Technical Report

BOUNDARY LAYER CALCULATION METHODS AND APPLICATIONS TO AERODYNAMIC PROBLEMS

Johannes Steinheuer

Dr.-Ing., Research Scientist, Institut für Aerodynamik der Deutschen Forschungs- und Versuchsanstalt für Luft- und Raumfahrt (DFVLR), Braunschweig, Germany,

1974

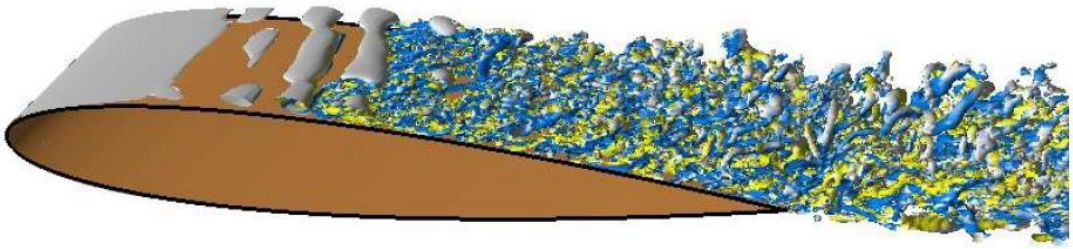

Contents

List of Figures

List of Tables

1. Introduction

1.1. General Remarks

The aerodynamic design of an aircraft may be characterized generally as the ability to develop such forms and shapes of an aircraft which will ensure a stable and controllable type of flow at a maximum efficiency. The basic flow to be achieved, for the Mach number range up to low-supersonic speeds, would ideally be the classical attached Kutta-Joukowsky flow[1]. The type of aircraft under consideration then is one having wings of large to moderate aspect ratio where the lifting surfaces are physically distinct from the propulsion units and from the fuselage. In the high subsonic speed range compressibility effects can be delayed to a certain extent by using swept wings, but still retaining the essential features of an attached flow. The aerodynamic design should be based on a full understanding of the fluid mechanics of the flow from which, either by theoretical considerations or by experimental research, design criteria and calculation methods are derived for the prediction of the aerodynamic properties of an aircraft.
Historically, the outstanding event by which our understanding of the physics of the flow around an obstacle such as an airplane was given its foundations, has been the introduction of the boundary-layer concept by Ludwig Prandtl (4 February 1875 - 15 August 1953) in 1904 [97] (see **figure A.1**). In this year of the 70th anniversary of that event it seems quite appropriate to recall that without the recognition that viscous forces, though small, play a crucial part in any flow, the experimentally observed finite drag in attached flows and the occurrence of separation could not be understood with the then existing and already highly developed perfect fluid theory on one hand or the Stokes viscous theory on the other. Prandtl's theory explained how viscosity exerts its influence on the flow in a thin boundary layer adjacent to the body surface. Drag is readily recognized as the sum of the shear forces in the thin boundary layer, and separation is the consequence of the retardation of fluid by viscous forces causing it to break away from the surface and thereby disturbing large areas of the flow field (stall). Since its foundation

[1] The Kutta-Joukowsky theorem is a fundamental theorem of aerodynamics, for the calculation of the lift on a rotating cylinder. It is named after the German mathematician Martin Wilhelm Kutta (* November 3, 1867 (Pitschen, Upper Silesia) , † December 25, 1944 (Fürstenfeldbruck, Bavaria)) and the Russian Nikolai Joukowsky (or Joukowski) (* January 17, 1847, (Orekhovo, Vladimir Governorate), † March 17, 1921 (Moscow)) who first developed its key ideas in the early 20th century. The theorem relates the lift generated by a right cylinder to the speed of the cylinder through the fluid, the density of the fluid, and the circulation. The circulation is defined as the line integral, around a closed loop enclosing the cylinder or airfoil, of the component of the velocity of the fluid tangent to the loop. The magnitude and direction of the fluid velocity change along the path.

boundary-layer theory has developed into a discipline of fluid dynamics of its own, standing comprising a broad variety of theoretical problems and practical applications. The analytic and numerical treatment of the boundary-layer equations has been greatly advanced, especially by the use of computers. Calculation methods have been devised in great number by which many problems of practical significance in aircraft aerodynamics could be solved, and of which this paper is trying to give a few examples.
Since the emphasis of this lecture course is on aerodynamic characteristics and their prediction, it seems appropriate first to point out in more detail the role of boundary-layer behavior and its influence on the aerodynamic characteristics. In view of the envisaged type of flow around an aircraft with wings of large to moderate aspect ratio, it is justified to do this by considering the two-dimensional flow over an airfoil section where most of the basic boundary layer phenomena are present.

1.2. The Influence of Boundary-Layer Behavior on the Aerodynamic Characteristics of Wing Sections

The low speed flow characteristics about a single airfoil, i.e. an airfoil without flaps[2] and slats[3] are well-known from wind-tunnel investigations as summarized in [5, 100, 126] giving data on lift vs. incidence, $c_{L,max}$ and drag coefficients for Reynolds numbers Re up to about 10^7. The Reynolds number is defined according to

$$Re := \frac{\rho u \mathscr{L}}{\eta} = \frac{u \mathscr{L}}{\nu} \ ,$$

with $\nu = \eta/\rho$ being the kinematic viscosity and $\mathscr{L}$ is a characteristic length of the considered system, e.g. the dimension of the airfoil.
From these experiments, one arrives at the following qualitative picture of the boundary-layer behavior and its influence on the aerodynamic coefficients. At small to moderate incidences the flow along the contour of the airfoil is completely attached, and an almost ideally potential flow pattern is established. The boundary layer starts on both sides of the stagnation point at the nose as a laminar boundary layer, undergoes transition beginning at some downstream position and extending usually over a relatively

[2] Flaps are devices used to improve the lift characteristics of a wing and are mounted on the trailing edges of the wings of a fixed-wing aircraft to reduce the speed at which the aircraft can be safely flown and to increase the angle of descent for landing. They shorten takeoff and landing distances. Flaps do this by lowering the stall speed and increasing the drag. Extending flaps increases the camber or curvature of the wing, raising the maximum lift coefficient - the lift a wing can generate. This allows the aircraft to generate as much lift, but at a lower speed, reducing the stalling speed of the aircraft, or the minimum speed at which the aircraft will maintain flight (see **figure A.3**).

[3] Slats are aerodynamic surfaces on the leading edge of the wings of fixed-wing aircraft which, when deployed, allow the wing to operate at a higher angle of attack. A higher coefficient of lift is produced as a result of angle of attack and speed, so by deploying slats an aircraft can fly at slower speeds, or take off and land in shorter distances. They are usually used while landing or performing maneuvers which take the aircraft close to the stall, but are usually retracted in normal flight to minimize drag.

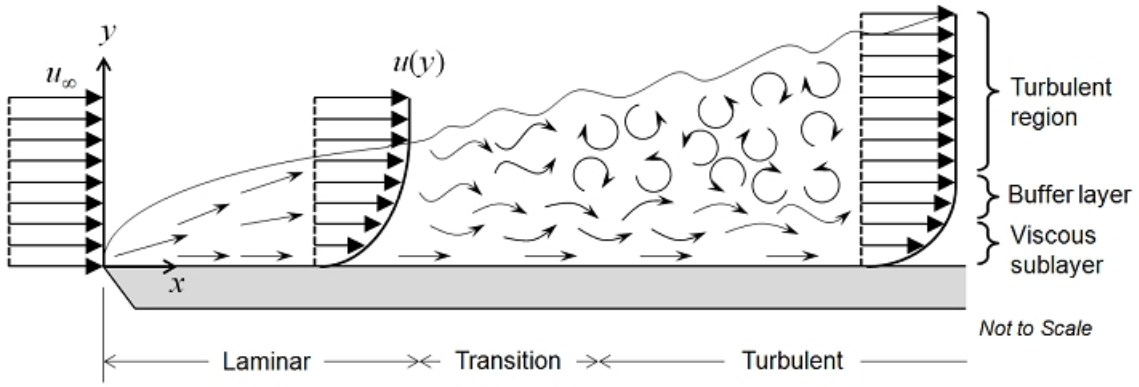

Figure 1.1.
Schematic drawing of a boundary layer over a flat plate

short distance, and continues as a turbulent boundary layer to the trailing edge where the boundary layers from the upper and lower sides merge to form a wake which is a turbulent thin shear flow (see **figure 1.1**). The location of the transition region depends on the pressure distribution, normally beginning at a small distance downstream of the point of minimum pressure, and on the Reynolds number. In general, increasing Reynolds number at a constant incidence decreases the boundary-layer thickness at any point, including the trailing edge which leads to an increase in circulation of the inviscid flow thus increasing the lift coefficient ${c_L}^4$, and the slope $\mathrm{d}\, c_L/\mathrm{d}\, \alpha$, while the pitching moment c_M becomes more positive. The profile drag c_D being composed of friction drag and pressure drag is generally reduced with Reynolds number by virtue of a decreasing pressure drag and also a reduction in friction drag. An indirect influence of the Reynolds number is brought about by a change in the transition location which is very sensitive to changes in pressure distribution. As the angle of incidence is increased at constant Reynolds number, the transition region moves forward on the upper side and rearwards on the lower side. On the other hand transition moves upstream on both sides with increasing Reynolds number at constant incidence. Thus the role of transition location as a Reynolds number dependent parameter is seen to have a prominent significance when it comes to extrapolating wind-tunnel measurements to the desired full scale data known as the scale effect to which some remarks will be made later on.
As the angle of incidence of an airfoil is further increased, eventually the boundary layer

[4] The lift coefficient is a dimensionless coefficient that relates the lift generated by a lifting body to the density of the fluid around the body, its velocity and an associated reference area. A lifting body is a foil or a complete foil-bearing body such as a fixed-wing aircraft. c_L is defined according to

$$c_L = \frac{L}{\frac{1}{2}\rho u^2 \cdot S} = \frac{2 \cdot L}{\rho \cdot u^2 \cdot S} = \frac{L}{q \cdot S} \ ,$$

where L is the lift force, ρ is the fluid density, u is the true airspeed, S is the planform area and q is the fluid dynamic pressure.

will separate from the surface at some point on the upper side. Depending on the section shape, the separation location and the Reynolds number significant differences occur as to the subsequent disturbance of the inviscid flow field. Two major characteristic types of separation can be distinguished (see **figure A.4**), i.e. (i) separation of the turbulent boundary layer at the trailing edge and (ii) separation of the laminar boundary layer near the leading edge. Rear separation of the turbulent boundary layer results from the increased positive or adverse pressure gradient as the lift increases with incidence. This type of separation occurs on thick airfoil sections with a well-rounded minimum pressure peak, and the transition lies at about the location of minimum pressure. The maximum lift is reached steadily with incidence as shown by the lift curve of **figure A.4** for the NACA 633-018 airfoil profile[5], indicating that the separation flow pattern is preserved even beyond the maximum lift. Raising the Reynolds number at constant incidence tends to push the separation point back again resulting in a gain of lift and thus allowing to achieve a higher $c_{L,max}$ value at a larger angle of incidence. However, lowering the Reynolds number eventually results in the separation of the laminar boundary layer on the forward part, i.e. before transition could take place. The once separated laminar boundary layer being unstable will very quickly turn turbulent and may then reattach again to the surface creating a closed separation region or bubble as shown for the cases ⓒ and ⓓ in **figure A.4**. This type of separation usually occurs with thinner airfoils, where the suction pressure peak is more pointed even at low angles of incidence. The bubble may behave in two distinct ways when after its establishment the incidence is raised or the Reynolds number is increased: it may shorten or it may enlarge, forming either a "short" or a "long" bubble. The contracting short bubble moves closer to the front and suddenly bursts when some critical incidence is reached, causing complete separation of the flow over the entire upper side of the airfoil. Consequently, the lift-curve (curve for the NACA 631-012 profile in **figure A.4**) has a sharp maximum with a drastic reduction of lift beyond this maximum and a corresponding drastic increase in drag. In contrast, the long bubble occurring at very thin airfoils extends rearwards with increasing incidence until it reaches the trailing edge. The lift slope decreases steadily during this process and the lift curve itself is rather flat around its maximum (curve for the NACA 64A006 profile in **figure A.4**). On profiles of moderate thickness the type of separation can change from the leading edge short bubble type to the trailing edge

[5] The NACA airfoils are airfoil shapes for aircraft wings developed by the **N**ational **A**dvisory **C**ommittee for **A**eronautics (NACA). The shape of the NACA airfoils is described using a series of digits following the word "NACA". The parameters in the numerical code can be entered into equations to precisely generate the cross-section of the airfoil and calculate its properties.
The NACA four-digit wing sections define the profile by:

1. First digit describing maximum camber as percentage of the chord,
2. Second digit describing the distance of maximum camber from the airfoil leading edge in tens of percents of the chord,
3. Last two digits describing maximum thickness of the airfoil as percent of the chord.

For detailed airfoil data see e.g. [33].

turbulent separation type. Also a range of Reynolds number may exist for which the two types are present simultaneously, e.g. a short bubble and turbulent rear separation, the latter being enhanced by the existence of the short bubble causing the adverse pressure gradient to be larger.
The main conclusion to be drawn is, that the lift characteristics of an airfoil are determined to a large extent by the boundary layer behavior being primarily dependent on Reynolds number. Transition location has a very important influence on the type of separation to be expected. No generally valid criteria exist by which the two types of bubble separation can be predicted. Only by a very detailed knowledge of the boundary layer development at every stage can one hope to predict quantitatively the aerodynamic characteristics of lift, moment and drag of airfoil profiles at least up to the point where separation first occurs. However, the calculation of the boundary layer development depends on the given pressure distribution which in turn is influenced by the boundary layer displacement effect. So, when trying to determine e.g. the lift by purely computational means, an iterative procedure is necessary in order to account for this interaction between inviscid outer flow and the boundary layer.
A much fuller account of the airfoil section characteristics and also of the following topics in connection with the general aspects of aircraft behavior at high angles of attack has been given in a recent review by G. J. Hancock [54]. The remarks made here are meant only to point out the role and significance of the boundary layer effects without attempting to be exhaustive.
The classical means of ensuring satisfactory landing and take-off performance of an aircraft is the addition of trailing edge flaps and leading edge slats to the basic wing. The development of the boundary layers around an airfoil with a flap and a slat is depicted in **figure A.5** together with measured pressure distributions reproduced from [40]. In addition to the phenomena connected with single airfoil flow, which may occur on each part of the multiple profile separately, there are essentially two more features to be considered. The first is the appearance of a separation bubble on the lower sides of the main airfoil and the slat, where the approaching turbulent boundary layer passes a contour discontinuity like that of the slat or highly curved parts of the profile contour like that at the flaps housing. The location of the reattachment point of these bubbles depends on the flap setting and the shape of the slat. Secondly, there exists an interaction between the wake of the slat and of the main profile and the boundary layer over the back of the main profile and the flap which will certainly influence the boundary layer characteristics and hence the overall profile behavior.
The typical boundary-layer development over the back of a profile with slat and flap can be deduced from the total pressure head distributions given in **figure A.6** as measured by Ljungstrøm [71]. Note that the only difference for the two cases shown is the different slat setting with a wider slat gap h_S in the upper diagram, resulting in a marked change in the boundary-layer development as influenced by the slat wake, and also in noticeable changes of the pressure distributions and the overall lift coefficient c_L. A very important practical problem with such configurations is the problem of finding the optimum positions of the slat and the flap with regard to maximum lift. **figure A.7** shows the results of wind-tunnel measurements for a drooped-nose profile with a slat for

three different slat angles and two Reynolds numbers according to E. Bartelt [40]. The pattern for positions of equal $c_{L,max}$ is quite irregular with the optimum locations being displaced considerably by small changes of the flap angle and a Reynolds number variation. These diagrams strikingly show that although flap and slat locations can be found in extensive and costly wind-tunnel experiments, the extrapolation of the experimental results to the full scale wing, i.e. to a higher Reynolds number is very doubtful. On the other hand, the prediction of the aerodynamic characteristics in such cases by purely computational means seems to be an almost insolvable task in view of the complexity of the problem. An attempted approach for the prediction of the optimum flap setting to attain maximum lift will be presented later. Very useful papers on the subject have been given by A. M. O. Smith [112] and D. N. Fostar [39].
If the Mach number Ma, which is defined according to[6]

$$Ma \coloneqq \frac{v_{\text{object}}}{v_{\text{sound}}}$$

is raised in the flow around an airfoil, a supersonic flow region is established on the upper surface which is terminated by a normal shock. Since a shock wave is a sudden flow compression, it is expected that there is a considerable influence on the boundary-layer development underneath. Although the flow upstream of the shock is supersonic, the inner regions of the boundary layer must be subsonic so that the compression is being spread out to some extent over the surface as shown in **figure A.8**. It depends very much on the shock strength and on the state of the approaching boundary-layer whether or not it will separate in this region. If separation occurs, this will drastically influence the inviscid flow and consequently also the aerodynamic properties of the profile. It is generally agreed that the approaching boundary layer should by all means be a turbulent one since a laminar boundary layer would almost invariably separate due to its very limited capability to withstand an adverse pressure gradient. This is the main reason why in wind-tunnel experiments the boundary layer is tripped to forced transition well ahead of the expected shock location.
The different types of separation phenomena as a consequence of the interaction of the shock with a turbulent boundary layer including various other aspects of the transonic flow over profiles and wings have been pointed out in several papers by K. H. Pearcey, e.g. in [95]. Recent reviews on the subject are also due to J. E. Greene [50, 51]. The two main models are depicted schematically in sketches ⓐ and ⓑ of **figure A.8**. Flow model A postulates the existence of a separation bubble underneath the shock which is growing in extent towards the rear with increasing incidence, i.e. with growing shock strength. The adverse pressure gradient over the rear part is not strong enough in this ease to induce rear separation which is to be expected for relatively thin and lightly loaded airfoils. However, for the thicker and more highly loaded sections used in modern designs, the pressure gradients in the rear subsonic flow are steeper so that flow model

[6] v_{object} is the velocity of the airfoil, etc. relative to the medium, and v_{sound} is the speed of sound in the medium or surrounding fluid respectively. At $Ma < 0.8$, the flow is to be said subsonic, for $Ma = 0.8 - 1.2$ the flow is called transonic and for $Ma = 1.2 - 5.0$ the flow is designated as supersonic.

B with separation from the trailing edge is expected to exist. Mixed types of flows may exist according to Pearcey, Osborne and Haines [95] with a bubble at the shock location and rear separation. Model B type separation, being essentially the analogue to the classical low speed turbulent trailing edge separation, is very sensitive to the local pressure gradient, the boundary-layer thickness δ, and the upstream history of the boundary layer. Even without separation, the interactions at the foot of the shock and at the trailing edge are locally strong as pointed out by J. E. Greene [51] and influence the overall flow behavior and hence the aerodynamic characteristics of the profile. Incipient rear separation also marks the onset of the very severe phenomenon of buffeting and it is of utmost practical importance to be able to predict the buffet boundaries as a function of Mach number and Reynolds number.

The above short description of examples of flows over single and multiple airfoils in the low speed range and the flow on an airfoil at high subsonic speeds may suffice to point out the eminent importance of the boundary layer in any flow situation. The extension of profile flow to the actual flow over wings with finite span, of course, must be taken into consideration in an actual design. However, the essential features of the boundary-layer development will not be changed radically by the inclusion of three-dimensionality as long as the aspect ratio of the wing remains large and the sweep angle in case of a swept wing is not too large, say less than 40 °. The problem of assessing the aerodynamic characteristics of a finite wing from the knowledge of its sectional behavior has been treated by Küchemann [67] and reviewed by Hancock [54] and by Williams and Ross [138] with many pertinent references. Since the aerodynamic characteristics of an aircraft are dominated by the properties of its lifting surfaces, it seems justified to leave aside the problems associated with fuselage interference. The boundary-layer aspect of the attached flow over the fuselage and other aircraft components such as engine nacelles is primarily concerned with the reduction of drag at low lift cruise speeds assuming attached flow conditions. Therefore, in the following survey on boundary layer calculation methods, essentially two-dimensional boundary layer flow is presupposed.

The purpose of boundary-layer calculations within the framework of the general objective of predicting the aerodynamic characteristics of a projected aircraft may be characterized as the ability (i) to positively define the state of flow, i.e. to decide if attached flow exists or if regions of separated flow must be expected, and (ii) to provide a quantitative measure of the effect that the boundary layer has on the aerodynamic characteristics, i.e. to be able to calculate the friction drag, the reduction of lift and the change of moment as compared to the non-viscous flow condition.

The difficulties encountered in achieving the first task are concerned not so much with the calculation of the attached boundary layer in the laminar or turbulent state but with the reliability of criteria for predicting the onset and extent of transition and hence turbulent separation. It may easily be visualized, that an inaccurate location of transition leads to wrong initial conditions for the calculation of the fully turbulent boundary layer and its characteristics including the location of possible turbulent separation, even if the method applied is quite satisfactory otherwise. This is especially true in the case where transition takes place over a laminar-turbulent separation bubble. The second task above implies the use of advanced criteria exceeding the well-known

Kutta-Joukowsky condition for the behavior of the external flow in the vicinity of the trailing edge. The treatment of the confluent boundary layers forming the wake in this region enters decisively into the subsequent recalculation of the entire inviscid flow field and is consequently responsible for the success in predicting the fractional drag and the reduction of lift due to the presence of the boundary layer. Thus, it must be realized that it is the combination of boundary layer calculation methods on the one hand and the utilization of adequate criteria of various types and at different stages in the computational process on the other hand which will determine the applicability and accuracy of a proposed overall prediction method.
In what follows, an attempt is made to give a survey on existing boundary layer calculation methods while the various criteria needed to complete the overall prediction method will not be treated in any greater detail.

2. The Boundary-Layer Concept

The concept of the boundary layer as introduced by L. Prandtl [97] in 1904 consists in the realization, that the flow around a (more or less streamlined) obstacle such as an airfoil can be subdivided into two distinct regions: (i) the main flow in which velocity gradients are so small that the influence of the viscosity η of the fluid may be disregarded completely, and (ii) the thin layer in the immediate vicinity of the surface of the body in which the gradient of the velocity in main direction of the flow is so large that a viscous shear force according to Newton's friction law $\tau = \eta \cdot \left(\frac{\partial u}{\partial y}\right)$ is produced and must be taken into account. While in the main region of the flow (which for simplicity may be viewed to be two-dimensional steady and incompressible), the Navier-Stokes equation reduce to the frictionless Euler equations characterized by the absence of vorticity and is therefore convertible to the Laplace potential equation. In the frictional region close to the wall, i.e. the boundary layer, the Navier-Stokes equations are reduced to Prandtl's boundary layer equations.
Written in the simplest form, i.e. for a steady two-dimensional incompressible boundary layer, the equations are:

$$\frac{\partial u}{\partial x} + \frac{\partial v}{\partial y} = 0 \ \text{(continuity equation)} \tag{2.1}$$

$$u\,\frac{\partial u}{\partial x} + v\,\frac{\partial u}{\partial y} = -\frac{1}{\rho}\cdot\frac{\mathrm{d}p}{\mathrm{d}x} + \frac{1}{\rho}\cdot\frac{\mathrm{d}\tau}{\mathrm{d}y} \ \text{(momentum equation).} \tag{2.2}$$

Equations (2.1) and (2.2) apply equally for laminar and turbulent boundary layers, if in the turbulent case the velocities u and v are understood as being time averaged mean quantities of the respective fluctuating velocities $u = \overline{u} + \overline{u'}$ and $v = \overline{v} + \overline{v'}$. The pressure-gradient term in equation (2.2) may be expressed by Bernoulli's equation as

$$\frac{1}{\rho}\cdot\frac{\mathrm{d}p}{\mathrm{d}x} = -U(x)\cdot\frac{\mathrm{d}U(x)}{\mathrm{d}x} \ , \tag{2.3}$$

where $U = U(x)$ is the velocity-distribution of the main stream assumed as given just outside the boundary layer of thickness $\delta(x)$, as depicted in **figure A.9**. The appropriate boundary conditions then are:

$$y = 0: \ \ u = v = 0; \ \ \lim y \to \delta: \ \ u = U(x) \ . \tag{2.4}$$

The shear stress $\tau = \tau(x, y)$[1] appearing in equation (2.2) formally as a thin, independent variable is expressed as

$$\tau = \frac{\partial u}{\partial y} \tag{2.5}$$

in the laminar case, and by

$$\tau = -\rho \cdot \overline{u' v'} \tag{2.6}$$

in the turbulent case[2], which in the boundary layer approximation is the so-called Reynolds shear stress or apparent turbulent stress as distinct from the Newton stress expressed by equation (2.5). For large Reynolds numbers, a necessary assumption when using boundary-layer theory, the Reynolds stress in fully developed turbulent flow exceeds the Newton stress generally by orders of magnitude. It is also usually assumed that the Reynolds stress is much larger than the turbulent normal stress which is an implication for equation (2.1) and (2.2) above to be valid in this simple form. For laminar boundary layers, the known relation equation (2.5) for the shear stress with the constant molecular viscosity η completes the set of partial differential equations (2.1) and (2.2). Therefore, together with the boundary condition, in principle, exact solutions of this system of equations are possible. The boundary-layer equations are of parabolic nature, implying that the solution for the unknown variables u and v which are to be determined within the strip-like domain between the body surface and the external flow region can be found by a stepwise marching procedure in the downstream direction. This means, that the solution at a location x is not influenced by conditions at a location downstream of x, the upstream conditions, however, affecting it very much generally. This property is often referred to as the boundary layer's memory capability for its upstream "history". Exact solutions for the laminar boundary-layer equations have been obtained for a wide range of external pressure (or velocity) distributions of which the similarity solutions are especially important. In these cases the external velocity distribution

$$U(x) \sim x^m \ , \tag{2.7}$$

with m being a dimensionless constant, allows the system of partial differential equations (2.1) and (2.2) to be reduced to one ordinary differential equation by removing

---

[1] A shear stress, denoted τ, is defined as the component of stress coplanar with a material cross section. Shear stress arises from the force vector component parallel to the cross section. Normal stress, on the other hand, arises from the force vector component perpendicular to the material cross section on which it acts. Any real fluids (liquids and gases included) moving along a solid boundary will incur a shear stress on that boundary.

[2] $\rho \cdot \overline{u' v'}$ is called the Reynolds stress tensor, which is defined according to

$$\tau_{i,j} = \rho \cdot \overline{u'_i v'}_j = \rho \cdot \begin{pmatrix} \overline{u'_1 v'_1} & \overline{u'_1 v'_2} & \overline{u'_1 v'_3} \\ \overline{u'_2 v'_1} & \overline{u'_2 v'_2} & \overline{u'_2 v'_3} \\ \overline{u'_3 v'_1} & \overline{u'_3 v'_2} & \overline{u'_3 v'_3} \end{pmatrix} \ .$$

The Reynolds stress tensor has the form of the divergence of a stress tensor (per unit mass).

the x-dependence from the equations which results in "similar" velocity profiles for all x-stations (Falkner-Skan equation, see [34]). These and other exact solutions of the laminar boundary-layer equations are fully described for example in the books of Hermann Schlichting [106] and L. Rosenhead [102]. The usefulness of exact solutions for the outer velocity distribution $U(x)$ according to equation (2.7) with continuously accelerated ($m > 0$) or continuously decelerated ($m < 0$) flows lies in the fact that they provide a good physical insight into the character of boundary-layer flows in general. Furthermore, approximate solution methods designed to be valid for the general case of a laminar layer with an arbitrary free-stream pressure distribution can be checked against these exact solutions. In fact, some of the approximate integral methods for the laminar case make direct use of the similarity velocity profile family gained by solution of the Falkner-Skan equation[3].
In order to formally complete the set of the partial differential equations (2.1) and (2.2) also for turbulent boundary layers, the Reynolds stress term in equation (2.2) and (2.6) is often replaced by the semiempirical relations known as the eddy-viscosity concept or the mixing-length concept of Prandtl. In the former case, the Reynolds stress is required to assume the form

$$-\rho \cdot \overline{u'\,v'} = \epsilon \cdot \frac{\partial u}{\partial y} \ . \tag{2.8}$$

where $\epsilon = \epsilon(x, y)$, the turbulent exchange coefficient or eddy-viscosity, is not a constant but varies from point to point. With the mixing-length theorem, the Reynolds stress is expressed by

$$-\rho \cdot \overline{u'\,v'} = \rho\,\ell^2 \cdot \left|\frac{\partial u}{\partial y}\right| \cdot \frac{\partial u}{\partial y} \tag{2.9}$$

where the mixing length $\ell = \ell(x, y)$ is also an unknown function. The mixing length is interpreted as that distance, which a turbulent fluid lump moves on the average in the y-direction before it is dissolved through a mixing process with other lumps and thus looses its identity. In a more modern interpretation, the mixing length is assumed to be a characteristic length scale for the transport of turbulent energy. Usually, it is tried to further break down the eddy-viscosity ϵ or the mixing length ℓ and relate them by suitable empirical functional relationships to the lateral distance y and the mean velocity and its derivatives. One such special assumption is von Kármán's similarity hypothesis[4]

[3] The Falkner-Skan equation (named after V. M. Falkner and Sylvia W. Skan) is a non-linear ordinary differential equation given as follows:

$$\frac{\partial^3 f}{\partial \eta^3} + f\frac{\partial^2 f}{\partial \eta^2} + \beta \cdot \left[1 - \left(\frac{\mathrm{d}f}{\mathrm{d}\eta}\right)^2\right] = 0 \ ,$$

with $\beta = \frac{2\,m}{m+1}$ and m being a constant. η is a transformed wall-normal coordinate (similarity variable). f is a dimensionless, scaled stream function, which is a function of η.

[4] Theodore von Kármán (* May 11, 1881 (Budapest, Austria-Hungary), † May 7, 1963 (Aachen, West Germany)) was a Jewish Hungarian-American mathematician, aerospace engineer and physicist who was active primarily in the fields of aeronautics and astronautics. He is responsible for many

$$\ell = \mathscr{K} \cdot \left| \frac{\left(\frac{\partial u}{\partial y}\right)}{\left(\frac{\partial^2 u}{\partial y^2}\right)} \right| \tag{2.10}$$

where $\mathscr{K}$ denotes an empirical constant. There has been much argument on the validity of the mixing-length and eddy-viscosity concepts from physical reasons (Bradshaw [16] and Rotta [105]). The most serious objection is, that the Reynolds shear stress is related to local mean flow quantities only whereas it is actually influenced also by the turbulence transport mechanisms, i.e. it should be more closely connected to turbulent properties of the boundary-layer flow including upstream -or "history"- effects of this turbulent process. Mathematically, however, the shear stress term must be related ultimately to the local independent space variables x and y whatever the degree of sophistication of the physical model may be to achieve this.

key advances in aerodynamics, notably his work on supersonic and hypersonic airflow characterization. He is regarded as the outstanding aerodynamic theoretician of the twentieth century (see **figure A.2**).

3. On the Structure of Boundary Layers

Before going further in the description of the main features of the various boundary-layer calculation methods, it seems appropriate to make some remarks on the structure of boundary layers. This is done again for two-dimensional incompressible boundary-layer flows giving the opportunity to recapitulate on the terminology used in boundary-layer theory.

3.1. Laminar Boundary Layers

As its denomination suggests, a laminar boundary layer consists of a well-behaved flow of stratified laminae of fluid moving along the solid surface of a body, **figure A.10**. Although there is a considerable momentum exchange between neighboring streamlines through the action of viscosity which produces the shear forces, the structure of the laminar boundary layer remains unaltered as long as it adheres to the wall. The thickness δ of the boundary layer is determined by the x-wise distribution of the external velocity $U(x)$ just outside the boundary layer. In general the thickness δ increases with x $\left(\delta \sim \sqrt{Re_x}\right.$ in laminar flat plate boundary layer, where $\left.U(x) = U_\infty = const.\right)$. Physically, this is explained by the decelerating effect of the shearing forces on a lamina of fluid causing the adjacent lamina of higher velocity to be pushed outwards in the y-direction. As a net result of this action, the outer flow is displaced somewhat away from the wall. The displacement is quantitatively expressed as the defect of mass flow in the boundary layer as compared to the ideal mass flow in the absence of the boundary layer by

$$U(x)\,\delta_1 = \int_0^\delta (U(x) - u)\,\mathrm{d}y \tag{3.1}$$

where here, for the incompressible case, the constant density ρ could be dropped. δ_1 then is the familiar displacement thickness.
If the prescribed free-stream velocity $U(x)$ is increasing, i.e. the pressure $p(x)$ decreases in the streamwise direction x ($\mathrm{d}p/\mathrm{d}x < 0$), the boundary-layer thickness δ (and δ_1) grows only very slowly. Much more interesting is the case of increasing pressure or adverse pressure gradient ($\mathrm{d}p/\mathrm{d}x > 0$), i.e. decreasing external velocity $U(x)$. In this case, the deceleration of the boundary-layer fluid becomes more pronounced. The boundary layer now quickly grows thicker and the velocity profile will soon show an inflexion point. The gradient $(\partial u/\partial y)_x$ at the wall, which is a measure for the local friction force exerted

to the wall, diminishes rapidly with persisting adverse pressure gradient. The eventual loss of all kinetic energy of a fluid particle adjacent to the wall under the combined influence of an increasing pressure and the shear forces leads to the stagnation of this particle. As a consequence, the particles on a neighboring streamline are forced to leave the surface and follow some path just above a dividing streamline which separates fluid coming from the upstream region from fluid, that is, of necessity, being pushed in from downstream in a reversed flow. This is the phenomenon of boundary-layer separation. At the point of separation, the dividing streamline intersects the wall at a finite small angle σ determined by the relation

$$\tan\sigma = -3 \cdot \frac{\left(\frac{\mathrm{d}\tau_w}{\mathrm{d}x}\right)_{x_S}}{\left(\frac{\mathrm{d}p}{\mathrm{d}x}\right)_{x_S}} \tag{3.2}$$

and the point of separation itself is determined by the condition, that the velocity gradient normal to the wall vanishes there:

$$\left(\frac{\partial u}{\partial y}\right)_{\substack{y=0,\\ x=x_S}} = 0 \;\text{ or }\; \tau_w\left(x_S\right) = 0 \;\; . \tag{3.3}$$

The appearance of an inflection point in the laminar boundary-layer velocity profile usually signalizes the inclination of the boundary layer to be unstable against small disturbances, i.e. at a sustained adverse pressure gradient, $(\mathrm{d}p/\mathrm{d}x > 0)$, the boundary layer will turn into its transitional state. Transition of this boundary layer from a pure laminar state into the fully developed turbulent state takes place over some distance in the streamwise direction, this transition length being mainly dependent on the outer pressure variation, on the roughness of the surface, and on the turbulence level of the outer stream. The onset of transition is marked physically by the appearance of an irregular and intermittent sequence of laminar and turbulent regions (turbulent spots). The theoretical prediction of transition onset is the subject of boundary layer stability theory, the first remarkable success of which are connected with the names of W. Tollmien and H. Schlichting [107], who were able to calculate the critical local Reynolds number $Re = U\,\delta_1/\nu$ for neutral stability on a flat plate boundary layer. The streamwise location x_i of this theoretical point of instability lies ahead of the actual region or point of transition. The transition point may be characterized to be that point in the streamwise direction, at which the regular oscillations appearing downstream of the instability point suddenly break down and are transformed into irregular patterns of high frequency which are characteristic of the fully turbulent motion.
It is not intended to go any further into the details of boundary-layer transition. Critical reviews of the subject of boundary-layer stability and transition were given by Betchov and Criminale [11], and Obremski et al. [90]. However, some remarks in view of an actual prediction method seem to be appropriate. There still is no rational method in existence to accurately predict transition from laminar to turbulent boundary-layer flow. Most of the earlier boundary-layer calculation methods make use of the concept, that transition takes place instantaneously at a transition point, the location of which is

taken as the point of minimum pressure or the point of instability which is determined roughly from correlation curves connecting the critical local Reynolds number based on the boundary-layer thickness with the local pressure gradient. In more refined methods, the actual transition point is taken as being downstream of the instability point by an amount taken from an experimental correlation curve such as those of Granville [49] or Smith and Gamberoni [114]. The most advanced methods realize the fact, that the transition from laminar to turbulent flow takes place over some finite surface distance. This is accomplished by slowly activating the turbulent eddy-viscosity ϵ over a finite surface length as based on an intermittency factor proposed by Chen and Thyson [22] which accounts for the intermittent appearance of turbulent regions in the transition region.
The transition mechanism dealt with above was concerned with boundary layers which remain attached during the transition process. As has been mentioned earlier, transition may alternatively take place through the mechanism of a laminar separation bubble followed by turbulent attachment. A basic review on this type of transition has been given by Tani [122]. Again the incorporation of criteria for a quantitative prediction of this type of transition relies heavily on experimentally observed correlation curves between bubble length, a suitable chosen pressure gradient coefficient, and the boundary-layer thickness at the point of laminar separation such as those given by Crabtree [25], Owen and Klanfer [91] and Gaster [43].

3.2. The Turbulent Boundary Layer

Let us now turn to a description of the main features of the fully developed turbulent boundary layer. It is characterized by the very vigorous mixing of fluid contained in it, where the velocity vector and other quantities like pressure, density and temperature (in the compressible case) fluctuate randomly with respect to space and time. Thus in a nominally two-dimensional turbulent boundary layer there is random motion also in the lateral direction. In contrast to the laminar boundary layer, a single momentary observation in a turbulent boundary layer would never give a repeatable result. Consequently the turbulent boundary-layer flow can only be described in terms of statistical quantities. Therefore the quantities u, v, p and ρ in equation (2.2), as already mentioned, are statistical mean quantities.
Despite the radically different internal structure of turbulent boundary layers, their general behavior and development under the influence of the free-stream velocity or pressure variation resembles much to that of a laminar boundary layer. With pressure decreasing in the x-direction, the turbulent boundary layer grows slowly in thickness, although at a faster rate ($\delta \sim x^{4/5}$ as compared to $\delta \sim x^{1/2}$ in the laminar case for flat plate boundary layer) while in a persisting adverse pressure gradient flow it eventually will separate from the wall. However, with the very vigorous mixing action present in the turbulent boundary layer, transfer of kinetic energy from the external flow is much greater than for laminar boundary layers resulting (i) in the fuller velocity profile $u(y)$, (ii) in the capability to endure much larger pressure gradients, and (iii) in higher fractional drag

forces on the wall.
Returning to the structure of the turbulent boundary layer, I do not intend to review the complicated theory of turbulence but I shall rather limit myself to the description of a generally accepted model of the turbulent boundary layer. For a full account of turbulence theory I may refer one to the recent publications by Bradshaw [16] and Rotta [105].
Figure A.11 shows a sketch of the turbulent boundary layer which may be regarded as a momentary picture of the vortex-like or eddying motion, the mean velocity profile being also indicated. From this, at first sight, it would seem to be impossible to deduce any principle of order. However, as we know, the mean boundary-layer thickness grows in the streamwise direction which means that a permanent entrainment of originally non-turbulent high-energy fluid takes place. This capture of fluid from the free stream is achieved by tangential viscous shear forces acting along the distorted and "wiggling" but distinct boundary layer edge which has been named therefore the "viscous superlayer". The high energy is then transported to the inner parts of the boundary layer by the largest turbulent eddies of a size in the order of the mean thickness δ of the boundary layer which enables them to be in contact with the irrotational outer flow in the first place. The turbulent energy is then exchanged among the eddies of smaller size which are forming and disappearing constantly. It is assumed, that eddies of all sizes are present but that eddies of widely different sizes have no direct influence on each other. An eddy of given size exchanges energy at an appreciable rate only with another eddy of nearly the same size. The energy exchange thus is comparable with a cascade process in which the biggest eddies lose energy to eddies one order of magnitude smaller, which lose energy to smaller eddies in their turn, and so on until the eddies are so small that they lose so much energy by direct action of viscous stress, that no smaller ores can be formed so that at last, all energy is converted into heat by direct viscous dissipation. The physical mechanism invoked for this cascade process is that of stretching of the eddies, which may be envisaged as line vortex elements, by the gradient of the mean velocity. Therefore the largest eddies can best interact with the mean flow as compared to small-sized eddies. Thus the large eddies whose lifetime is also large, carry most of the turbulent energy and Reynolds stresses while the scale of the smallest eddies is determined by the magnitude of the molecular viscosity.

3.3. The Reynolds Stress Equation

It is now clear, that the turbulent shear stress needed in the momentum equation, equation (2.2), is not likely to be determinable from consideration of mean flow properties only, such as the mean local velocity gradient as suggested by the eddy viscosity concept or the mixing length concept. For this reason, turbulence research workers as Bradshaw and Rotta demand the use of transport equations, which can be derived from the Navier-Stokes equations and by which the transport of any turbulence quantity such as the the Reynolds stress $-\rho \cdot \overline{u'\,v'}$ or the turbulent kinetic energy $\mathbf{k} = 1/2 \cdot \overline{q'^2} = 1/2 \cdot \left(\overline{u'^2} + \overline{v'^2} + \overline{w'^2}\right)$ can, in principle, be described. Since the Reynolds stress enters the boundary layer momentum equation directly, let us consider the ap-

propriate transport equation. For a two-dimensional turbulent incompressible boundary $\rho = const.$ we have:

$$\underbrace{u\,\frac{\partial \overline{u'\,v'}}{\partial x} + v\,\frac{\partial \overline{u'\,v'}}{\partial y}}_{\text{advection by mean flow}} + \underbrace{\overline{v'^2}\cdot\frac{\partial u}{\partial y}}_{\text{generation by interaction with mean flow}} - \underbrace{\overline{\frac{p'}{\rho}\cdot\left(\frac{\partial u'}{\partial y}+\frac{\partial v'}{\partial x}\right)}}_{\text{redistribution by pressure fluctuations}} \tag{3.4}$$

$$+ \underbrace{\frac{1}{\rho}\cdot\frac{\partial \overline{p'\,u'}}{\partial y}}_{\text{Transport by velocity fluctuations}} - \underbrace{\nu\cdot\overline{(u'\,\nabla^2\,v' + v'\,\nabla^2\,u')}}_{\text{destruction by viscous forces}} = 0\ .$$

The physical meaning of the different terms is indicated. Similarly, the transport equation for the turbulent kinetic energy $\overline{q'^2/2}$ reads:

$$\underbrace{\frac{1}{2}\cdot u\,\frac{\partial \overline{q'^2}}{\partial x} + \frac{1}{2}\cdot v\,\frac{\partial \overline{q'^2}}{\partial y}}_{\text{advection}} + \underbrace{\overline{u'\,v'}\cdot\frac{\partial u}{\partial y}}_{\text{production}} \tag{3.5}$$

$$+ \underbrace{\frac{\partial}{\partial y}\cdot\left(\overline{p'\,v'} + \frac{1}{2}\cdot\overline{q'^2\,v'}\right)}_{\text{transport by diffusion}} + \underbrace{\epsilon_d}_{\text{viscous dissipation}} = 0\ .$$

Also, transport equations for other turbulent fluctuating quantities such as $\overline{u'^2}$, $\overline{v'^2}$ and $\overline{w'^2}$ can be derived, which all have the same structure as the above equations (3.4) and (3.5). To make these equations solvable, one must represent the individual terms by empirical functions of the Reynolds stress. This is what is often referred to as "modeling" or "closure" of the transport equations.
It is not my intention, to go any further into the details of modeling the turbulent transport equations. I just wanted to indicate the general feature of this approach to complete the momentum equation, equation (2.2), by introducing additional partial differential equations pertaining to the Reynolds stresses instead of purely empirical formulae. However, I would like to draw your attention to one point. For high Reynolds number boundary layers the assumption can be made that in the transport equation for the turbulent energy, equation (3.5), the production of energy is equal to the dissipation, with all other terms negligibly small. This means that whatever amount of turbulent energy is produced by the large size eddies and transferred from big to small eddies, will be dissipated by viscous action eventually. The controlling parameter then is the production term, and energy dissipation is independent of viscosity. Then ϵ_d, in equation (3.5) can be expressed by the relation

$$\epsilon_d = c \cdot \left(\frac{\overline{q'^2}}{2} \right)^{\frac{3}{2}} \cdot \frac{1}{\mathscr{L}} \ , \tag{3.6}$$

where $\mathscr{L}$ is a length scale of the big eddies and c is a dimensionless proportionality factor. With the additional assumption made by P. Bradshaw [14], that the ratio of the Reynolds shear stress to the turbulent energy is constant, i.e.

$$-\overline{u'\,v'} = a \cdot \overline{q'^2} \ \ (a = const.) \ , \tag{3.7}$$

and equating ϵ_d from equation (3.6) with the production term from equation (3.5), one arrives at the expression

$$-\overline{u'\,v'} = \xi^2 \cdot \mathscr{L}^2 \cdot \left(\frac{\partial u}{\partial y} \right)^2 \tag{3.8}$$

with $\xi^2 = (2\,a)^3/c^2$. This relation is identical with equation (2.9) for the mixing length concept, if $\ell = \xi \cdot \mathscr{L}$. The derivation of the mixing length formula from the transport equation for the turbulent kinetic energy, equation (3.5), seems somewhat artificial, it shows however that the required information on the Reynolds stress can be obtained from these equations which relate one turbulent quantity to another turbulent quantity, as in equation (3.7), and that under special assumptions the same relation is retrieved, which originally has been a hypothesis. In the case of high Reynolds number boundary layers, the mixing length formula turns out indeed, to be a good approximation. For other cases of thin shear layers as the turbulent wake or jet flow it might not be so adequate (see [16, 18, 105]). Calculation methods, which are based on the system of partial differential equations embracing both, those for the mean flow velocities, equation (2.1) and (2.2), and those for the transport of turbulent quantities such as the Reynolds stress, equation (3.4), and the turbulent kinetic energy, equation (3.5), are called turbulence field methods. Some of these methods will be listed later.

3.4. The Two-Layer Model

Having recognized the usefulness of the mixing length concept, it is appropriate to recapitulate its consequences on the boundary layer velocity profile. In the case of incompressible two-dimensional flow over a smooth surface and in the absence of strong x-wise pressure gradients, the shear stress is almost independent of distance from the surface and equal to the wall shear stress τ_w. For the mixing length ℓ, being a measure for the size of the eddies in the vicinity of the wall, the reasonable assumption is made, that it is proportional to the distance y from the wall,

$$\ell = \mathscr{K} \cdot y \ . \tag{3.9}$$

Introducing this into the mixing length formula, equation (2.9), one has

$$\sqrt{\frac{\tau_w}{\rho}} = \mathscr{K} \cdot y \cdot \frac{\partial u}{\partial y} = u_\tau \ , \tag{3.10}$$

which integrates to the familiar logarithmic velocity profile

$$\frac{u}{u_\tau} = \frac{1}{\mathscr{K}} \cdot \ln\left(\frac{y \cdot u_\tau}{\nu}\right) + C \ . \tag{3.11}$$

where $\mathscr{K} = 0.4$ is the von Kármán constant, and $C = 5.0$ is an integration constant determined from experiment. In equation (3.10) u_τ is the so-called shear stress velocity, being introduced as a convenient measure of the constant wall shear stress τ_w. The range of validity of the law-of-the-wall, equation (3.11), extends from about 1 to 2 % of the mean total thickness δ (see **figure A.11**). The usual representation of the law-of-the-wall velocity distribution is that in a semi-logarithmic plot as in **figure A.12** ⓐ, which shows the velocity distribution u/u_τ according to equation (3.11) together with experimental results according to Coles [23].
The narrow region from $y = 0$ at the wall to about 0.2 % of δ is not included in the velocity distribution of the law-of-the-wall. In this region, the turbulent eddy motion is more or less damped out as a consequence of the adherence condition $u(0) = 0$. This very thin layer is essentially laminar and it must carry the constant shear stress τ_w as a laminar shear stress to the wail very much like a Couette flow between a stationary and a moving parallel wall. The distribution of velocity in this viscous sublayer is accordingly a linear one

$$\frac{u}{u_\tau} = \frac{u_\tau \cdot y}{\nu} \ , \tag{3.12}$$

which is also shown in **figure A.12**. A continuous single function for the velocity distribution $\frac{u}{u_\tau}$ extending right from the wall $y = 0$ which comprises the linear relation, equation (3.12), as well as the logarithmic part according to equation (3.11), can be achieved by modifying the linear relation for the mixing length, equation (3.9), suggested by Van Driest [130]

$$\ell = \mathscr{K} \cdot y \cdot \left[1 - \mathrm{e}^{-\left(\frac{y \cdot u_\tau}{A \cdot \nu}\right)}\right] \ , \tag{3.13}$$

where the empirical value $A = 26$ gives good agreement with experiment.
The outer portion of the boundary layer, which extends from about $y = 0.2 \cdot \delta$ up to the outer edge $y = \delta$ (see **figure A.11**) does not obey the law-of-the-wall. This is best seen by replotting in **figure A.12** ⓑ the curves of **figure A.12** ⓐ to show the velocity defect $(U(x) - u)/u_\tau$ as a function of the wall distance y/δ, where δ is taken to be that point for which $u/U(x) = 0.995$. Also shown is the law-of-the-wall curve as the straight line in this semi-logarithmic graph. Comparing the experimental data with the logarithmic law, one observes first that they deviate from it appreciably in the region $0.2 < y/\delta < 1$, and second that the experimental curves for the two different Reynolds numbers fall together into one single curve. For this behavior of the outer portion of the

turbulent boundary layer, D. Coles [24] has developed his wake model also called the law-of-the-wake. Under this concept, the whole boundary layer is visualized essentially as a turbulent half-wake flow which is constrained by a wall. The wake-like behavior, if apparent from the intermittent character of the outer boundary layer where, at a fixed distance $y/\delta \leqslant 1$, turbulent flow is alternating with rotation-free flow. Furthermore, the outer velocity profiles are quite sensitive to external pressure gradients $\mathrm{d}\,p/\mathrm{d}\,x$. On the other hand, the logarithmic inner part of the boundary layer is almost completely defined by the magnitude of the wall shear stress τ_w appearing as the shear stress velocity $u_\tau = \sqrt{\tau_w/\rho}$ in the velocity distribution, equation (3.11).
From this idea of two distinct scales determining the turbulent boundary layer flow, Coles developed a two-parametric standard representation of the velocity distribution by extending the logarithmic part to include an additional wake part.

$$\frac{u}{u_\tau} = \frac{1}{\mathscr{K}} \cdot \ln\left(\frac{y \cdot u_\tau}{\nu}\right) + C + \frac{\Pi}{\mathscr{K}} \cdot w\left(\frac{y}{\delta}\right) \quad , \tag{3.14}$$

where

$$w\left(\frac{y}{\delta}\right) \equiv w\,(\chi)$$

is Coles wake function, which may be approximated by either of the two following equations

$$w\left(\frac{y}{\delta}\right) = w(\chi) = 1 + \sin\left[\frac{\pi}{2} \cdot (2\,\chi - 1)\right] \tag{3.15}$$

or

$$w(\chi) = 2 \cdot \sin^2\left(\frac{\pi}{2}\,\chi\right) \quad . \tag{3.16}$$

In equation (3.14), Π is a new parameter, which will determine the magnitude of the wake-part and which is dependent strongly on the streamwise pressure gradient. In **figure A.13** the composition of a complete boundary-layer profile is illustrated.
The standard two-layer velocity-profile representation in the form of equation (3.14) plays an important role in the boundary layer calculation methods, which are based on the integrated form of the boundary layer equations. Thus e.g., on putting $u = U(x)$, the free-stream velocity, and $y = \delta$, the local friction law is obtained in the form

$$\frac{U(x)}{u_\tau} = \frac{1}{\mathscr{K}} \cdot \ln\left(\frac{\delta \cdot u_\tau}{\nu}\right) + C + \frac{2}{\mathscr{K}}\,\Pi \quad . \tag{3.17}$$

Given the constants $\mathscr{K} = 0.4$, $C = 5.0$ (for a smooth wall), and the kinematic viscosity ν as well as the local free-stream velocity $U = U(x)$, the last equation determines any one of the three parameters u_τ, δ, and Π, if the other two are known. For instance, the local skin friction parameter

$$c_f = \frac{\tau_w}{\frac{\rho}{2} \cdot U(x)^2} = 2 \cdot \left(\frac{u_\tau}{U(x)}\right)^2 \tag{3.18}$$

is expressible by equation (3.17) as a two-parametric function

$$c_f = c_f\left(\delta, \Pi\right) = c_f\left(H_{1,2}, Re_{\delta_2}\right) \quad . \tag{3.19}$$

Just as we replaced here the wall shear velocity u_τ by the local skin friction parameter, one may replace also δ and Π by suitable other form parameters, as indicated in equation (3.19). The most commonly used form parameters are the thickness ratio $H_{1,2} = \delta_1/\delta_2$ and the local Reynolds number $Re_{\delta_2} = \delta_2 \cdot U(x)/\nu$ based on the momentum thickness δ_2.
Since we have derived the law-of-the-wall, equation (3.11), for the inner boundary-layer region from the mixing-length concept, one might expect that also the outer region can be adequately described by it. This is indeed possible, if one assumes the mixing length to be constant, i.e.

$$\ell = \lambda \cdot \delta \quad , \tag{3.20}$$

where $\lambda = 0.09$ is a constant. This constant mixing layer assumption was applied to the case of plane turbulent mixing layer of a uniform flow over a region of quiescent fluid by W. Tollmien [127] and by Spalding and Patankar [92]. Properly scaled, the solution for velocity distribution is almost identical with Coles wake function, giving strong support to the applicability of using the constant mixing layer concept to the outer part of the turbulent boundary layer.
Equally, it has been shown by application in boundary layer calculation methods (e.g. by Cebeci-Smith [113]), that also the use of the eddy-viscosity concept according to equation (2.8) results in an adequate representation of turbulent boundary layers. Noting from equation (2.8) and equation (2.9), that ϵ can be expressed in terms of the mixing length as

$$\epsilon = \rho\, \ell^2 \cdot \left|\frac{\partial u}{\partial y}\right| \quad , \tag{3.21}$$

this is not surprising from the discussion above on mixing length. Again the algebraic expressions for the eddy viscosity will differ in two regions of the boundary layer. For the inner wall layer, the eddy viscosity is usually taken to be that resulting from equation (3.21) with the mixing layer ℓ varying linearly with distance from the wall as given in equation (3.9), or with the Van Driest extension as given in equation (3.10). Thus, the eddy viscosity formulation for the inner region of an incompressible boundary layer is

$$\epsilon = \rho\, \mathscr{K}^2\, y^2 \cdot \left[1 - \mathrm{e}^{\left(-\frac{y \cdot u_\tau}{A \cdot \nu}\right)}\right]^2 \cdot \frac{\partial u}{\partial y} \quad . \tag{3.22}$$

For the outer region the eddy viscosity is taken to be a local constant of the form

$$\epsilon = \kappa \cdot \rho \cdot U(x) \cdot \delta_1(x) \tag{3.23}$$

where the constant $\kappa = 0.0168$, $U(x)$ and δ_1 are the local values of the free-stream velocity and the displacement thickness.

4. Boundary Layer Integral Equations

In the foregoing paragraph some aspects of the structure and general behavior of boundary layers in two-dimensional incompressible flow have been discussed. The starting point has been the system of partial differential equations, equation (2.1) and (2.2), which form the basis for the so-called direct calculation methods using some finite difference computational procedure. These methods have become feasible only through the use of high-speed computers with appreciable memory capacity. Because of the difficulty of solving partial differential equations without a computer, the methods developed earlier, especially those for airfoil boundary-layer calculations are based on the integral relationships that can be obtained from the basic equations (2.1) and (2.2). Since these so-called integral methods are, and will persist to be in use, it is proposed to briefly outline their main features.

A general way of obtaining integral relations (see e.g. Thompson [125]) is to multiply the boundary layer momentum equation, equation (2.2), by the product $u^m\, y^n$ $(m, n \in \mathbb{N}_0)$ and to integrate over the distance y from the wall to the boundary layer edge. The velocity component v is eliminated by means of the continuity equation, equation (2.1), beforehand. A doubly infinite family of ordinary differential equations (depending on the integer values for m and n) are formally obtained, called the moment-of-momentum equations. In general, only the first two members of this family are used in calculation method. Omitting all the mathematical manipulations of their derivation, these are

$$\frac{\mathrm{d}\,\delta_2}{\mathrm{d}\,x} + (H_{1,2} + 2) \cdot \frac{\delta_2}{U(x)} \cdot \frac{\mathrm{d}\,U(x)}{\mathrm{d}\,x} = c_f \tag{4.1}$$

the momentum integral equation ($m = 0$, $n = 0$) and

$$\frac{\mathrm{d}\,\delta_3}{\mathrm{d}\,x} + 3 \cdot \frac{\delta_3}{U(x)} \cdot \frac{\mathrm{d}\,U(x)}{\mathrm{d}\,x} = c_{Diss} \tag{4.2}$$

the kinetic energy integral equation ($m = 1$, $n = 0$), with the following definitions (including δ_1, from equation (3.1))

$$\delta_1 = \int_0^\infty \left(1 - \frac{u}{U(x)}\right) \mathrm{d}y \ ; \ \text{(displacement thickness)} \tag{4.3}$$

$$\delta_2 = \int_0^\infty \left(\frac{u}{U(x)}\right) \cdot \left(1 - \frac{u}{U(x)}\right) \mathrm{d}y \ ; \ \text{(momentum thickness)} \tag{4.4}$$

$$\delta_3 = \int_0^\infty \left(\frac{u}{U(x)}\right) \cdot \left[1 - \left(\frac{u}{U(x)}\right)^2\right] \mathrm{d}y \ ; \ \text{(energy thickness)} \tag{4.5}$$

$$\left.\begin{array}{ll} H_{1,2} & = \delta_1/\delta_2 \ (= H) \\ H_{3,2} & = \delta_3/\delta_2 \ (= H^\star) \end{array}\right\} \text{(shape factors or form parameters)} \tag{4.6}$$

$$c_f = \frac{\tau_w}{\frac{1}{2}\rho U(x)^2} \ \text{(skin friction coefficient)} \tag{4.7}$$

$$c_{Diss} = \frac{2}{U(x)^3} \cdot \int_0^\infty \left(\frac{\tau}{\rho}\frac{\partial u}{\partial y}\right) \mathrm{d}y \ \text{(energy dissipation coefficient)} \ . \tag{4.8}$$

With the definition of the local Reynolds number based on the momentum thickness δ_2

$$Re_{\delta_2} = \frac{\delta_2 \cdot U}{\nu} \tag{4.9}$$

the momentum integral equation (4.1) can also be written as

$$\frac{\mathrm{d}\, Re_{\delta_2}}{\mathrm{d}\, x} + (H_{1,2} + 1) \cdot \frac{Re_{\delta_2}}{U(x)} \frac{\mathrm{d}\, U(x)}{\mathrm{d}\, x} = \frac{U(x)}{v} \cdot \frac{c_f}{2} \ . \tag{4.10}$$

In the laminar case, the velocity distribution in the boundary layer can be represented by a polynomial of the form

$$\frac{u}{U(x)} = a\,\chi + b\,\chi^2 + c\,\chi^3 + d\,\chi^4 \quad \left(0 \leqslant \chi = \frac{y}{\delta} \leqslant 1\right) \ , \tag{4.11}$$

as used in the Kármán-Pohlhausen method, which when introduced into the definitions (4.3), (4.4), (4.5) and (4.7) and into the momentum integral equation (4.1) finally results in the single ordinary differential equation

$$\frac{\mathrm{d}\ (\delta_2^2/v)}{\mathrm{d}\, x} = \frac{1}{U(x)} \cdot F(\kappa) \ , \tag{4.12}$$

which can be solved for a given free-stream velocity distribution $U(x)$. In equation (4.12) $F(\kappa)$ is an algebraic function, sometimes called the auxiliary function. A linear approximation for this function is

$$F(\kappa) = a - b \cdot \kappa \quad (a = 0.47, \ \ b = 6) \ , \tag{4.13}$$

which, when inserted into equation (4.12), allows a simple quadrature giving the well-known formula

$$\delta_2^2(x) = \frac{0.47 \cdot v}{U(x)^6} \cdot \int_{x=0}^{x} U(x)^5 \mathrm{d}x \tag{4.14}$$

applicable for the approximate calculation of laminar boundary layers.
The reason for reviewing this Kármán-Pohlhausen laminar method (for details see H. Schlichting [106]) is, to point out that the momentum integral equation (4.1) can be solved with the help of one additional auxiliary function $F(\kappa)$, the argument κ of which can easily be represented as a function of $H_{1,2}$ and c_f. This pattern for a solution procedure is seen to be followed in almost all integral methods, also in the turbulent case. However, the auxiliary relation needed, is usually not an algebraic function but an ordinary differential equation of the form

$$\delta_2 \cdot \frac{\mathrm{d}H_{1,2}}{\mathrm{d}x} = f_1\left(H_{1,2}, Re_{\delta_2}, \frac{\delta_2}{U(x)} \cdot \frac{\mathrm{d}U(x)}{\mathrm{d}x}\right) \ . \tag{4.15}$$

An equation of this kind will account for the second term in equation (4.1). The only unknown left then is the local skin friction coefficient c_f. Fortunately, this can be related to the local velocity profile quite accurately by means of a relationship of the general form

$$f_2\left(c_f, Re_{\delta_2}\right) = 0 \ , \tag{4.16}$$

of which equation (3.17) in connection with the standard turbulent two-layer model would be an example. Other well-known examples are the empirical skin-friction formulae by Ludwieg and Tillmann [73]

$$c_f - 0.246 \cdot 10^{-0.678 \cdot H_{1,2}} \cdot \left(Re_{\delta_2}\right)^{-0.268} = 0 \tag{4.17}$$

and by Squire and Young [119]

$$c_f - 0.0576 \cdot \left[\log\left(4.075 \cdot Re_{\delta_2}\right)\right]^{-2} = 0 \ . \tag{4.18}$$

Note, that in the last formula any dependence of c_f on $H_{1,2}$ is neglected, which will lead to too large values of c_f near separation of the boundary layer.
The auxiliary equation of the type of equation (4.15) need not have $H_{1,2}$ as the main dependent variable. There are other shape factors in use such as the energy thickness ratio $H_{3,2}$ defined by (4.6). If $H_{3,2}$ is to be used, then the auxiliary equation is derived from equation (4.2) for the integral mean kinetic energy. This approach seems to have been particularly favored by German research workers such as Truckenbrodt [128], Walz [133], and Rotta [103]. By combining equation (4.2) with equation (4.1), the appropriate auxiliary equation is obtained in the form

$$\delta_2 \cdot \frac{\mathrm{d}H_{3,2}}{\mathrm{d}x} = \left(H_{1,2} - 1\right) \cdot H_{3,2} \cdot \frac{\delta_2}{U(x)} \frac{\mathrm{d}U(x)}{\mathrm{d}x} + c_{Diss} - \frac{1}{2} H_{3,2} \cdot c_f \ , \tag{4.19}$$

where for the dissipation coefficient c_{Diss}, defined in (4.8), different empirically established relations can be used. An early suggestion by Truckenbrodt [128] is

$$c_{Diss} = 0.0112 \cdot (Re_{\delta_2})^{\frac{1}{6}} \quad . \tag{4.20}$$

It is based on the evaluation of a number of non-equilibrium boundary layers. A more refined relation is one which can be derived from equations (4.1) and (4.2) assuming the magnitude of $H_{3,2}$ to be independent of x (see Rotta [104]).

$$c_{Diss} = \frac{1}{2} c_f \cdot H_{3,2} \cdot \left(1 + \frac{H_{1,2} - 1}{H_{1,2}} \cdot \Gamma\right) \quad . \tag{4.21}$$

Here, Γ the so-called equilibrium parameter and is implicitly related to $H_{1,2}$ by a formula suggested by Nash [84]

$$\frac{H_{1,2} - 1}{H_{1,2} \cdot \sqrt{c_f/2}} = 6.1 \cdot \sqrt{\Gamma + 1.81} - 1.7 \ . \tag{4.22}$$

Using equation (4.17) for c_f, c_{Diss} can be calculated as a function of $H_{1,2}$ and Re_{δ_2}, thus completing the system of the two ordinary differential equations, equations (4.1) and (4.19), which then can be solved simultaneously by a Runge-Kutta procedure delivering as output all interesting boundary layer parameters such as c_f and δ_1.
Another relatively modern approach is that introduced by Head [56] in his famous entrainment method. Head departs from the continuity equation (2.1) which on integration over y from $y = 0$ to $y = \delta$ and using the definition for displacement thickness, equation (4.3), gives

$$\frac{\mathrm{d}}{\mathrm{d}\,x} \left[U(x) \cdot (\delta - \delta_1)\right] = v_e = U(x) \cdot c_E\,(H_1) \tag{4.23}$$

where v_e is the normal velocity (in y-direction) at the nominal outer edge of the boundary layer, also called the entrainment rate, and H_1 is a new form parameter defined as

$$H_1 := \frac{\delta - \delta_1}{\delta_2} \quad . \tag{4.24}$$

The physical interpretation of equation (4.23) is, that the mass flow in the turbulent boundary layer is a function of the large scale eddies, characterized by the length scale $\delta - \delta_1$ referenced to the momentum thickness δ_2. The form parameter H_1 is correlated to the usual form parameter $H_{1,2}$ by the empirical relationship

$$H_1 = 1.535 \cdot (H_{1,2} - 0.7)^{-2.715} + 3.3 \ , \tag{4.25}$$

while the functional form of the entrainment rate coefficient c_E is taken to be

$$c_E = 0.0306 \cdot (H_1 - 3)^{-0.653} \quad . \tag{4.26}$$

Both, equation (4.25) and (4.26) are curve fits of Head's original charts for c_E and H_1 as gained from experiments. It is interesting to note, that the entrainment equation (4.23)

can be brought into the general form of the auxiliary equation (4.15) giving, with the help of equation (4.1),

$$\delta_2 \cdot \frac{\mathrm{d}\, H_{1,2}}{\mathrm{d}\, x} = U(x) \cdot \frac{\mathrm{d}\, H_{1,2}}{\mathrm{d}\, H_1} \cdot c_E - H_1 \cdot \frac{1}{U(x)} \frac{\mathrm{d}}{\mathrm{d}\, x} \cdot (U(x) \cdot \delta_2) \quad . \tag{4.27}$$

With Head's method, very good results are obtained for airfoil-type boundary-layer flows predicting also separation quite well. The method was improved more recently by Head and Patel [57], whereby the development of $H_{1,2}$ with x conforms better to flows with high shear stress, i.e. high entrainment rates and to decelerating flows in strong adverse pressure gradients.

The integral methods mentioned so far are all based on empirical relationships between local quantities at one given station x, taking account of the upstream history only through the auxiliary equation which physically provides a measure for the deformation of the velocity profile as it develops with x. Turbulence properties enter the equation only through empirical information on the skin friction, for example equation (4.17) and (4.18), and the dissipation coefficient, (4.21) and (4.22). These are connected to local mean flow properties. From what has been discussed in the previous chapter on the need for using the turbulence transport equations in order to adequately describe the history effects, when using complete (differential) methods, it appears necessary to also incorporate turbulence transport equations in integral methods.

This has been attempted by several authors, e.g. McDonald and Camarata [52], Hirst and Reynolds [60] with the most recent development, I know of, by J. E. Green et al. [52]. All these methods start out by considering the transport equation for turbulent kinetic energy, equation (3.5), to gain an additional ordinary differential equation that will describe the streamwise change of the turbulent shear stress. The approach to achieve this, however, is quite different for the references just quoted. In [76], the turbulent kinetic energy transport equation is used in an integrated form, yielding an equation which governs the variation of the mixing-length distribution in the x-wise direction. The two other integral equations used are the momentum integral equation, equation (4.1) and a y-moment-of-momentum integral equation ($m = 0, n = 1$).

Hirst and Reynolds [60] also use the integral turbulent kinetic energy equation as a starting point and, by an assessment of the relative importance of the terms contained in it, arrive at a relatively simple equation for the turbulent energy balance in the outer region of the boundary layer, i.e. balance between the net downstream convection of turbulent energy and the turbulent energy locally supplied to the outer layer from the inner region near the wall,

$$\frac{\mathrm{d}}{\mathrm{d}\, x} \left(\frac{1}{2}\, Q^2 \cdot I \right) = const. \cdot u_\tau \cdot Q^2 \tag{4.28}$$

where the integral quantities Q and I are defined as

$$Q^2 = \frac{1}{I} \cdot \int_0^\delta u\, \overline{q'^2}\, \mathrm{d}\, y \quad , \tag{4.29}$$

and

$$I = \int_0^\delta u \, \mathrm{d}\, y = U(x) \cdot (\delta - \delta_1) \quad . \tag{4.30}$$

By postulating that the entrainment rate $v_e = \mathrm{d}\, I / \mathrm{d}\, x$ according to equation (4.23) is linearly related to the square root of the turbulent kinetic energy, an ordinary differential equation for the entrainment rate is obtained from equation (4.28)

$$\frac{\mathrm{d}}{\mathrm{d}\, x} \left(\frac{v_e^2}{2} \cdot I \right) = K_1 \cdot u_\tau \cdot v_e^2 \tag{4.31}$$

where $K_1 = 0.14$ is an empirical constant. Thus this "turbulence model equation", equation (4.31), the entrainment equation, equation (4.23), and the momentum integral equation (4.1) together with equation (3.17) as a matching condition, form the system of ordinary differential equations to be solved.
In the new method of Green et al. [52] consideration of the turbulent kinetic energy equation starts out from its differential form as used originally by Bradshaw, Ferris and Atwell [19] in their famous finite difference method. By again assessing all terms, an ordinary differential equation for the maximum shear stress occurring within the boundary layer is derived. By invoking also a universal relationship between the c_f-value of this maximum shear stress and c_E, an ordinary differential equation is obtained

$$\delta_2 \cdot (H_1 - H_{1,2}) \cdot \frac{\mathrm{d}\, c_E}{\mathrm{d}\, x} = F \left(c_E \, , c_f \, , \frac{\delta_2}{U(x)} \, , \frac{\mathrm{d}\, U(x)}{\mathrm{d}\, x} \right) \tag{4.32}$$

called the "lag equation" which is a rate equation for the entrainment coefficient c_E. The use of equation (4.32) requires some additional empirical relations for H_1 as a function of $H_{1,2}$ and c_f as function of the friction coefficient $c_{f,0}$ for the flat plate boundary layer as well as some empirical formulae for the equilibrium values of c_E and $(\delta_2 / U(x) \cdot \mathrm{d}\, U(x) / \mathrm{d}\, x)$. The joint solution then of the momentum integral equation (4.1), the entrainment equation in the form of equation (4.27) and the above lag equation (4.32) completely determines the development of the boundary layer. This method was extended to wakes which seems to make the method especially attractive for the aircraft aerodynamicist. Green's report [52] also contains the complete scheme of the calculation procedure for the compressible case.
Another assumption to include the history effect is due to Rotta [104]. The reasoning is, that the dissipation coefficient c_{Diss}, needed in the energy integral equation (4.2) when this is used as the auxiliary equation, does not immediately react to changes of the turbulent velocity profile and of the pressure gradient. To account for this relaxation effect, c_{Diss} as calculated at station x is considered to be the effective value for the downstream station $x + \Delta x$. The lag length Δx is assumed to be four times the local boundary-layer thickness δ. This assumption is plausible in as far as this distance corresponds roughly to the decay length of a turbulent eddy. Substantial improvement could be achieved by this simple principle.

5. Classification of Calculation Methods

From the discussion in the preceding section, a classification on the existing boundary layer calculation methods can be inferred. **Table 5.1** summarizes schematically the procedure for a boundary layer calculation. The problem at hand must be properly defined: (i) by the general flow characteristics, i.e. the undisturbed free-stream velocity and the Reynolds number based on a characteristic length scale, (ii) by the initial conditions for a wall surface point from which the calculation is to be started, and (iii) by the boundary conditions, the most important of which is the given velocity or pressure distribution at the outer edge of the boundary layer as obtained by potential theory. The desired result is the determination of all boundary layer parameters, as indicated, of which, from the engineering point of view, the skin friction coefficient $c_f(x)$ and the displacement thickness $\delta_1(x)$ are the most important ones. Equally important is the prediction of the locations of the transition point x_t and the separation point x_s, which may be laminar or turbulent.

In order to perform a boundary layer calculation, one must decide on the calculation method to be used. A gross criterion for distinction between the calculation methods is given by the mathematical solution procedure, i.e. wether one uses a so-called Complete Field Method or an Integral Method. The former involves the numerical solution of the partial differential equation for continuity and momentum directly while the latter embraces the numerical solution of ordinary differential equations for the momentum integral and some suitable form parameter. In laminar boundary-layer calculations, the direct methods need no further input since the stress term $\partial\tau/\partial y$ is uniquely defined by Newtons law $\tau = \eta \cdot (\partial u/\partial y)$. In Integral methods, however, some empirical information on the velocity profiles to be inserted and the laminar wall shear stress τ_w is needed usually being supplied from local similarity conditions as obtained from exact laminar solutions. For turbulent boundary layers, both methods need empirical input concerning the turbulent or Reynolds shear stress in the direct methods and concerning the skin friction coefficient, the energy dissipation integral, and the entrainment coefficient in the integral methods.

As has been pointed out previously, a second distinction between methods may be made by asking wether this empirical information is obtained from consideration of mean field quantities or from consideration of the turbulence quantities. This criterion will then again divide each type of methods (complete or integral) into two branches. For the complete methods **table 5.2** indicates this distinction. Eddy viscosity and mixing length methods normally are based on empirical expressions for ϵ and ℓ, in which mean field quantities such as the derivatives of the mean velocity are appearing (see equations

Problem definition: (Input)	Generell flow characteristics $U(x)_\infty$, $\mathscr{L}$, ν, Re	Initial conditions at $x = x_0$ $u = u(y)$; δ, δ_1, δ_2, $H_{1,2}$	Boundary conditions at $y = 0$: $u = v = 0$, at $y = \delta$: $U(x)$ or $p(x)$
Result (Output)	(i) Solution at all $x > x_0$ for: velocity profile $u(x, y)$ boundary Layer thickness: δ, δ_1, δ_2, δ_3 skin friction: c_f form parameters: $H_{1,2}$, $H_{3,2}$	(ii) Prediction of Transition point x_t or transition-zone: laminar separation point: $x_{l,s}$ turbulent separation point: $x_{t,s}$ $\Rightarrow$ both, if existent	
Solution Procedure	Complete Field Methods:	Integral Methods:	
Mathematics	Numerical solution of the partial differential equations for continuity and momentum	Numerical solution of coupled ordinary differential equations for momentum integral and appropriate form-parameters	
Physics on	Reynolds stress $-\rho \cdot \overline{u' v'}$	Skin friction c_f energy dissipation integral c_{Diss} entrainment c_E	

Table 5.1.
Boundary Layer calculation scheme

Mathematics	Numerical solution of the partial differential equations of continuity and momentum by finite difference procedures			
Physics	Derivation of the Reynolds shear stress $-\rho \cdot \overline{u' v'}$ coupled to characteristics of the			
	Mean flow field. Reynolds stress determined by empirical algebraic relations for		Turbulence field. Reynolds stress determined from differential transport equations for	
	eddy viscosity	mixing length	eddy viscosity	turbulent kinetic energy
Assumptions	$-\rho \cdot \overline{u' v'} = \underline{\epsilon} \cdot \frac{\partial u}{\partial y}$ $\epsilon = \epsilon(y)$ at $x = \text{const.}$	$-\rho \cdot \overline{u' v'} = \rho\, \underline{\ell}^2 \cdot \left(\frac{\partial u}{\partial y}\right)^2$	$\underline{\epsilon} = \epsilon(x, y)$	$-\rho \cdot \overline{u' v'} = \mathbf{k} \cdot \underline{\overline{q'^2}}$ or $-\rho \cdot \overline{u' v'} = \mathbf{k} \cdot \sqrt{\underline{\overline{q'^2}} \cdot \ell}\, \frac{\partial u}{\partial y}$
Authors (representative)	Mellor-Herring [78] Spalding-Patankar [92] Cebeci-Smith [113]		Nee-Kovasznay [89]	Bradshaw-Ferris [19] Beckwith-Bushnell [10]

Table 5.2.
Complete Field Methods

(3.13) and (3.22), (3.23)). The second group of complete methods utilizes turbulence transport equations for the determination of the Reynolds stress. Transport equations may be formulated for eddy viscosity ϵ as for example in the Nee-Kovasznay method or, more usually for the turbulent kinetic energy $\overline{q'^2}$ which then necessitates a postulated relation connecting this quantity to the Reynolds stress. Two such relations are stated in **table 5.2**. The last row of the table lists the origin of some methods representative for the different treatment.

In **table 5.3** a tentative survey on the integral methods is made. The empirical input concerning the physics of turbulence consists of correlation function for the skin friction coefficient c_f, the integral energy dissipation coefficient c_{Diss}, and for the entrainment coefficient c_E. Furthermore, an auxiliary ordinary differential equation for the development of a typical form parameter H is needed, the functional form of which depends on the empirically based correlations between the pressure gradient parameter $(\delta_2/U(x))\,(\mathrm{d}U(x)/\mathrm{d}x)$, the form parameter H being considered, the local Reynolds number Re_{δ_2}, and one at the coefficients c_f, c_{Diss} or c_E. One nay now make a distinction between methods in which all correlation functions used in the auxiliary equation are developed from mean flow integral equations or from equations for a turbulent property. Thus, if the integral energy equation is used, this involves assumptions on the functional relationship of the dissipation coefficient c_{Diss} with the form parameter $H_{3,2}$, while with integrated continuity equation an assumption for the functional relationship between the entrainment rate c_E and the form parameter H_1 is needed. In this category of methods are also included those methods which utilize integrated forms of higher moments-of-

<table>
<tr><td>Mathematics</td><td colspan="4">Numerical solution of coupled ordinary differential equations for the momentum integral and one or more form parameters</td></tr>
<tr><td>Physics</td><td colspan="4">(i) Correlations between integral properties:
$c_f = c_f\,(H_{1,2}, Re_{\delta_2})\,;\;\; c_{Diss} = c_{Diss}\,(c_f, H_{3,2})\,;\;\; c_E = c_E\,(c_f, H_1)$;
(ii) Auxiliary differential equations for form parameter H:
$\delta_2 \cdot \frac{\mathrm{d}H}{\mathrm{d}x} = F\left(\frac{\delta_2}{U(x)}\frac{\mathrm{d}U(x)}{\mathrm{d}x}, H, Re_{\delta_2}, c_\varsigma\right)$
where: $H = H_{1,2}$, $H_{3,2}$, H_1 and $c_\varsigma = c_f$, c_{Diss}, c_E</td></tr>
<tr><td>Auxiliary equation developed from</td><td colspan="2">mean flow integral equation for
energy | entrainment</td><td>moment of momentum</td><td>turbulent property equations for kinetic energy</td></tr>
<tr><td>Assumptions concerning</td><td>c_{Diss}</td><td>c_E</td><td>$c_f\,(\epsilon \text{ or } \ell)$
$c_{Diss}\,(\epsilon \text{ or } \ell)$</td><td>$\overline{q'^2}$, ϵ_d, c_{Diss}, c_E
(history effects from the turbulence field)</td></tr>
<tr><td>Authors (representative)</td><td>Truckenbrodt [128]
Rotta [104]
Walz-Geropp-Felsch [36]
Alber [6]
Zwarts [141]</td><td>Head-Patel [57]
Michel-Quémard [80]</td><td>Nash-Hicks [86]
Herring-Mellor [78]</td><td>McDonald [76]
Hirst-Reynolds [60]
Green et al. [52]</td></tr>
</table>

Table 5.3.
Integral Methods

momentum, where it is possible to incorporate algebraic formulae for eddy viscosity or mixing length into the functional form of the integral coefficient under consideration, e.g. the shear stress integral and the energy dissipation integral. The second group of integral methods relies on true turbulence property equations, i.e. mostly the transport equation for turbulent kinetic energy. From it, a third ordinary differential equation is developed which will provide for the dissipation coefficient or entrainment coefficient needed in the auxiliary equation and the basic momentum integral equation.
The distinction between integral methods based on mean flow integral equations and on turbulent property relations is not so clearcut as for the direct methods. Thus, some of the moment-of-momentum methods, e.g. McDonald and Camarata [76], employ a differential equation of the turbulence as a basis to account for history effects in a similar way as for the methods of Hirst-Reynolds [60] and Green et al. [52]. Much more information on the classification of boundary layer calculation methods are given in the papers by W. C. Reynolds [99], P. Bradshaw [16, 17], and Launder and Spalding [69].

6. Examples of Boundary-Layer Calculations

When looking for comparative calculations in the literature, it is not easy to find examples where the computations were performed with several different methods for the same flow configuration except for the extensive comparisons made at the Stanford conference [2,3] for incompressible turbulent boundary layers. Therefore it is proposed to show two examples from this source for two cases where the experimental pressure distributions resemble those for the suction side of an airfoil.
The first example is that for the flow around an elliptical airfoil-like section of Schubauer and Klebanoff [109], where the pressure gradient first is negative, then strongly positive with eventual separation as seen in **figure A.14**. This figure shows the result of computations by the competitive methods. The first column gives the development of the form parameter $H_{1,2}$, the second contains the local skin-friction curve c_f, and the third is for the local momentum thickness Reynolds number Re_{δ_2}. The dots represent the corresponding measurement. It is seen, that virtually all methods predict these boundary-layer characteristics very well up to the point of maximum velocity (at about $x = 18$ ft) but that deviations begin to show quite distinctly in the strong adverse pressure gradient region up to the separation point which lies at about x_s ft. On the left I have marked the different methods according to the category which they belong to, with the additional marking of those methods that were rated first-class at Stanford. From this comparison, no general superiority of any of the three types of methods can be deduced. Note, however, the consistently good prediction of all three parameters as computed by the complete field method of Bradshaw and Ferris [19]. This is attributable to the fact, that they have accounted for three-dimensional effects, i.e. the convergence of the flow as it approaches separation. Also allowance has been made in the Bradshaw-Ferris calculations of longitudinal curvature effects. It is therefore not surprising that most of the other methods, which were applied to this case without these corrections could not predict the boundary-layer development in the adverse pressure gradient region as well. In order to show that also an integral method is capable of taking account of convergence and curvature effects, let us look on the results of test calculations from Green's new lag entrainment method [52] for the same example. **figure A.15** reflects the predictions assuming two-dimensionality by the solid line. The dotted line shows the effect of allowing for flow convergence in such a way that the Re_{δ_2}-curve is forced to match the experimental data. The effect on $H_{1,2}$ and c_f then is to halve the discrepancy between the previously calculated and measured values. The further allowance for longitudinal curvature then will again improve the calculations considerably, so that even the separation point is predicted satisfactorily. The conclusions are (i) that an integral

method such as Green's is not inferior to a complete field method if it is capable of handling secondary effects, (ii) that on the other hand a good method should possess the built-in capability to allow for such secondary effects in order to be able to judge from the results of comparative calculations on the possible deviations from a nominally two-dimensional experiment.
The second example is on the experiment of Schubauer and Spangenberg [110] the velocity-distribution of which is shown at the top of **figure A.16**. This is a case of a severely retarded flow in which the slope of the adverse pressure gradient increases with x as occurs typically on the upper side of a lifting airfoil. **Figure A.16** again gives the result from Stanford, where not all competitors have run this case which was not mandatory. Most of the methods again performed very well with the integral methods of Rotta (RO) and Walz (FG) not being in any way inferior to the complete methods like that of Herring and Mellor (HM2) or Spalding-Patankar (NP). These methods predict the incipient separation equally well and in accordance with experiment. The representation of Green's lag entrainment results in **figure A.17** reveals that the history effect on the development of turbulence structure does have an influence when comparison is made to the results of Head's method without the lag equation used by Green.
In the light of the conclusions drawn in the introduction concerning the importance of being able to predict the separation point accurately, it is appropriate to show some comparisons gained from different methods. I have found this comparison in the paper by Cebeci et al. [21] from which **figure A.18** is taken. It shows the predicted separa-tion points for the experimental pressure distribution on a NACA 66.2-420 airfoil at various angles of attack. The experimental separation points are to be inferred as the point, where the velocity levels off to the horizontal constant value after the step descent. The best prediction quality then is to be attributed to those methods which come closest to this point. Of the new methods, those of Head and Cebeci-Smith are the most satisfactory ones under this criterion, while the older methods of Stratford [121] and Goldschmied [47] predict separation too early. Here again the competition between a complete method (Cebeci-Smith) and an integral method (Head) is undecided. This example together with the foregoing examples, where also separation was present, show that with the best methods available at present turbulent separation can be predicted with confident accuracy.
As to the prediction of transition, the situation is not as encouraging. Although the qualitative nature of the transition process for low-speed boundary layers remaining attached is known, no sure criteria have yet been developed for the onset and the streamwise extent of the transition region. However, with some of the presently available boundary layer methods remarkable success is achieved for the development of boundary-layer characteristics, especially the skin friction coefficient if the point of onset and length of transition region are assumed known. **Figure A.19** gives an example of calculations through the transition region by McDonald and Fish [55] performed with a complete finite difference method. The method uses the turbulent kinetic energy transport equation which essentially provides the development and change of an effective viscosity to be used in the simultaneous solution of the differential boundary-layer equations. By inserting a small but nonzero value of the free-stream turbulence level (which is the pa-

rameter to the curves in **figure A.18** into the energy-transport equation, the increasing production of turbulent shear stress is triggered and followed up to the point of fully turbulent flow. In **figure A.20** the comparison between measurement and calculated prediction of the development of the shape parameter $H_{1,2}$ and the momentum thickness δ_2 is made for a transitional boundary layer. The agreement is very good. This is an encouraging example of how the modern boundary-layer methods are able to tackle the difficult problem of transition, provided that there is some additional information for its onset and extent. A similar method was proposed by Harris [21].

7. Compressible Boundary Layers

Modern aircraft are operating in a Mach number range extending up to $Ma = 3$, if we disregard the designs for space crafts such as the space shuttle. Special importance is directed to the high subsonic Mach number range representing the cruising speed of modern transport aircraft. Consequently, also the boundary layer under these conditions including boundary layer shock-wave interaction must be taken into account. Not attempting to be complete at all, I propose to describe in this paragraph some of the phenomena and effects which will influence or change the behavior of boundary layers in compressible flow as distinct from the incompressible case and to indicate in which way boundary layer calculation methods are extended to incorporate these compressibility effects.

In laminar compressible boundary layers, the main sources for deviation from the incompressible behavior are the generation of heat by viscous shear stresses (i.e. dissipation) as the velocity gradients increase with Mach number, leading to temperature gradients. Also the temperatures in the free stream at the boundary-layer edge and at the wall surface with or without heat transfer differ in general, giving rise to heat transport across the boundary layer in addition to the convection heat transport. Furthermore, the density of the fluid will vary appreciably across the boundary layer according to the thermodynamic state. Density and temperature variations will lead to a variation also of the molecular viscosity. So, besides the velocity boundary layer, there will be a thermal boundary layer, if either the main stream temperature differs from the temperature of the wall or / and if there is a significant amount of dissipation in the velocity boundary layer. Compared with incompressible flow, at least four additional quantities must be taken into account in the calculation of compressible boundary layers: the Mach number as a measure of compressibility and frictional heat, the Prandtl number as a measure of the diffusion (or transport) of heat, viscosity change with temperature, and heat transfer across the wall, determining the temperature distribution along the wall. Accordingly, all phenomena known from the behavior of the incompressible boundary layer will be affected in one or the other way, the main effects being: (i) The temperature increase towards the wall, as occurs with adiabatic surfaces (no heat transfer) thickens the boundary layer, leading to a decrease of skin friction coefficients with Mach number. (ii) In flows with heat transfer to the wall, the heat transfer coefficient is also reduced with Mach number. (iii) The reduction of skin friction enhances separation. (iv) Laminar compressible boundary layers are less stable, i.e. transition Reynolds number from laminar to turbulent decreases with Mach number up to $Ma = 3.5$. Wall cooling on the other hand stabilizes the boundary layer again and delays transition.

As to calculation procedures for the laminar compressible boundary layer, there are powerful methods in existence of the complete field type by which the full nonlinear par-

tial differential equations can be solved by finite difference techniques. These methods are devised to include foreign gas injection and chemical reaction of several gas species present in a high-temperature laminar boundary layer. A review on these methods was given by Blottner [13]. But also the integral method have been developed to a satisfactory degree of accuracy for engineering purpose, e.g. by Geropp (see Walz [133]).
A third type of method which has proven to be very powerful for incompressible and compressible laminar boundary layer calculations is the so-called GKD method (Galerkin-Kantorovich-Dorotnitzyn) also known as the multimoment method or the method of integral relations. This method is a generalization of the Kármán-Pohlhausen method, but instead of using only the one integral equation for momentum, equation (4.1), many moment-of-momentum equations are solved simultaneously. Representative for this type of boundary-layer method is the work of Abbott and Bethel [4] for incompressible laminar boundary layers and of Nielsen et al. [48] for compressible laminar boundary layers. A specially useful feature of the GKD-methods for laminar boundary layers is the fact, that they are able to compute formally past the laminar separation point, while with finite difference methods this, in general, cannot be achieved. In summarizing then, it may be safely stated that for the calculation of laminar compressible boundary layers a number of sufficiently accurate methods are at our disposal. In view of the application to two-dimensional boundary layers over airfoil sections, the calculation of the laminar portion does not seem to become a critical problem except for the prediction of transition from laminar to turbulent.
For turbulent compressible boundary layers, the effect of Mach number on the general behavior qualitatively follows that of laminar boundary layer at least in the high subsonic to moderately supersonic Mach number range considered here. Regarding external turbulent boundary layers on typical aerodynamic shapes, both skin friction and heat transfer coefficients decrease with Mach number. The effort or the various empirical techniques to account for compressibility effects in turbulent boundary layers were directed to give quantitative predictions of skin friction and heat transfer by introducing suitable parameters such as the wall-to-free stream temperature ratio. Quite good correlation formulae for skin friction due to Wilson [139] and Van Driest [129] and for heat transfer due to Spalding and Chi [116] were developed in this way. In the light of the modern methods for turbulent boundary-layer methods, however, this parametric approach must be valued as an attempt to circumvent the actual solution of the turbulent boundary-layer equations and the consideration of the turbulence characteristics.
The main effect of Mach number and the accompanying heating on the turbulence structure is the additional appearance of temperature and pressure fluctuations which produce density fluctuations, so that there is a strong interaction between the velocity and temperature distribution. Consequently the fluctuating part of pressure, temperature and density enter the boundary layer equations which of course must be augmented by the energy equation usually written as an equation for temperature or total enthalpy. Without going into any details of the derivation of these equations, let me point out the most important results regarding the incorporation of compressibility effects into them. For Mach numbers below about $Ma = 5$, Morkovin's hypothesis [81] holds, which says that the density fluctuations to the mean density are small and that therefore the

turbulence structure is not influenced, being the same as in incompressible boundary layer. This means, that compressibility does not affect the functional form of the usual incompressible models of the turbulent eddy viscosity and mixing length as also shown by Maise and McDonald [75]. Consequently, these concepts are extensively used in calculation methods of complete field type, the model of eddy viscosity ϵ for the momentum transport $\left(-\rho \cdot \overline{u'\,v'} = \epsilon \cdot \frac{\partial u}{\partial y}\right)$ being analogously applied to define a thermal eddy conductivity λ_T, in order to treat the term $-\rho \cdot \overline{v'\,H'} = (\lambda_T/\epsilon_{Diss}) \cdot \left(\frac{\partial H}{\partial y}\right)$, and an effective turbulent Prandtl number $Pr_t = c_P \cdot \epsilon/\lambda_T$, usually assumed to be constant and equal to unity. Also the integral methods are extended to compressible boundary layers in which however even more empiricism concerning the relationships between the various form parameters, the skin friction coefficient and the energy dissipation coefficient are needed. Recent reviews of compressible methods were given by Beckwith [9] and by Peake et al. [94].

As an example of the capability of calculation methods for the prediction of a boundary layer in compressible flow, the results of the experiment of Winter et al. [140] for high speed flow over a waisted body of revolution are compared first with the results of the field method of Herring and Mellor [58] and second with those found by the compressible version of the integral lag entrainment method of Green et al. [52]. **Figure A.21** shows the flow situation and the measured pressure distributions for two different free-stream Mach numbers. In **figure A.22** is shown the skin friction and momentum thickness distributions as calculated by the field method of Herring and Mellor, which are compared with the measured data obtained by surface pitot tubes. **Figure A.23** presents the result of Green's calculations in a plot with different scales. Shown here are also the results as obtained with Head's method and the curves for which corrections for curvature, lateral strain and dilatation were made. Such secondary effects are provided for in Green's lag entrainment method. These comparisons show, that both field and integral methods will produce good to fairly good agreement with measurements. None of the two methods can be said to be superior to the other, except may be for the shorter computer time in Green's integral method.

In connection with high subsonic Mach number flows, of course, the appearance of shocks brings about a new situation for boundary layer calculation capabilities. In aircraft aerodynamics, the most important example of shock and boundary-layer interaction occurs on transonic airfoils or wings. It will be shown in section 9.4 in which way boundary layer calculations through the interaction region below a normal shock on an airfoil serves as a means of predicting buffet onset on a wing. A deeper insight into the general problem of interaction between shock waves and boundary layers may be gained from the review article of Green [51].

8. Three-Dimensional Boundary Layers

From the aircraft aerodynamicist's point of view, the interest for calculating three-dimensional boundary layers is prompted by the need for more accurate predictions of skin friction drag than are possible by the conventional application of the flat plate estimate. For instance, the drag of a swept wing may be in serious error because of the neglect of three-dimensional flow effects on the development of the boundary layer. In the mid semispan of a swept wing, the actual boundary layer "run" is longer than the geometric chord because the inviscid flow above the surface follows a curved path. In addition, as the boundary layer looses energy, the spanwise pressure gradient causes it to drift outboard thus further increasing the "run". Therefore, the boundary layer near the trailing edge of swept wings is significantly thicker than on a two-dimensional section, in general, thereby increasing also the pressure drag by interaction with the inviscid flow. Also the three-dimensional separation characteristics on a swept wing are totally different from their two-dimensional counterpart. Of course, also the flow over the fuselage is three-dimensional and the determination of its drag should strictly be based on calculations of the three-dimensional boundary layer instead of by the method for equivalent bodies of revolution.
When speaking of three-dimensional boundary layers, it is again assumed that they are defined as being the thin layer next to the surface of the body to which the viscous effects of the flow are confined. The inviscid main-stream flow in a three-dimensional case will depend on all three space coordinates, one of which may be envisaged to be the normal to the surface at every surface point, so that within the boundary layer approximation the pressure variation along these normals can be ignored. Two effects are immediately apparent, which were absent in the two-dimensional case. The first is due to lateral convergence or divergence of the three-dimensional main flow streamlines parallel to the surface and the second is introduced by the curvature of these streamlines. While streamline convergence (or divergence) results in a change in boundary-layer thickness different from the two-dimensional development, the lateral curvature of the outer streamlines gives rise to a secondary flow in the boundary layer also called the cross-flow. It is defined as the component of velocity parallel to the surface but perpendicular to the inviscid outer streamline. This effect is qualitatively well understood in being the consequence of the full lateral pressure gradient acting on the fluid of reduced velocity within the boundary layer, causing the boundary layer fluid to evade towards the concave side of the potential streamlines. The full complexity of three-dimensional boundary layer flow reveals itself when it comes to separation, two typical examples of which are depicted in **figure A.24**. Sketch ⓐ represents the case where a "bubble" is formed inside of which fluid is carried along with the body. Only at the singular point S

the behavior of two-dimensional separation zero-wall-shear stress is seen to exist while the confluent wall shear stress lines (or wall "stream lines") forming the curved line of separation, suggest that the wall shear stress along this line is nonzero. Sketch ⓑ shows the formation of a free shear layer due to confluent wall stream lines. The extent of the viscous region, attached or free, is indicated by the shaded projected areas. In sketch ⓒ the situation of case ⓑ is illustrated for the flow over a yawed or swept wing with three-dimensional separation. These examples show, that the concepts of boundary-layer theory may be applicable upstream of and away from separation lines but that in the vicinity of separation they may not be adequate.

At present, the calculation methods for three-dimensional boundary layers is in a state of vigorous development. Recent reviews have been given by Eichelbrenner [32], Nash and Patel [88] and Wheeler and Johnston [136, 137], Horlock et al. [61] and Fernholz [37]. A paper on the numerical treatment of three-dimensional boundary-layer problems was presented at an AGARD-VKI (**A**dvisory **G**roup for **A**erospace **R**esearch and **D**evelopment-**V**on **K**ármán **I**nstitute) short course by Krause [65], which includes a large bibliography. For the laminar case, methods of the finite-difference type have been successfully applied to a number of flows including the laminar three-dimensional boundary layer at the forward stagnation point of an ellipsoid and the flow along the leading edge of an infinite swept wing. It may be noted that these numerical methods are not restricted to boundary layers with small cross-flow or small spanwise pressure gradients. Also the problem of transition in three-dimensional boundary layers has been considered by Hirschel [59]. As to the methods for calculating three-dimensional turbulent boundary layers, these may again be divided into complete or integral methods. The complete methods developed so far are extensions either of finite difference methods for laminar boundary layers with the inclusion of a suitable expression for the Reynolds shear stress or of established two-dimensional turbulent methods. With a lateral velocity component present, the Reynolds shear stress must now be considered as a vectorial quantity. The eddy-viscosity or mixing length concept are again utilized, e.g. in [30,35,66], with special assumptions regarding their functional form for the two components of the local flow direction. Other methods [15, 85, 135] use the turbulent energy equation in the vector form as proposed by Bradshaw [15]. However, the predictive quality of these complete field methods depends critically on the assumptions on the lateral shear stress component, especially close to the wall by which the local flow angle will be determined.

The situation seems to be a little better for the integral methods developed so far, [26,31,83,115]. The basic assumption in all of these methods is, that the streamwise component of the boundary-layer velocity is analogous to that in the two-dimensional case. As shown by Cumpsty and Head [26], the entrainment concept seems to be suited best for three-dimensional methods. Of course, the two integral-equations for the streamwise direction (the momentum integral equation and entrainment shape parameter equation) are completed by the addition of the momentum integral equation for the cross flow. The three equations then contain more than three unknowns, however, and to make the problem solvable, a coupling between the crosswise and the streamwise velocity profiles is introduced. The assumption made on the representation of the two profile types and

their interconnection form the essential difference between the various methods. For the cross-flow profile the simplest formula is that due to Mager [74]

$$\frac{w}{u} = \left(1 - \frac{y}{\delta}\right)^2 \cdot \tan\beta \tag{8.1}$$

where w and u are the crosswise and streamwise velocity components respectively, y is the wall distance along a normal to the surface, and β is the angle between the wall streamline and the local external streamline. The famous triangle representation according to Johnston [64] may be written as

$$\frac{w}{u} = \begin{cases} \tan\beta & \text{for } \frac{u}{U(x)} \leqslant 1 - \frac{\tan\beta}{A} \\ A \cdot \left(1 - \frac{u}{U(x)}\right) & \text{for } \frac{u}{U(x)} \geqslant 1 - \frac{\tan\beta}{A} \end{cases} \tag{8.2}$$

with

$$A = \frac{\tan\beta}{\left(\frac{0.1}{\cos\beta \cdot \sqrt{c_f}} - 1\right)} \ ,$$

where $U(x)$ is the external velocity and c_f is the streamwise component of the skin friction. Still another formula has been proposed by Eichelbrenner [31]

$$\frac{w}{U(x)} = \tan\beta + B \cdot \frac{u}{U(x)} - (\tan\beta + B) \cdot \left(\frac{u}{U(x)}\right)^2 \ , \tag{8.3}$$

where B is a known function of β and c_f. The limiting angle β then is essentially the form parameter to be determined from the solution of the crosswise momentum integral equation. Michel et al. [64] have used a cross-profile representation of the general form:

$$\frac{w}{U(x)} = \Phi \cdot \delta \cdot f(y/\delta) \ , \tag{8.4}$$

where Φ is the geodesic curvature to the outer free-stream, and the function $f(y/\delta)$ is determined from a differential equation of similarity type. Note that the Mager and Johnston representations do not allow for crossover profiles while Eichelbrenner's and Michel's expressions do.

As to the predictive qualities of the above methods, an assessment is difficult to make, since adequate experiments are scarce. For instance, comparisons with measurements of Cumpsty and Head [27] on a swept wing model showed serious discrepancies especially in the growth of the streamwise momentum thickness, while the wall cross-flow angle β was predicted quite well by their calculation method. Similar results were obtained from a comparison between the method of P. D. Smith [115] and an experiment with curved duct flow by Vermeulen [132], where, except for the streamwise momentum thickness, the prediction was generally satisfactory. Good overall agreement is claimed by Michel et al. [79] of the results of their method with the measured boundary layers on swept

wings and in front of a blunt body.
In closing these remarks on three-dimensional boundary layer calculation methods, allow me to cite part of the conclusions drawn of Eichelbrenner's recent review article [32]: "*In laminar flow, several fairly reliable methods for the calculation of three-dimensional boundary layers have been developed. Far less satisfactory is the state of the art in three-dimensional turbulent flow, where, to date, only integral methods are available; even these methods depend still on too many simplifying assumptions to be trusted in the general case.*"

9. Prediction of Aerodynamic Characteristics Using Boundary Layer Calculation Methods

As mentioned in the introduction, the inviscid free-stream over a lifting body is influenced by the presence of the boundary layer. Even in the case of the two-dimensional flow over an airfoil we have seen, that the interaction may become very strong especially when separation (bubble or rear separation) occurs. But also when the boundary layer remains attached, the pressure distribution is affected. From the aircraft aerodynamicist's point of view, not the boundary layer as such but these interaction effects constitute the problems that one wishes to solve with the help of boundary layer calculation methods. It is therefore proposed to review some of the problems for which boundary layer methods have been successfully applied. These are: (i) attached flow over a single airfoil, (ii) attached flow over an airfoil with a slotted flap, (iii) flow over single and flapped airfoil with rear separation, and (iv) shock induced rear separation on straight and swept wings determining buffet-onset limits.

9.1. Attached Flow over a Single Airfoil

The general principles of the way in which the pressure distribution and hence the lift are changed as compared to the potential theory, are well-known and have been described by Thwaites [126]. The main influence is the displacement effect of the boundary layer and the wake. The procedure then is to recalculate the potential flow around the airfoil with the boundary layer displacement thickness added to the airfoil geometric coordinates. At this stage, however, this seemingly straight-forward procedure already shows its drawbacks. The first inviscid potential flow calculation uses the Kutta condition at the trailing edge, having generally a nonzero trailing edge angle to determine the overall circulation (i.e. the lift) of the airfoil. But what condition is to be applied in the second potential flow calculation? It is known, that the prediction for the overall lift depends critically on exactly the condition specified at the trailing edge region with the boundary layers from the upper and lower surfaces having different thickness. If one applies the criterion that the vorticity contained in the two merging turbulent boundary layers must be equal and opposite at the trailing edge this, together with the boundary layer approximation that $\partial p/\partial y = 0$ leads to the conclusion, that the velocities at the upper and lower edges of the beginning wake are equal. The experiment shows, that this con-

dition is wrong, also the lift coefficient at a given angle of attack of the airfoil obtained by applying this condition is much too low. It was therefore argued, that a pressure difference across the two boundary layers is induced at the trailing edge by the curvature of the ensuing wake. **figure A.25** depicts this situation at the trailing edge. The formula

$$\frac{\Delta c_L}{c_L} = \frac{c_D}{w} \tag{9.1}$$

for the relative lift reduction was given by Spence [117] in which, however, the unknown drag coefficient must be estimated from approximate formulas like that of Squire and Young [119]. The above formula is only a crude approximation which underestimates the lift reduction especially with increasing angles of incidence. Later Spence and Beasley [118] developed another formula arguing that the nonzero vorticity in the wake will induce a circulation about the whole airfoil as is the case with a jet flap. By interpreting the effect of the wake to be analogous to the jet effect they arrived at the nonlinear expression

$$\frac{\Delta c_L}{c_L} = \Lambda \cdot \sqrt{c_D} \ , \tag{9.2}$$

with $\Lambda = -0.214$. In this formula, again the profile drag coefficient c_D would have to be calculated approximately again from the Squire-Young formula. Steinheuer [120] found, that quite good agreement with experiment is achieved by leaving the form of equation (9.2) unchanged but replacing c_D by the overall skin friction coefficient c_F as defined by

$$c_F = \oint \frac{\tau_w(s)}{\rho \cdot U(x)_\infty^2} \, \mathrm{d}\, s \ , \tag{9.3}$$

where the integral is taken around the profile contour, leading to

$$\frac{\Delta c_L}{c_{Lo}} = \Lambda \cdot \sqrt{c_f} \ . \tag{9.4}$$

Here, c_{Lo} is the value of the lift coefficient of the potential flow calculation using the original Kutta condition, and Λ was found to have the empirical value $\Lambda = 2$. This formula is very convenient insofar as it does not necessitate the calculation of the wake, and c_f is easily obtained from the skin friction distribution of a boundary-layer calculation. Another advantage is, that the formula, equation (9.4) can be applied to multiple airfoils as well. **Figure A.26** shows a comparison of the calculated lift curve with the experiments of Brebner and Bagley [20] with two different Reynolds numbers.
A different line of approach to the problem is that employing the concept of reduced camber, a measure of which is the added total displacement thickness of the boundary layer at the trailing edge. This method has been perfected by Powell [96]. For the ratio of the displacement thickness to chord length, the assumption is made that it assumes half of the value of the drag coefficient at a specified distance downstream of the trailing edge. The drag coefficient again has to be known in advance and is calculated by a method due to Nash and McDonald [87] based on the momentum thickness at the trai-

ling edge. The special feature of Powell's method is, that a potential source and vorticity distributions placed along an effective camber line are sought for, which is determined from the calculated displacement thickness added to the original airfoil contour. This results effectively in a change of angle of incidence. The usual Kutta condition is applied and the source and vorticity distributions are found by fulfilling the boundary conditions at the displacement surface of the camber-modified airfoil. An iterative procedure is then set up, where the pressure distribution from a potential flow calculation is updated according to the change in effective camber, and boundary-layer calculations are performed with this new pressure distribution. Convergence is reached after about 10 iterations.
The method of Powell described above has been found to give good general agreement with measured pressure distributions, if the comparison is made at the same value of the lift coefficient. However, when the solution is sought for a given angle of incidence, the method overestimates the lift coefficient by up to 10 %, i.e. it underestimates the reduction of lift due to the boundary-layer effect. This is the case with all methods that have been proposed so far like that of Bhateley and Bradley [12] and of Giesing [46]. The discrepancies are attributed to the uncertainty of the older nominally two-dimensional wind-tunnel experiments, as evidenced by the more recent investigations of Firmin and Cook [1].
An interesting discussion on the subject of the interaction of the outer flow with the confluent boundary layers and the wake in the trailing edge region of an airfoil has recently been given by Green [51]. A theoretical model for the immediate vicinity of the trailing edge is developed envisaging the confluent boundary layers to be effectively inviscid, but with rotational shear layers with slip velocity at the surface. The main result of Green's discussion is, that a correlation between the shape parameter $H_{1,2}$ of the upper surface turbulent boundary layer approaching the ideally sharp trailing edge and accompanying pressure rise could be established, resulting in a lower pressure (higher velocity) at the edge of the upper surface boundary layer than at a corresponding point at the edge of the lower surface boundary layer. This is in qualitative accord with the formula developed by Giesing [46]. It is not known whether Green's trailing edge flow model has been incorporated into a prediction method.

9.2. Attached Flow over an Airfoil with a Slotted Flap

The need for still more efficient high-lift devices for use in RTOL and STOL[1] aircraft has led to extensive research activities mostly on the experimental side as far as full three-dimensional configurations are concerned. The basis for theoretical studies, however, still is the simplest case of a high lift device, i.e. the airfoil with one trailing edge flap. With the modern methods for the calculation of the potential flow around multiple airfoils, such as those developed by Riegels and Jacob [101], Giesing [46] and Bhateley

[1] RTOL - Reduced TakeOff and Landing, STOL - Short TakeOff and Landing

and Bradley [12], the prospect of developing a prediction method including viscous effects has come within reach.
The typical development of the viscous layers around an airfoil with a slotted flap has already been shown in **figure A.5**. This case has been extensively studied at RAE [38,41] and at NLR [28, 68] experimentally and theoretically. The difficulties imposed on the theoretical analysis lie mainly in the appearance of two features: (i) the mixing of the wake from the main airfoil and the boundary layer of the upper surface of the flap, and (ii) the presence of a closed zone of separation (or bubble) on the lower surface of the main airfoil near to the trailing edge. The interaction of the wake and boundary layer at optimum lift at a given incidence and flap deflection has been found to be relatively weak, meaning, that the two shear layers retain their separate identities almost to the flap trailing edge. However, this is only true as long as the relative translational position of the flap (characterized e.g. by the gap width and the trailing edge overlap) is such that the flow at the slot exit contains an essentially inviscid core. **Figure A.27** shows schematically the flow situation, where sketch ⓐ applies to the favorable situation just described. Sketch ⓑ below shows the effect on the slot flow, when the gap has become too narrow. The limiting streamline, by which the recirculation bubble is bounded in the situation of sketch ⓒ, no longer reattaches to the lower side of the main airfoil ahead of its trailing edge but is swept down below the lower side of the flap. This then gives rise to separation over the back of the flap or even the back of the main profile, resulting in a substantial loss in the overall-lift of the flapped airfoil.
A more detailed picture of the mechanism of flow in the slot region is gained from the results of a recent investigation made by W. Schröder [12], here at the VKI, on a thin airfoil with flap. **Figure A.28** shows some treasured pressure distributions over the upper and lower sides of the main wing and the flap for a decreasing gap width of the flap nose location at constant overlap. These parameters being determined by the coordinates d and s. Beginning with the case or the largest gap width, $s/c = 1.8$ %, it is seen, that the pressure coefficient reaches its full potential value of unity at the flap's stagnation point, while the pressure within the bubble forms a relatively low plateau, rather sharply bounded towards the trailing edge by a pressure peak which marks the reattachment point. This peak lies just ahead of the overlap location marked by the arrow. When the gap is diminished, the stagnation pressure at the flap nose becomes less than unity, indicating that low-energy fluid is shed over the flap nose. Correspondingly, the overall-lift is reduced. Also the pressure level at the bubble location is reduced and the region of separated flow extends upstream beyond the discontinuous corner of the contour. Surprisingly, however, with still non-separated flow over the main airfoil's trailing edge and over an appreciable part of the flap back, the flow through the slit still is maintained as evidenced by the sharp pressure fall just ahead of the trailing edge. The still noticeable pressure peak here suggests, that the bubble structure continues to be maintained, its bounding streamline, however, being formed of fluid of reduced kinetic energy. Three distinct regions of flow are tentatively indicated in the accompanying sketch of the slot flow: region I is the region of irrotational potential flow with full total pressure energy, region II is composed of rotational fluid forming a free shear layer origi-

nating from the separated boundary layer of the lower side of the main airfoil and region III is the closed recirculating bubble region. The described mechanism of the slot flow is strongly supported by the smoke visualization pictures made by Schröder, of which the obtained smoke contours are presented in **figure A.29**. These smoke contour lines roughly correspond to the line of division between the regions II and III of the previous figure.

The prediction method devised by the author [120] for the calculation of the optimum lift as dependent on the flap-setting, especially with respect to gap width and overlap at given flap angle, incidence, and Reynolds number assumes, that the bubble region can be replaced by a solid fairing contour for the calculation of the potential flow and hence the pressure distribution and the lift coefficient. This approach has been used previously by Labrujere et al. [68] and Werlé [134] for the analogous situation of the flow around the lower side of a slat to successfully calculate the pressure distribution. However, as the replacement contour is not known a priori, it is chosen to coincide with the fairing contour used in the experiments of Foster et al. [41] in the particular example, for which the first comparative calculations were made. The potential flow was calculated by means of the method of Giesing [46] for multiple airfoils, and a boundary-layer calculation was performed using Walz's integral method [133]. With the values of gap width and overlap as parameters, a series of potential flow and boundary-layer calculations were made, in which the lift reduction due to the boundary layer displacement effect was computed from equation (9.4) applied to the main airfoil and the flap individually. It turned out that, by varying the flap position, the boundary-layer calculation predicted either completely attached flow along the fairing contour right down to the trailing edge or the occurrence of separation at a point well upstream of the trailing edge. In **figure A.30** a comparison of calculated and measured values of the total lift is made for a case where the gap width is varied at a constant overlap distance. It is seen, that the experimentally found optimum gap width very well coincides with the point of flap position for which the calculations predict the occurrence of separation. Note further, the relatively small error of the absolute values of the lift coefficient as compared to the experimental values in the range of predicted attached flow.

The weak point of the proposed prediction method, of course, is the a-priori assumption to be made for the replacement contour in the bubble region. However, this difficulty should be overcome by exploiting the results of Schröder's experiment which showed, that the point of bubble reattachment always lies just ahead of the flap nose position (see **figure A.28**) and that the bubble contour line for the case of optimum lift forms a well-behaved curve which can probably be approximated by a cubic (see **figure A.29**).

The potentialities of a prediction method as that described above are immediately apparent. Not only the extensive (and expensive) wind-tunnel measurements to determine an optimum slot configuration would be greatly reduced by a preceding computational survey, but also the transfer of the low Reynolds number wind-tunnel results to the actually intended high Reynolds number configuration could be made with much more confidence.

9.3. Airfoil Flow with Separation

The prediction of incipient trailing edge separation for a given airfoil section is of extreme importance in the design of aircraft wings of moderate sweep angle, especially for the low speed range at take-off and landing. The purely theoretical determination of the maximum lift of wings with mechanical high lift devices such as single or multiple trailing edge flaps and slats or other fore-flaps is rendered especially difficult not only because of the mutual influence of the inviscid flow around the different parts of the wing, but also by the fact that the maximum lift of the configuration is almost always associated with moderate rear separation already established on one of the elements forming the complete section. While a prediction method for the general three-dimensional compressible case seems remote for a long time to come, the incompressible two-dimensional problem such as the one depicted in **figure A.31** has been attacked with some success by Jacob [62] and Bhateley and Bradley [12].

Following Jacob, I wish to outline briefly his line of approach and show some recent examples of his method, [63]. The concept of simulating the flow over an airfoil with a separated region ahead of the trailing edge is, to add to the otherwise classically determined potential flow (i.e. with Kutta-condition fulfilled at the trailing edge) a source distribution along that part of the contour where separation is present. From the development of a preceding boundary-layer calculation, the separation point has been determined. The added source distribution will then alter the original pressure distribution over the upper side of the airfoil and a new boundary-layer calculation (using Rotta's method [103] will predict the separation point to lie at some other location, as in the preceding run. The area of simulating source flow is altered accordingly and a new pressure distribution is calculated. This process of alternatingly calculating the potential flow and boundary-layer development is continued, until the assumed location of the separation point coincides with the predicted one. In order to avoid a stagnation point to occur in front of the outflow region, the source distribution is modeled in such a way that the streamline forming the surface ahead of separation leaves the surface smoothly, i.e. with zero-slope. Further the problem is made determinable by requiring an equal pressure (or velocity) to prevail at a point L shortly upstream of the trailing edge on the lower side, at a point 0 above the trailing edge through which the separation streamline passes, and at the separation point s itself. As soon as convergence of the iteration process is achieved, all section characteristics can be determined for the particular case considered, i.e. for a given angle of incidence and given flap settings. By repeating the calculation for a range of angles of incidence, of flap deflection angles, and of flap positions, the dependence of the lift coefficient on any of these parameters can be predicted for attached flow and flow with trailing edge separation. Also Reynolds number dependence is included through the use of boundary-layer calculations. Note, however, that up to the present the boundary-layer calculations have been used solely for the purpose of determining the separation point while boundary layer displacement effect is not included.

To show the potentialities of Jacob's method I propose to show two examples from his recent report [63]. The first example is on the flow over a hypothetical flapped airfoil

with a NACA 23012 main section (see **figure A.32**) and a flap, the section shape of which is a 20 % replica of the main airfoil. Graph ⓐ shows the $c_L(\alpha)$ curve for three different flap deflection angles δ_F and two different Reynolds numbers. With the smaller Reynolds number (solid line curves) separation occurs first on the main wing, causing immediate separation on the flap as well. For $\delta_F = 20°$, in contrast, the flap flow is separated already at zero angle of incidence and separation over the main wing occurs at about $\alpha = 8.5°$. A very interesting behavior is exhibited for the higher Reynolds number $Re = 10^7$ (broken line curves). Again with the flap angles $\delta_F = 0°$ and $10°$, separation is predicted to first occur over the main profile while the flow remains attached up to considerable higher angles of incidence. At the high flap deflection angle $\delta_F = 20°$ now the flow separates first over the flap while it continues to remain attached on the main airfoil causing the $c_L(\alpha)$-curve to again rise to a second peak value, where then separation takes over also to the main airfoil. In the graph ⓑ the boundaries for the different types of separation behaviors are shown, i.e. no separation, separation on flap only, separation on main airfoil only, and separation on both main airfoil and flap, depending on the angle of incidence and on the flap deflection angle. Note that at the lower Reynolds number $Re = 10^6$ the domain, where there is separation on the main airfoil only, is degenerated to a very narrow range of possible angles of incidence.
The second example treats the case of a main airfoil with drooped nose and an additional slat (as seen in **figure A.33**). The main profile here is a modified NACA 64-210 section. The reference chord c is therefore taken to be that of the unmodified profile. The figure shows the calculated pressure distribution at a given slat position and an effective angle of incidence of $\alpha = 20°$ corresponding to equal values of lift coefficient of the calculation and of the measurements by Baumert [8]. The transition point was taken as the point of laminar separation. Considering that the displacement effect of boundary layer is not accounted for, the agreement between the theoretical and the measured pressure distribution is most satisfactory, although the measured separation point seems to lie slightly downstream of the predicted location. The flexibility of the method may be demonstrated by **figure A.34**, where for the same profile at a given flap position the measured $c_L(\alpha)$-curve (dotted line) is seen to have two maxima, the first of which corresponds to slat separation at about $\alpha = 33°$, followed by the second peak at $\alpha = 40°$ for main wing stall. The solid line curve represents the result of the calculations and the broken line curve corresponds to the experimental curve corrected for an effective angle of attack at an infinite aspect ratio. First of all, it is noted that the computed curve exhibits correctly the existence of the two maxima. The deviations from the corrected experimental curve may be attributed to the inexplicable difference of about two degrees in incidence at zero lift and to the boundary layer displacement effect not accounted for in the calculations. In closing this paragraph then, it can be stated without exaggeration, that Jacob's prediction method has now come to a degree, that it may be applied with confidence to explore numerically the low speed aerodynamic characteristics of an airfoil with slats and even multiple flaps in the design state with only a very reduced number of wind-tunnel runs necessary for assurance.

9.4. Prediction of Buffet Boundaries for a Wing in Transonic Flow

One of the important problems in modern aircraft design is constituted by the appearance of a normal shock on the upper surface of a wing or airfoil involving an interaction between shock and boundary-layer development. Specifically, shock-induced boundary-layer separation marks the phenomenon of buffeting, loosely defined as the state of very severe random oscillations of the aerodynamic forces on a wing. Buffeting thus poses structural limits to the range of flight conditions attainable. The influence of buffet onset on the flight envelope (curve $c_{L,max}$ versus Mach number) for a transport aircraft with wings of large aspect ratio and moderate sweep angle is depicted in **figure A.35** schematically. In incompressible flow (range I), the maximum lift is determined by separation phenomena induced by adverse pressure gradients involving either rear separation or bubble bursting as discussed previously. Range II, beginning at a Mach number of about $Ma = 0.3$ is characterized by the appearance of a small supersonic zone around the airfoil nose at high angles of incidence with $c_{L,max}$ decreasing with increasing Mach number. An extended supersonic flow region terminated by a normal shock is encountered in range III, beginning at about $Ma > 0.6$. Here now, the maximum lift is rapidly falling off with Mach number. It is in this range that buffeting is the constraining factor. The diagram includes the curve for drag rise close to which the operating point for cruise of an aircraft is usually chosen, so as to keep some margins ΔMa and Δc_L with respect to the $c_{L,max}$ or buffet-onset curve.
Adopting flow model B according to the classification of transonic separation types (see **figure A.8**) after Pearcey et al. [95], F. Thomas [123] has been the first to develop a purely computational method to predict the onset of buffeting which hitherto could only be obtained by wind-tunnel and flight tests. The method relies on the argument, that if buffet-onset is the consequence of boundary-layer separation behind a normal shock on a transonic wing, it was to be expected that the problem could be solved by employing boundary-layer methods. The analytical steps in the method of Thomas as applied to two-dimensional airfoils are as follows:

1. Using available semi-empirical [111] or theoretical [82] methods, the pressure distribution including the position of the shock is calculated assuming the flow to be attached and inviscid,

2. With the above pressure distribution a boundary-layer calculation along the upper surface of the airfoil and through the shock region is performed to determine the separation point by one of the available boundary layer calculation methods for compressible turbulent flow,

3. Steps 1. and 2. are repeated for a series of flight conditions (Mach number) and the movements of the obtained separation points and the shock position are determined as shown schematically in **figure A.36**,

4. In [123] buffet-onset was taken as being the condition where the boundary layer separation point and the shock position coincide (point A in **figure A.36**). Later, with some revisions in the analysis components, it was assumed [124] that buffeting occurred at the condition where the separation has moved forward from the trailing edge to 90 % of the chord (point B in **figure A.36**).

The above criterion for buffet-onset has been discussed by Thomas and Redeker [124] and by Gentry and Oliver [44, 45], who made comparative calculations using different methods in the computational steps 1. and 2. above. Some of the results of Thomas' method as compared to wind-tunnel and flight test results are shown in **figure A.37** where c_{LB} denotes the lift coefficient for buffet-onset. For these two-dimensional examples the agreement between predicted and measured buffet limits is very satisfactory.
The first attempts of Thomas [123] to extend his method also to swept wings by applying the independence principle for an infinite swept wing and by correcting the results obtained for the section airfoil normal to the leading edge by the cosine law, were successful only for wings of moderate sweep. For large angles of sweep the neglect of the truly three-dimensional boundary-layer development produced too optimistic limits of buffet-onset. Therefore Redeker [98] (see also [124]) extended the incompressible boundary layer entrainment method of Cumpsty and Head [26] for the three-dimensional boundary layer flow over swept wings to include compressibility. A weak-shock concept is adopted which does not lead to separation of the boundary layer ahead of the shock, and again it is assumed, that three-dimensional separation marked by confluent wall streamlines sets in first at the trailing edge and moving up towards the shock position. Also the 90 %-chord criterion for buffet-onset is adopted.
In **figure A.38** the results of the example calculations taken from [98] are shown. In case ⓐ the buffet boundaries for the fighter aircraft F-86A, as determined in flight test [42], are compared with the results of Redeker's method and with the quasi-two-dimensional method of Thomas. It is seen, that accounting for three-dimensionality results in much better agreement with experiment. In case ⓑ the comparison extends to two wings of different thickness ratios and sweep angles at equal aspect ratio and drag-rise Mach number. The wind-tunnel experiments made in the Göttingen transonic-tunnel [131] revealed, that in spite of the equal drag-rise Mach number the thinner wing with less sweep is more favorable with respect to the buffet boundaries. This is also reflected in the theoretical prediction which is in very satisfactory agreement with experiment.
The foregoing examples show convincingly, that again with the help of boundary-layer methods a complex problem in aircraft design is made amenable to analytical prediction.

10. Some Remarks on the Scale Effect

By scale effect, generally the differences are understood which exist between the results obtained from model testing in a wind-tunnel and the result of the full scale flight test with respect to any aerodynamic characteristic being investigated. The principle cause for these differences is the dependence of various flow phenomena on Reynolds number which is, in general, not the same in the flow at model scale and at full scale. This Reynolds number dependence gives rise to serious problems in the extrapolation of model test results to the conditions of full scale or vice-versa in the ability to simulate properly full scale conditions in a model test, e.g. by artificially fixing of boundary-layer transition.

In actual wind-tunnel testing besides the Reynolds number simulation, although of prime importance, other aspects must be considered, some of which are: tunnel wall constraints, model support interferences, elastic model strength, model surface conditions, the representation of components such as the engines. Also, the free-stream turbulence level, given as

$$I_{Tu} \equiv \frac{u'}{U(x)_\infty} \quad , \tag{10.1}$$

where u' is the root-mean-square of the turbulent velocity fluctuations and $U(x)_\infty$ is the mean free-stream velocity (Reynolds averaged), may become very important as it influences the onset of transition from laminar to turbulent boundary-layer flow. In the discussion to follow, all these effects will not be considered, the major attention being given to the pure Reynolds number effect. Recent reviews of various influences on the scale effect have been given by Hall [53], Green [51], Little [70], and Paterson [93].

The study of the Reynolds number scale effect consists of essentially the study of the complex interactions between boundary-layer development and the external inviscid flow. Thus, again, the basic boundary-layer phenomena will determine the sensitivity of the flow of a given model-configuration to scale effects. In the two-dimensional airfoil flow these are: (i) attached boundary-layer flow, either laminar or turbulent, (ii) transition from laminar to turbulent flow, (iii) complete laminar separation, (iv) laminar separation with subsequent turbulent reattachment over short and long separation bubbles, (v) turbulent separation, (vi) turbulent reattachment, e.g. downstream of the shock-boundary layer interaction zone in the flow over a transonic airfoil, and (vii) the wake development. Although in most occasions the real flow is three-dimensional, it is expected that the study of the basic two-dimensional boundary-layer phenomena will provide the criteria for assessing scale effects, as for instance the effects on a swept wing being discussed by considering a sheared wing of infinite span. The above mentioned boundary-layer

phenomena may be subdivided into two categories according to their effect on the flow field as a whole. Strong interaction is provoked usually by the phenomena (iii) and (v) involving complete detachment of the outer flow over an appreciable portion of the surface. Phenomena (i), (ii) and (vii) belong to the weak interaction category while the items (iv) and (vi) involving closed separation region play an intermediate role. However, it must be born in mind, that phenomena which only weakly affect the outer flow locally are responsible in many cases for the appearance of strong interaction. Thus, e.g. transition from laminar to turbulent being highly Reynolds number dependent, influences by its location and streamwise extent the subsequent development of the turbulent boundary layer and hence the possible turbulent separation at a location relatively far downstream of the transition zone. Another example is the change of a separation bubble from the short to the long type depending on the Reynolds number. Typical pressure distributions obtained at ONERA as referenced in [54] are shown in **figure A.39**. At the higher Reynolds number (higher velocity V_0) a short bubble exists up to a 14° angle of incidence causing the kinks in the c_f-curves but otherwise not affecting the pressure distribution. At the lower Reynolds number the short bubble apparently bursts into the formation of a long bubble at about 8° incidence, resulting in the deterioration of the suction peak pressure close to the leading edge. This example exhibits the inherent dangers in extrapolating low Reynolds number data to full scale Reynolds number if, as in this case, a fundamentally different type of boundary layer free-stream interaction phenomenon comes into existence within the range of Reynolds numbers over which the extrapolation is desired. An example of this kind has actually occurred with the C-141 airplane as reported on by Loving [72] and demonstrated in **figure A.40**. Turbulent boundary-layer separation in flight test was much more downstream on the wing than had been predicted by wind-tunnel tests. The downstream shift of the shock and the increased circulation around the wing changed considerably the pressure distribution and hence the location of the lift-center causing in turn different trim requirements and greater loads on the fuselage structure than were anticipated in the design.
The above examples lead to the following conclusions:

1. Reynolds number scale effects may arise from a change in any part of the boundary-layer flow, the most significant sources of deviation being associated with boundary-layer transition and boundary-layer separation,

2. Extrapolation of results from one Reynolds number to another may lead to significant errors in the prediction of the aerodynamic characteristics at the desired full-scale Reynolds number.

One solution for remedy in this situation is to enlarge the capability of the experimental facilities in such a way, as to always make full-scale experiments. In fact, the need for larger wind-tunnels especially in the regime of transonic speeds has been established by the AGARD HIRT Group [29] (**Hi**gh **R**eynolds Number Wind **T**unnel). The second possibility, not as an alternative but rather as a complementary means, is to develop new,

and refine existing calculation methods comprising methods for the calculation of inviscid flow fields and boundary layers. The latter must be supplemented by increasingly reliable methods or criteria to determine transition and separation in detail. Furthermore, methods are needed by which the interactions between the inviscid and viscous flow regimes are predictable realistically so as to allow for a feedback of the influences of one flow type on the other. A composite prediction method may then be conceived, built up by way of evolution, in which only the best component methods available are utilized. Although the evolution of such an ideal method seems to be remote at the present, the progress made in the last decade in developing numerical procedures, both for the calculation of external flow fields and of the boundary layer provides an optimistic outlook into the future. As encouraging first steps into the right direction I would consider the examples of sections 9.1 to 9.4, where composite methods have been devised to attack Reynolds number dependent problems (calculation of maximum lift coefficient of a multiple airfoil, determination of buffet-onset boundaries), which hitherto were not thought to be solvable.

A. List of Illustrations

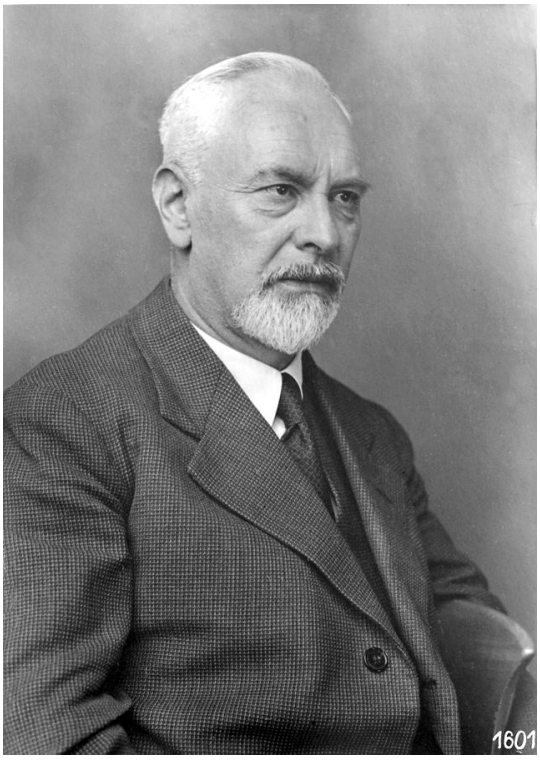

Figure A.1.
*Ludwig Prandtl, * 4 February 1875 in Freising, Upper Bavaria, German Empire, † 15 August 1953 (aged 78) in Göttingen, West Germany*

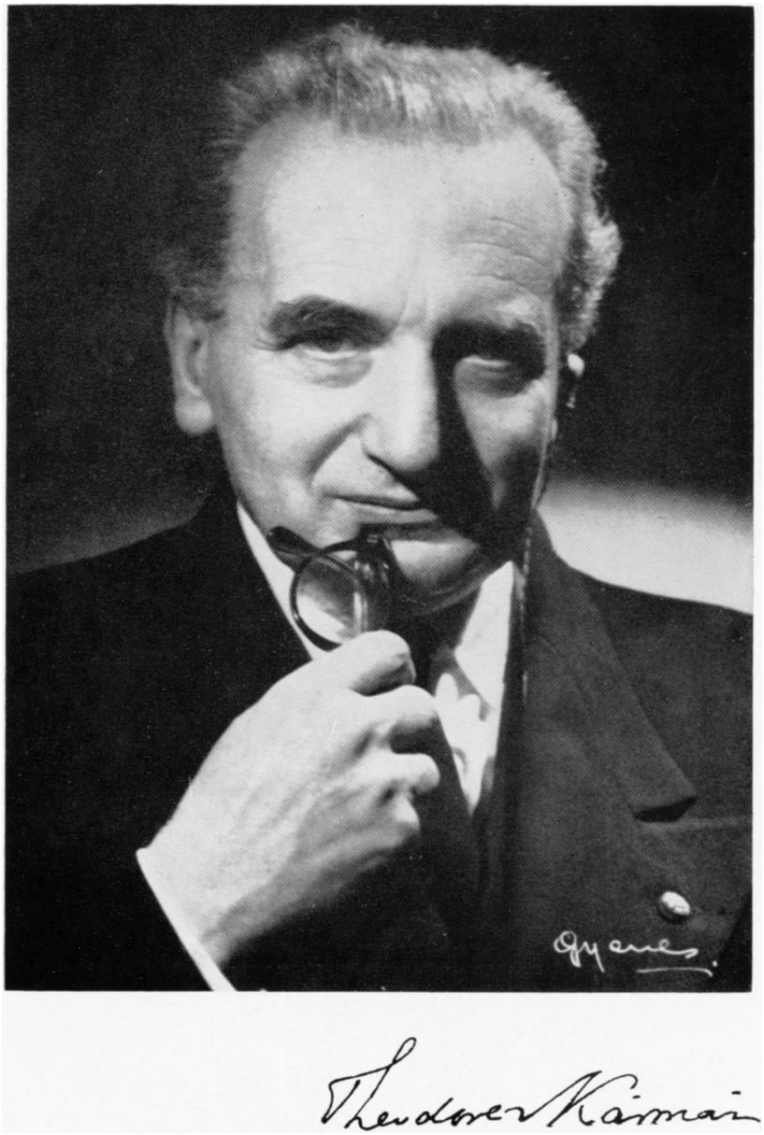

Figure A.2.
Portrait of Theodore von Kármán (May 11, 1881, Budapest (Austria-Hungary) - May 7, 1963, Aachen (West Germany))

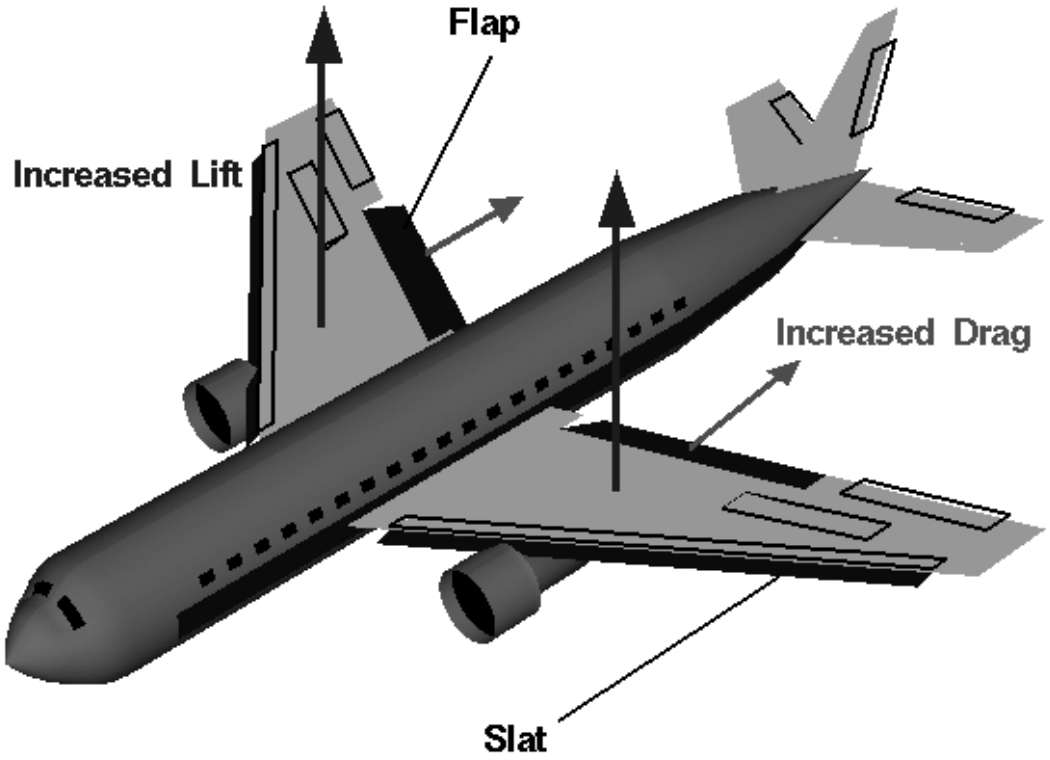

Figure A.3.
Illustration of slats and flaps of an airplane and corresponding lift and drag

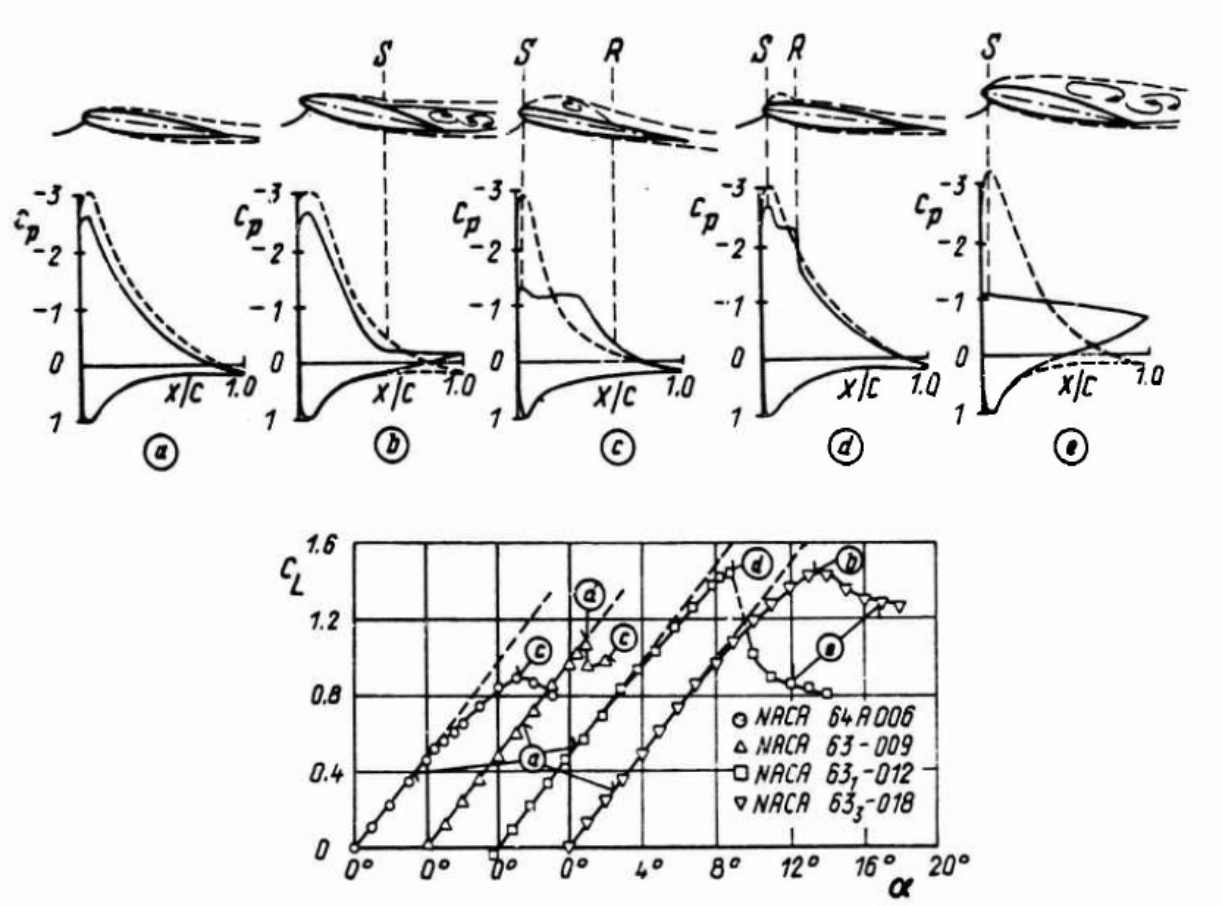

Figure A.4.
Effects of the boundary layer on the pressure distribution and the lift characteristics of single airfoils (schematically)

ⓐ *with attached boundary-layer flow*
ⓑ *with trailing edge separation*
ⓒ *with leading edge separation and long bubble*
ⓓ *with leading edge separation and short bubble*
ⓔ *with leading edge separation*
– – – – – *inviscid flow*
——◯—— *viscous flow*
S separation point

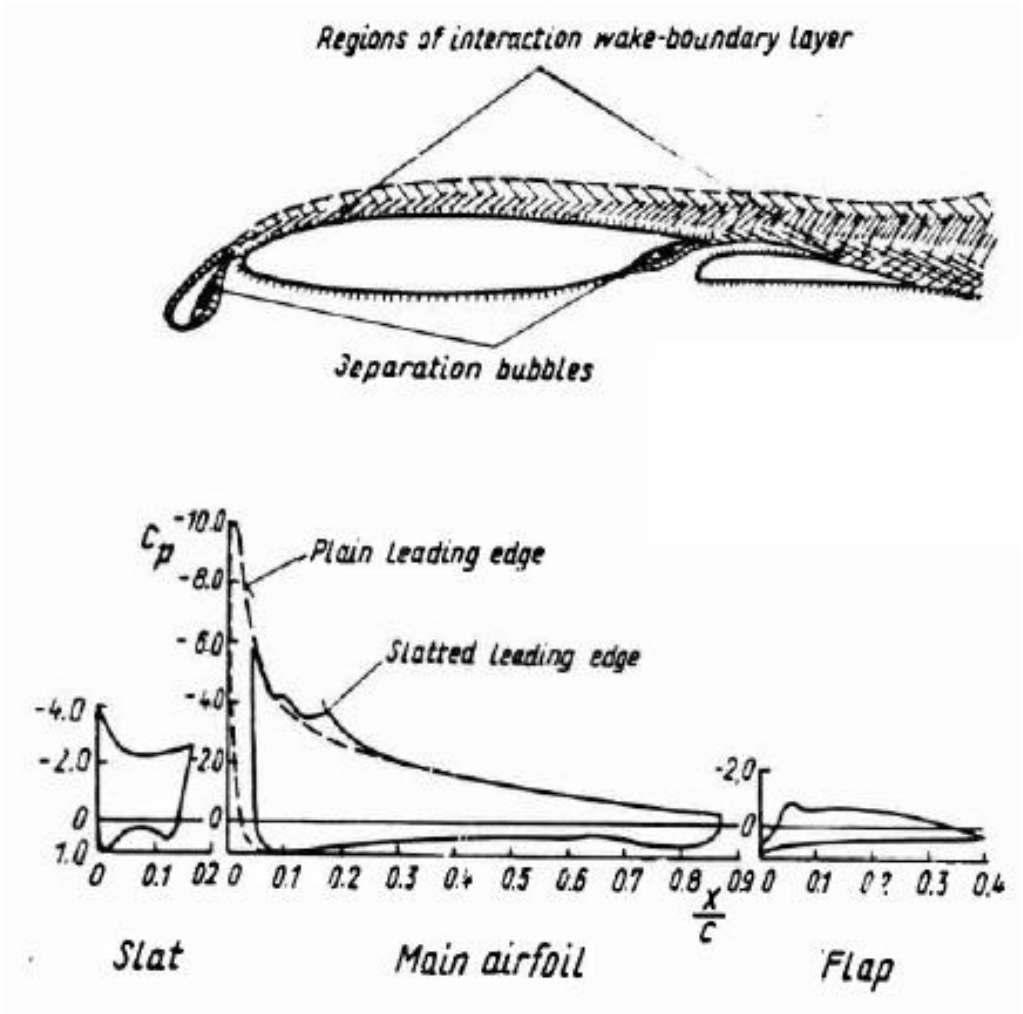

Figure A.5.
Boundary-layer development and typical pressure distribution for the flow over an airfoil with leading edge slat and trailing edge flap, from [40]

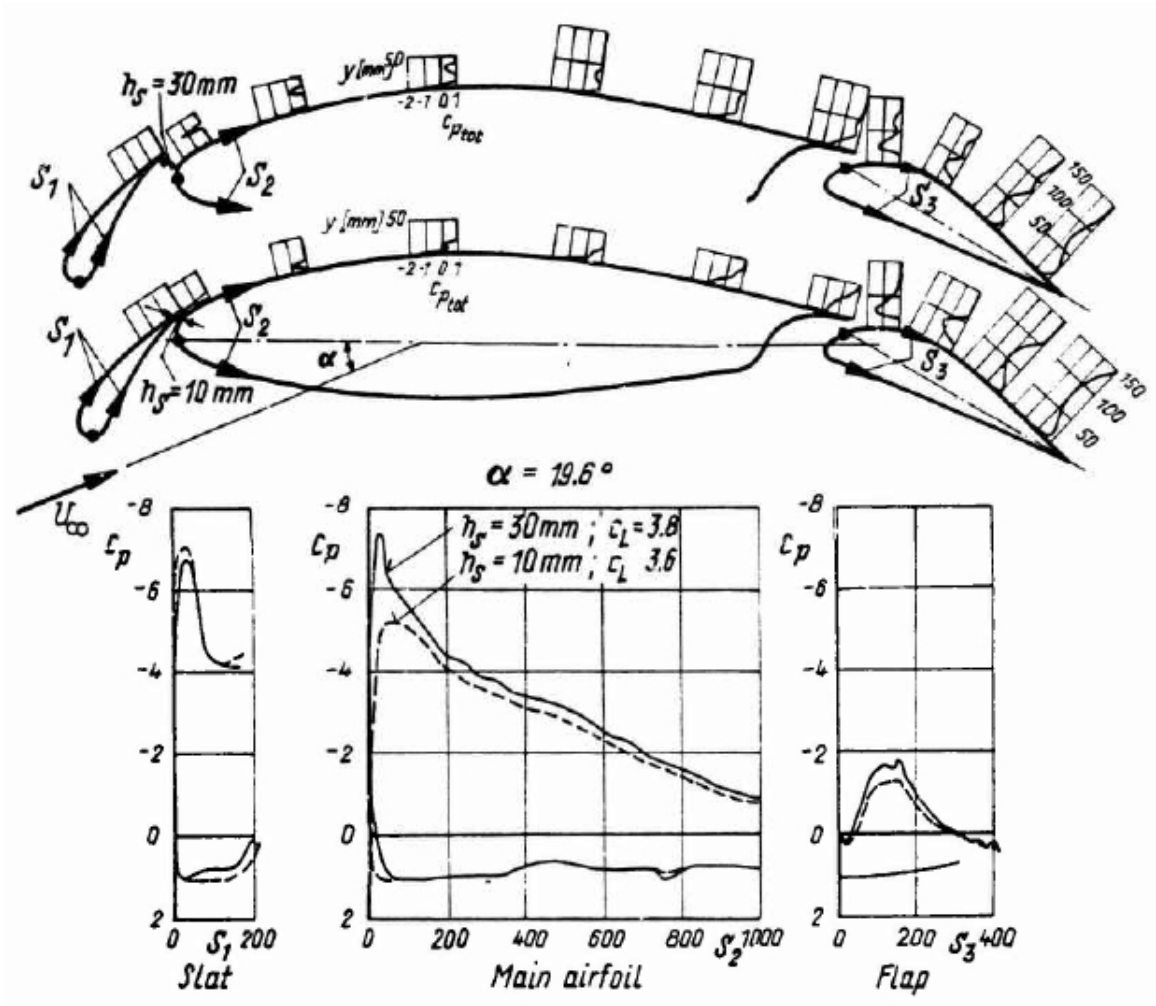

Figure A.6.
Development of the total head pressure in the boundary-layer flow over an airfoil with slat and flap. Comparison of measured static pressure distributions for two different flap settings, from [71]

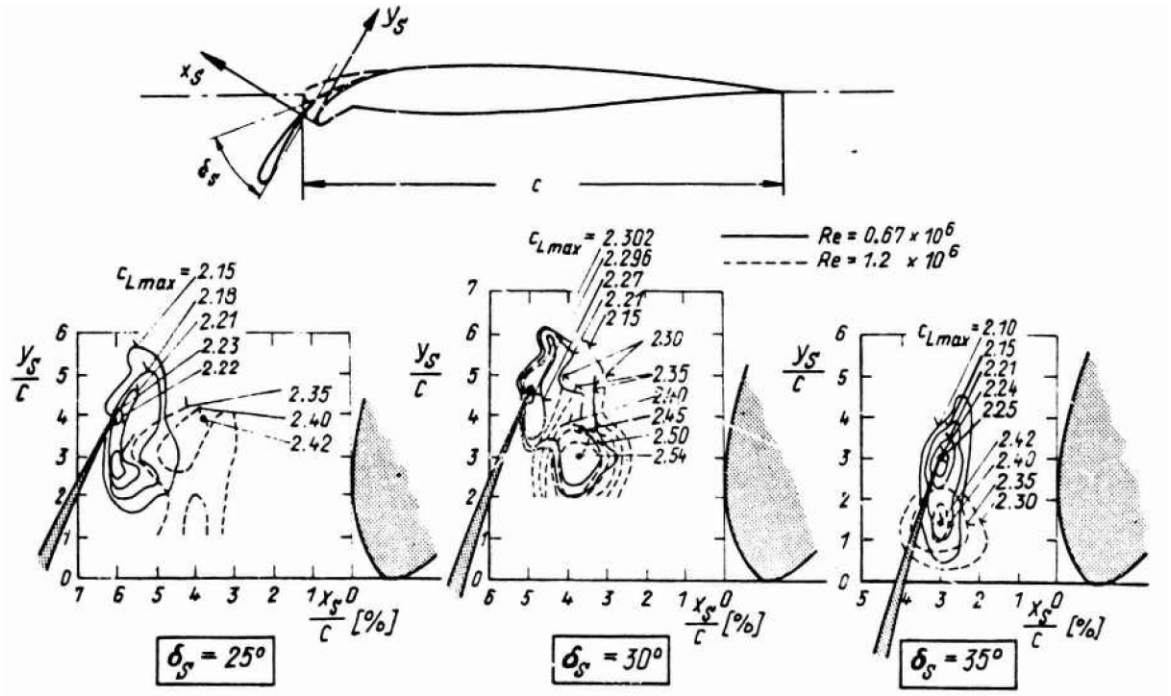

Figure A.7.
Effect of Reynolds number on the optimal slat position for maximum lift at three different flat angles for flow over a slatted airfoil with drooped nose, after [7]

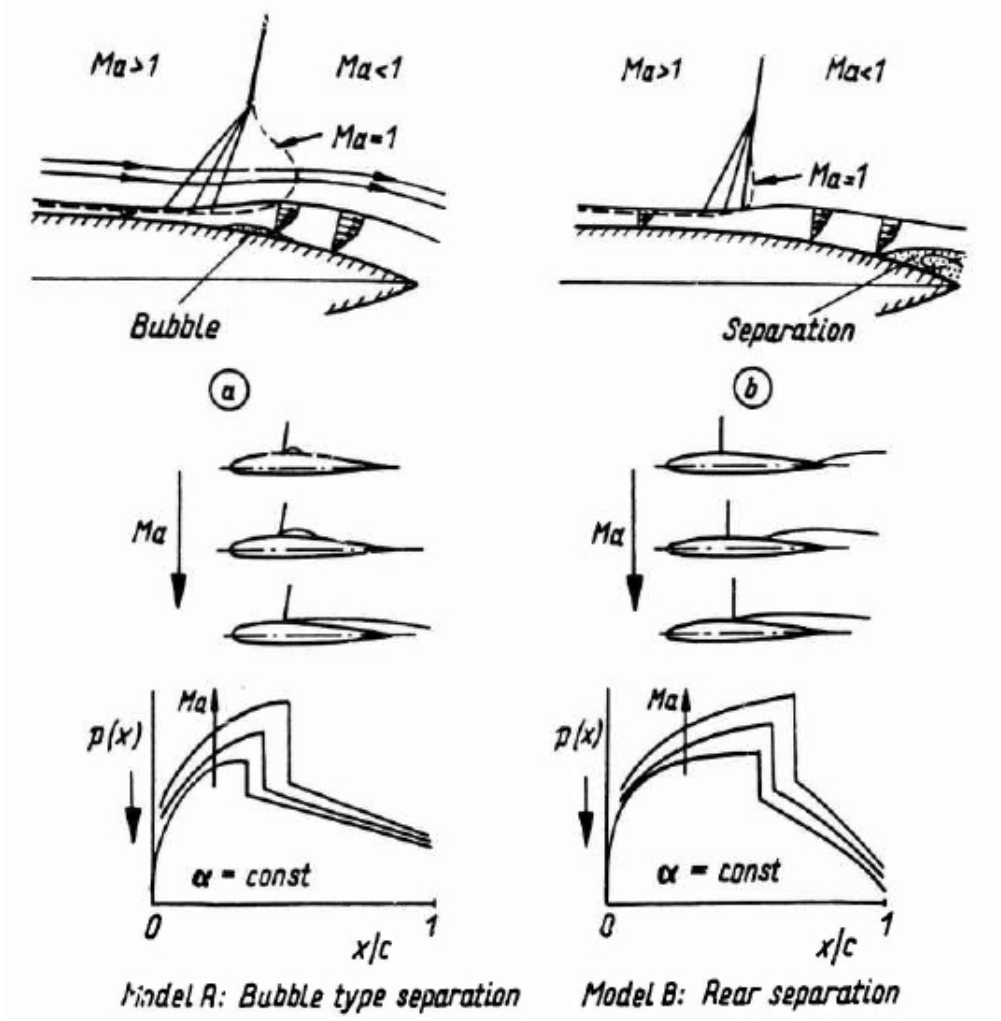

Figure A.8.
Flow models explaining shock induced separation effects on transonic airfoils

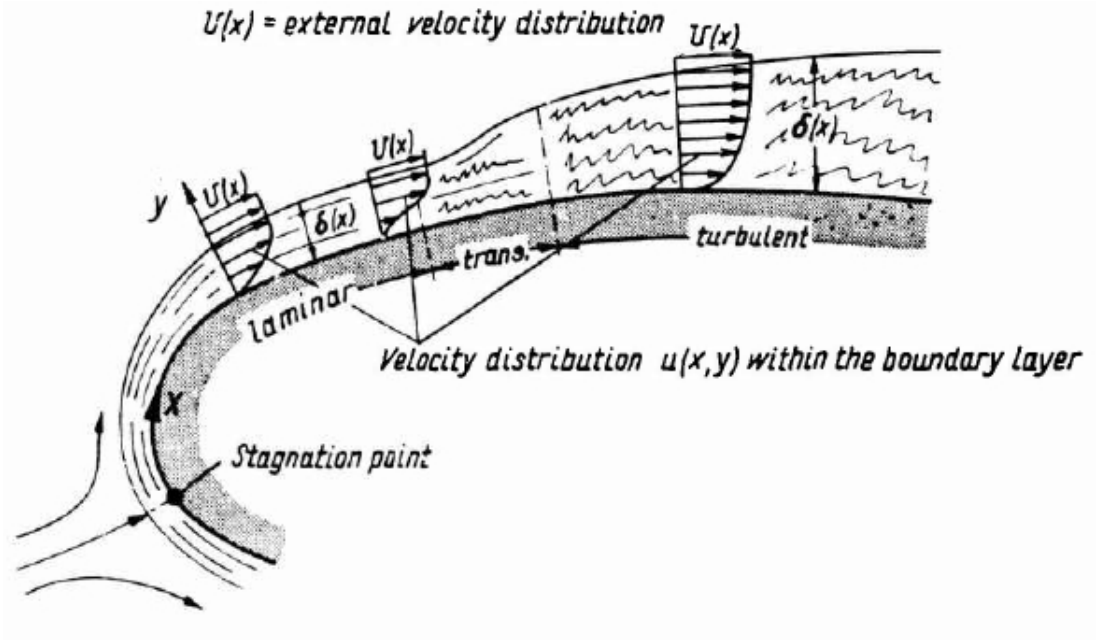

Figure A.9.
Development of an attached boundary on an airfoil-like body (schematically)

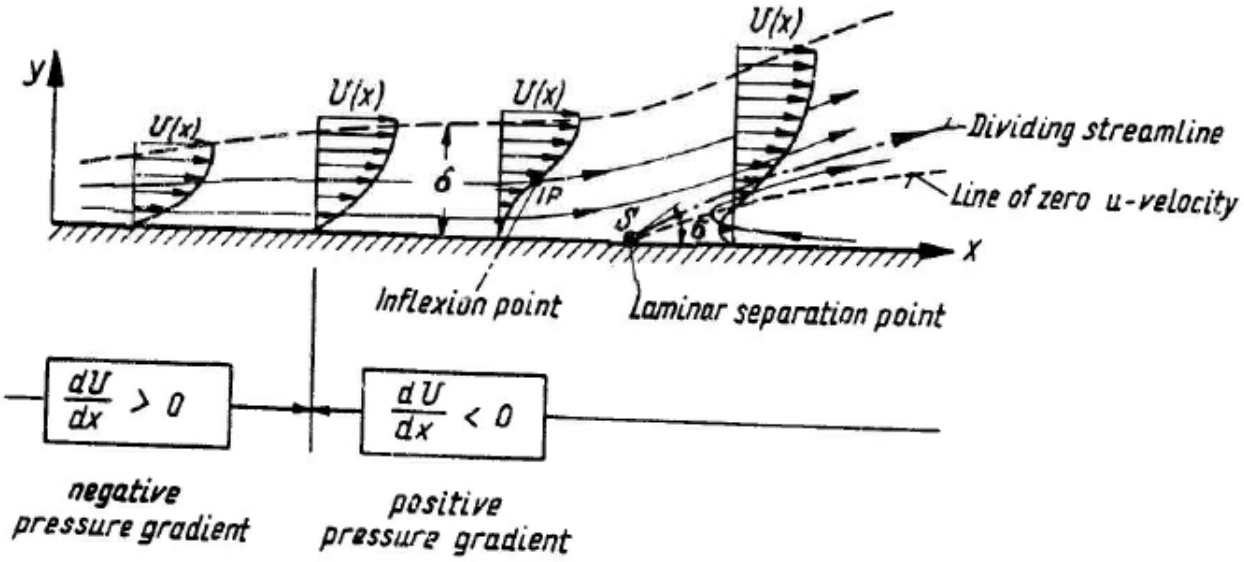

Figure A.10.
Laminar boundary-layer development including separation (schematically)

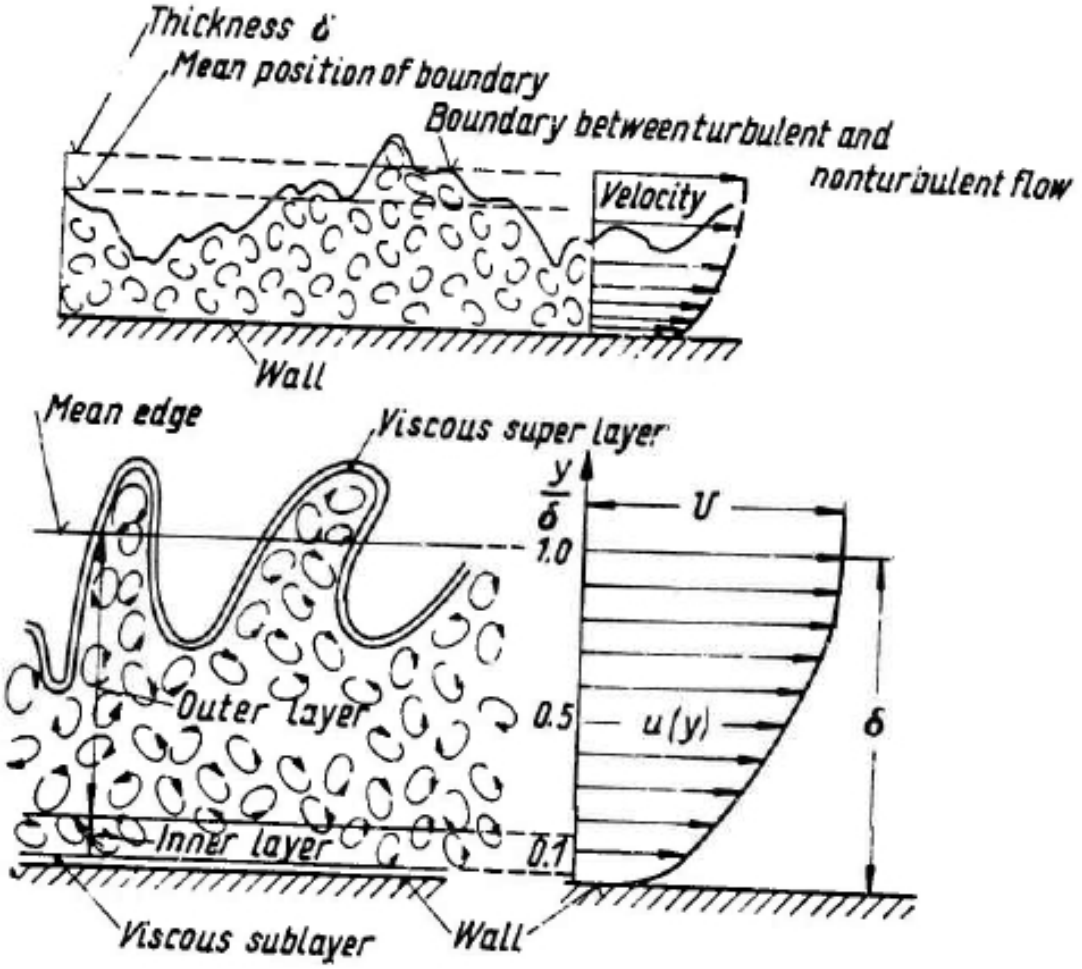

Figure A.11.
Schematic sectional view of a turbulent boundary layer and mean velocity profile

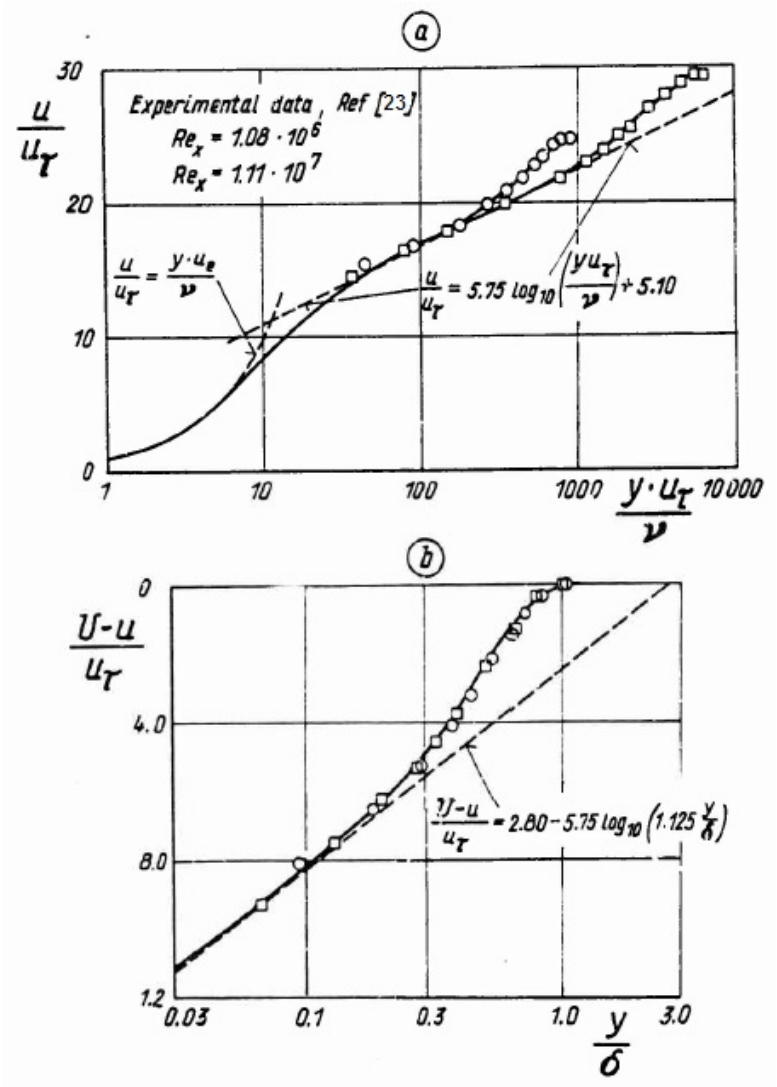

Figure A.12.
Logarithmic representation of the velocity distribution of a turbulent boundary layer
ⓐ *In wall-orientated coordinates (law-of-the-wall)*
ⓑ *In edge-orientated coordinates (velocity-defect-law or law-of-the-wake)*

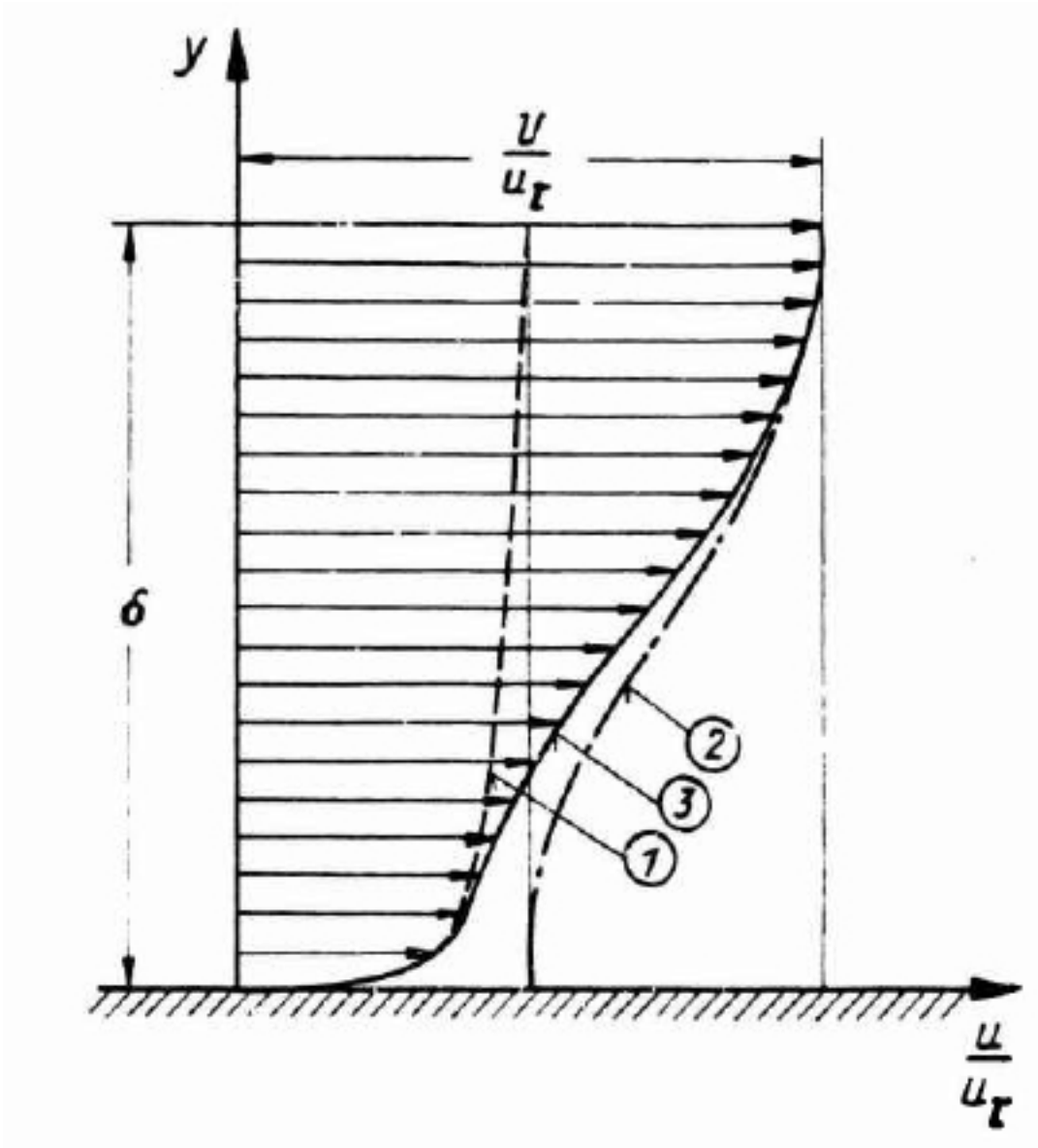

Figure A.13.
Composite velocity profile of a turbulent boundary layer

$$\underbrace{\frac{u}{u_\tau}}_{③} = \underbrace{\frac{1}{\varkappa}\ln\left(\frac{y\cdot u_\tau}{\nu}\right)+C}_{①} + \underbrace{\frac{\pi}{\varkappa}\cdot\omega\left(\frac{y}{\delta}\right)}_{②}$$

① *Law-of-the-wall component*
② *Wake component*
③ *Composite velocity profile*

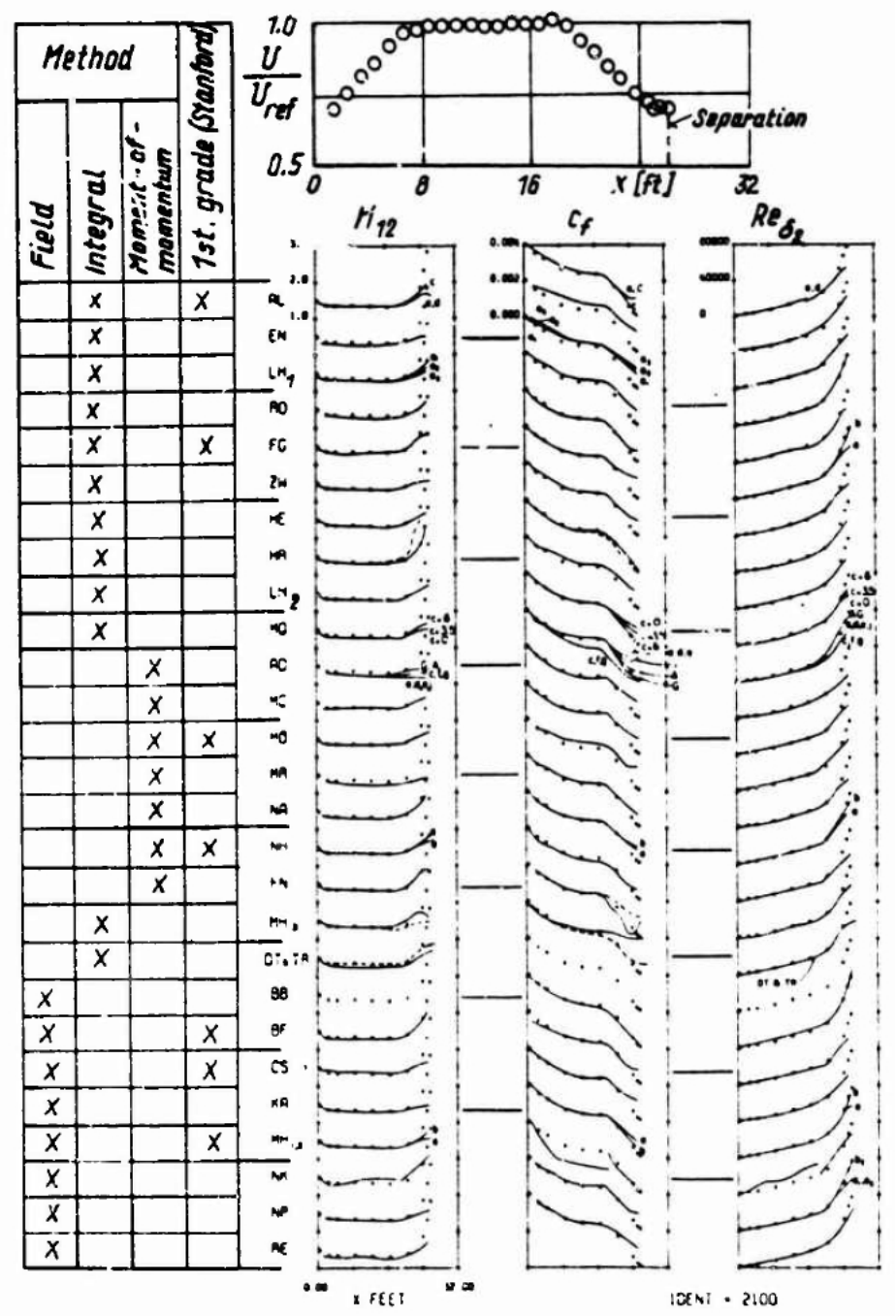

Figure A.14.
Results of different boundary layer calculation methods applied to the experimental case of Schubauer and Klebanoff [109] as presented at the Stanford Conference [2, 3]

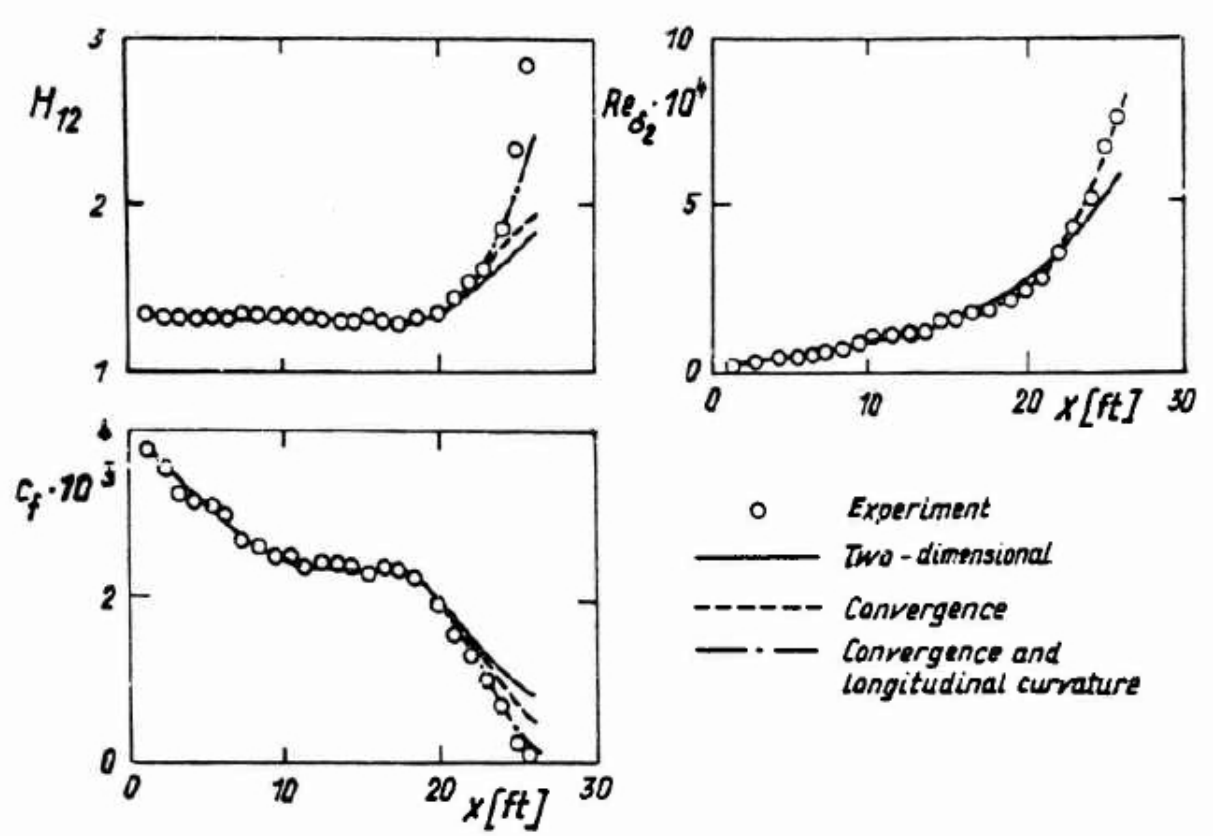

Figure A.15.
Results of the calculation method of Green et al. [52] applied to the experimental case of Schubauer and Klebanoff [109] including the effects of convergence and longitudinal curvature

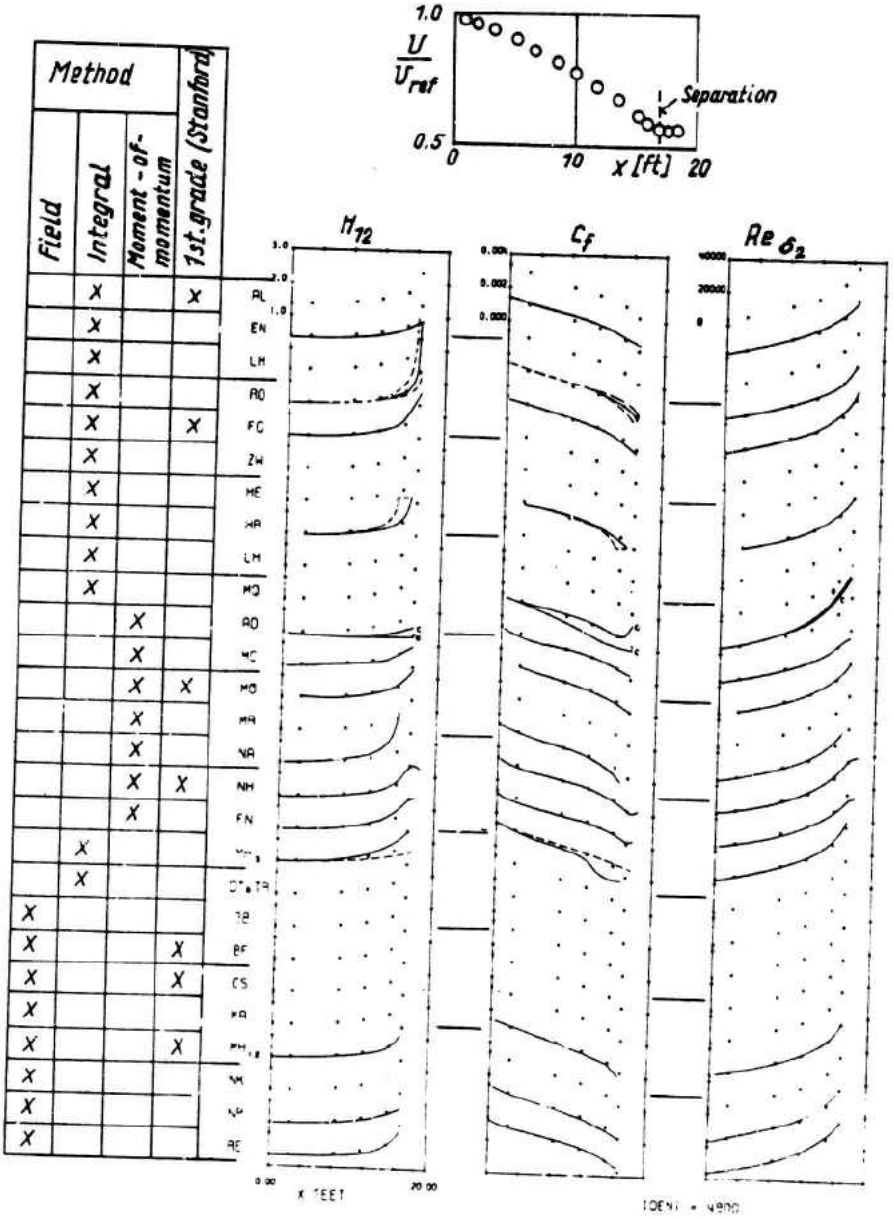

Figure A.16.
Results of different boundary Layer calculation methods applied to the experimental case of Schubauer and Spangenberg [110] as presented at the Stanford Conference [2, 3]

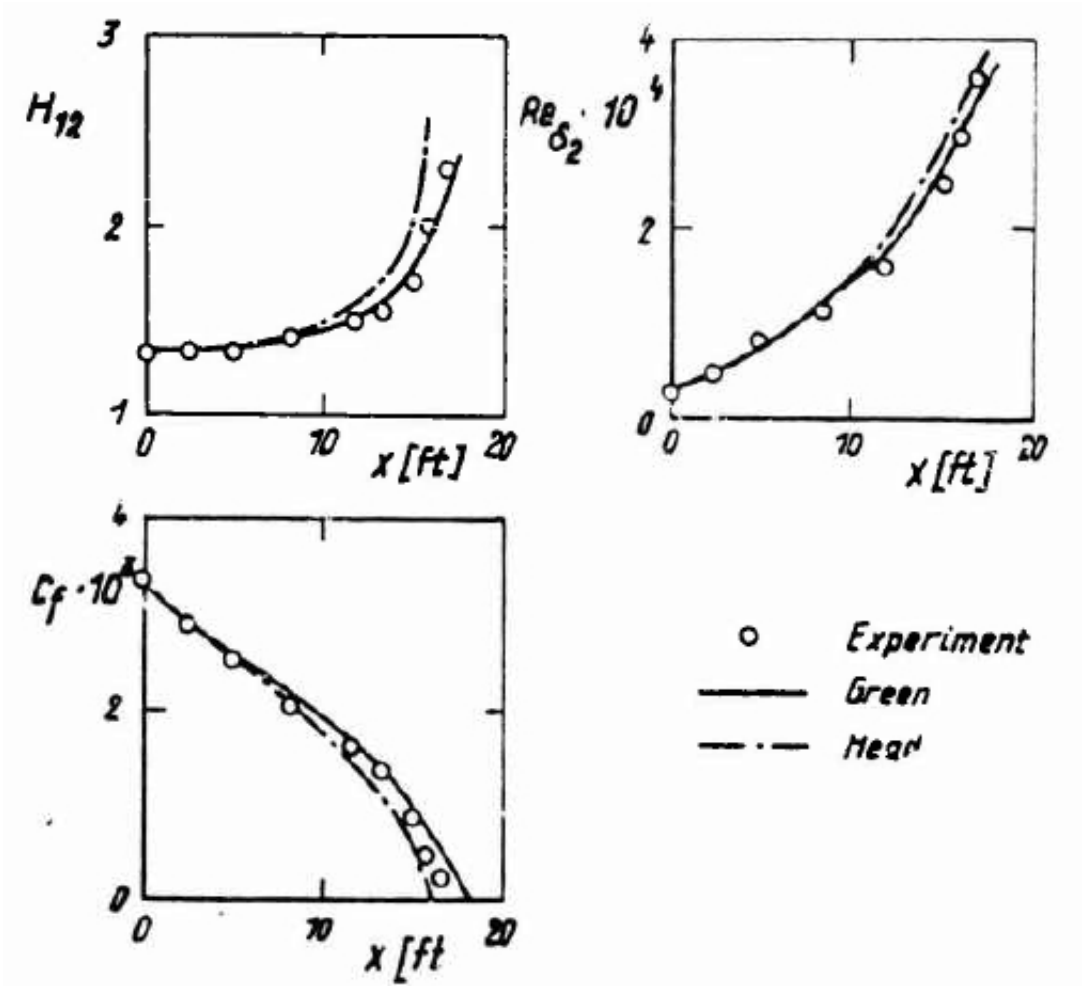

Figure A.17.
Results of the calculation method of Green et al. [52] and Head [56] applied to the experimental case of Schubauer and Spangenberg [110]

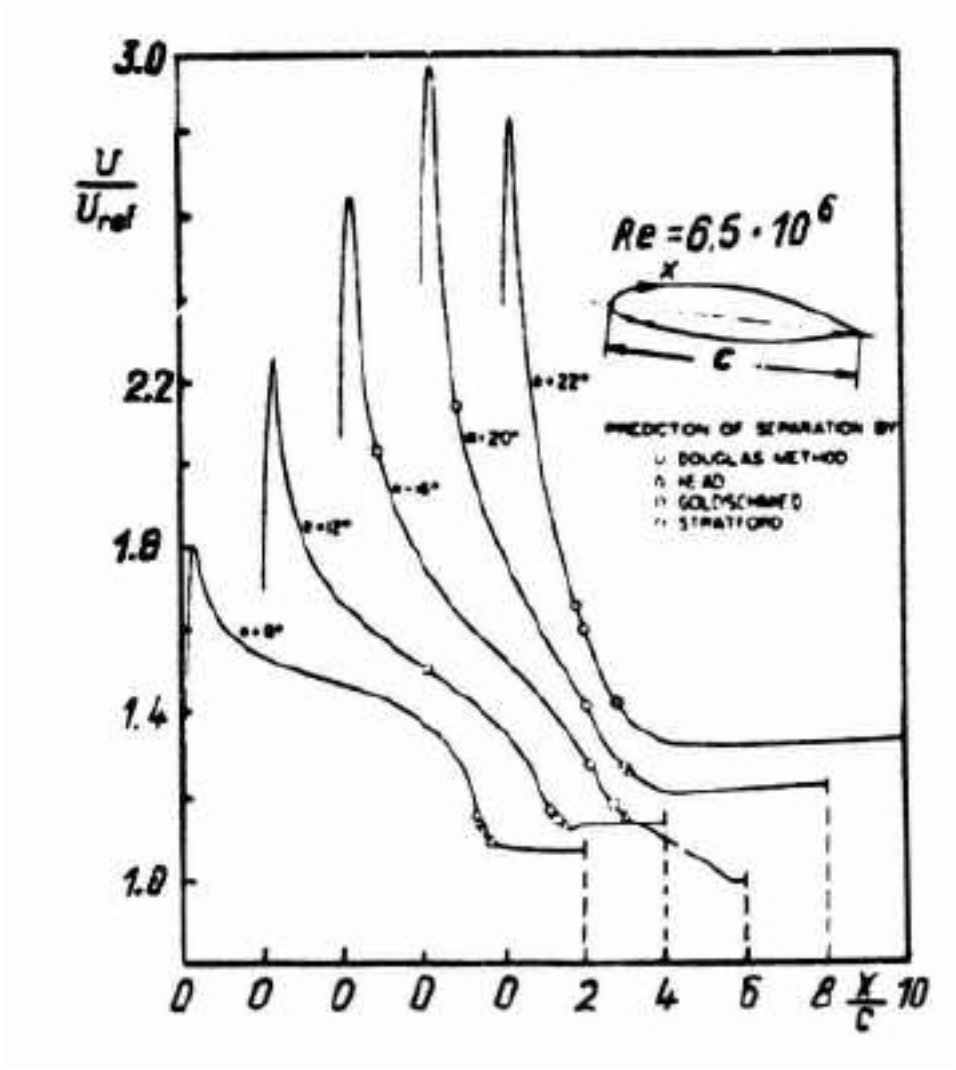

Figure A.18.
Predicted separation points for the experimental pressure distribution on the NACA 662-420 airfoil, from [21]

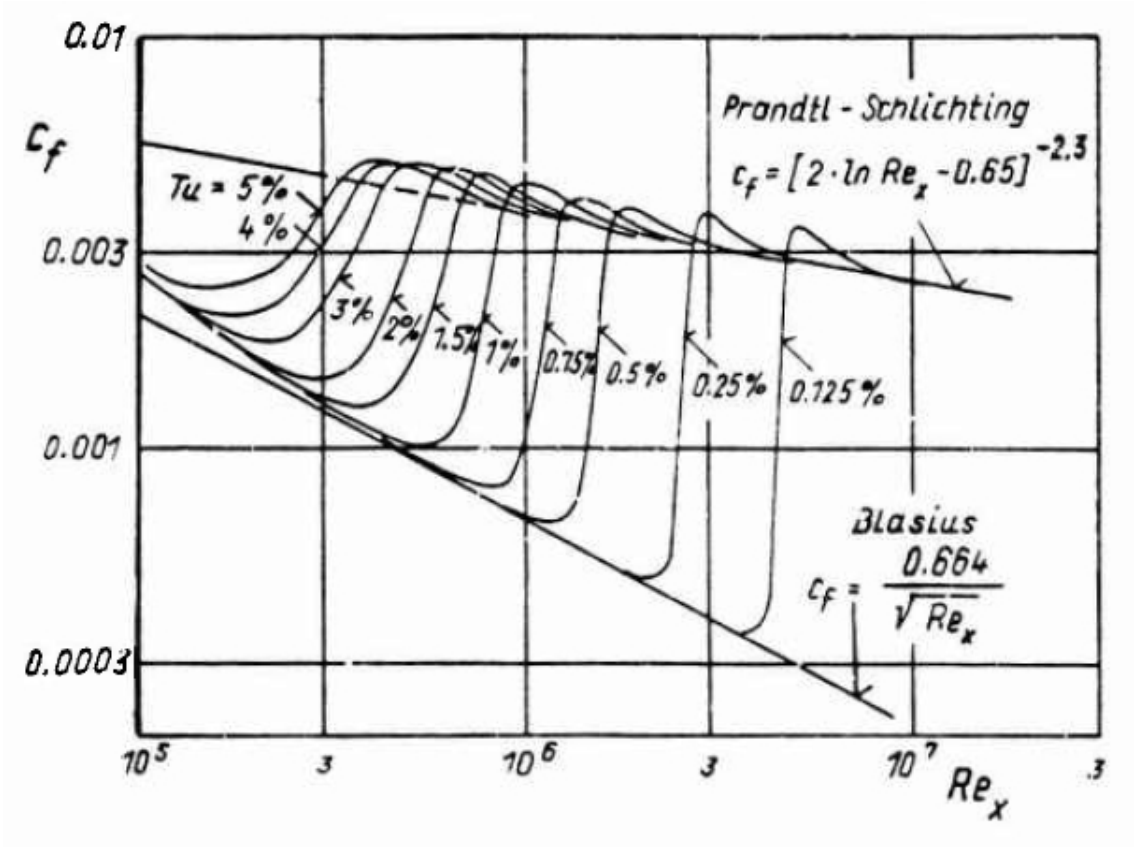

Figure A.19.
Calculated skin-friction coefficient of the transitional flat plate boundary layer for different levels of free-stream turbulence, from [55]

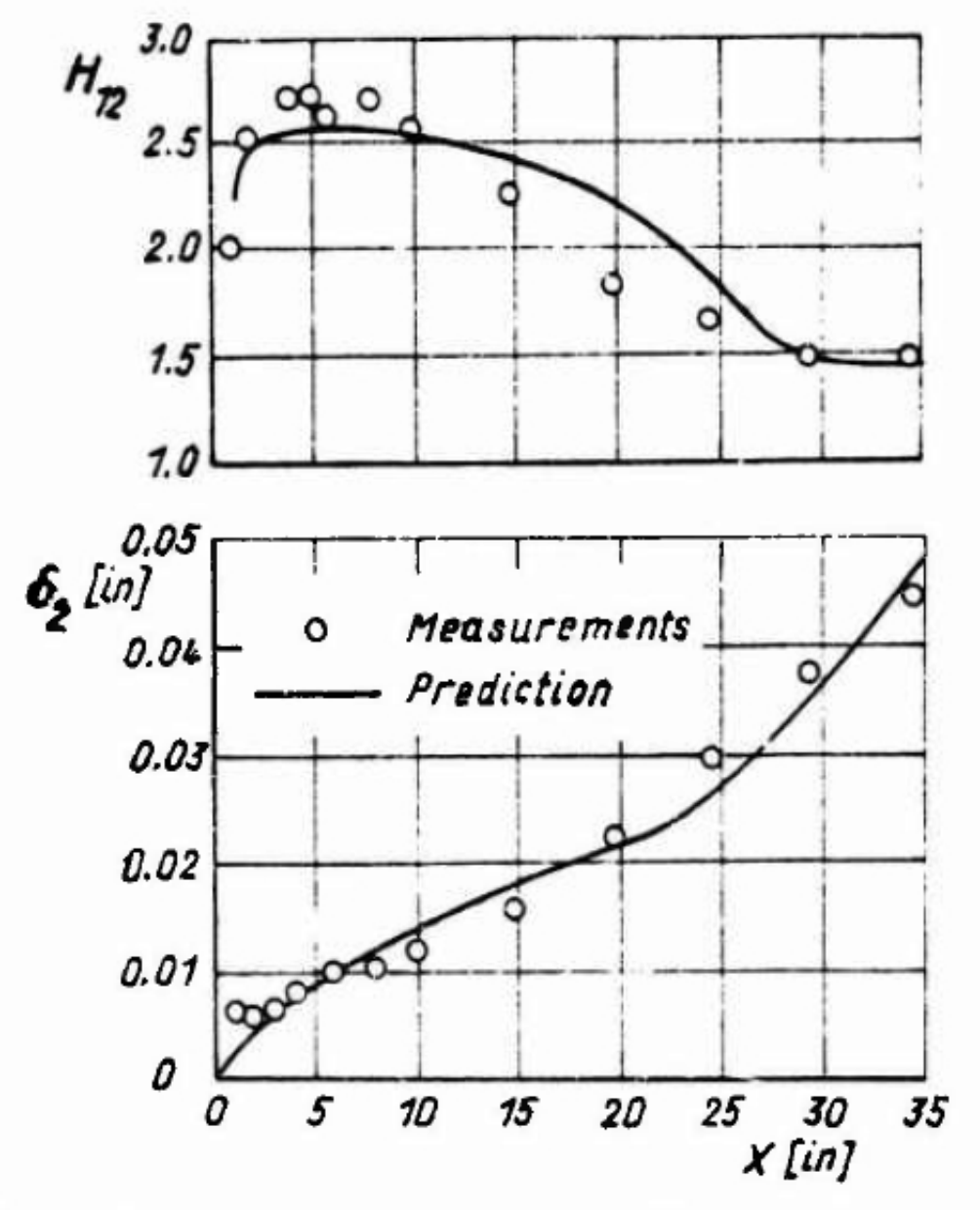

Figure A.20.
Calculated shape parameter and momentum thickness of a transitional boundary layer in comparison with measurements, from [77]

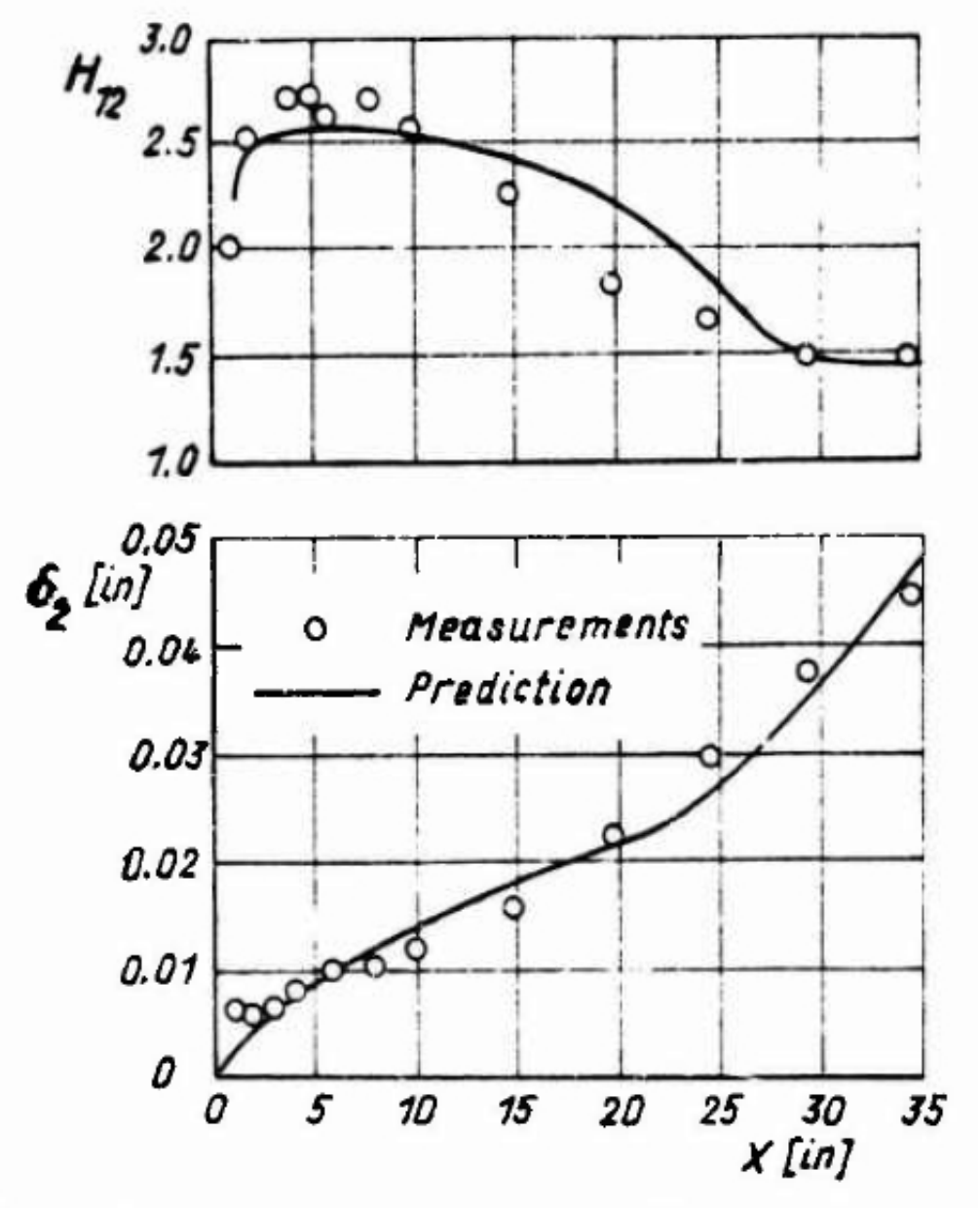

Figure A.21.
Geometry and measured pressure distribution for waisted body of revolution, after Winter at al. [140]

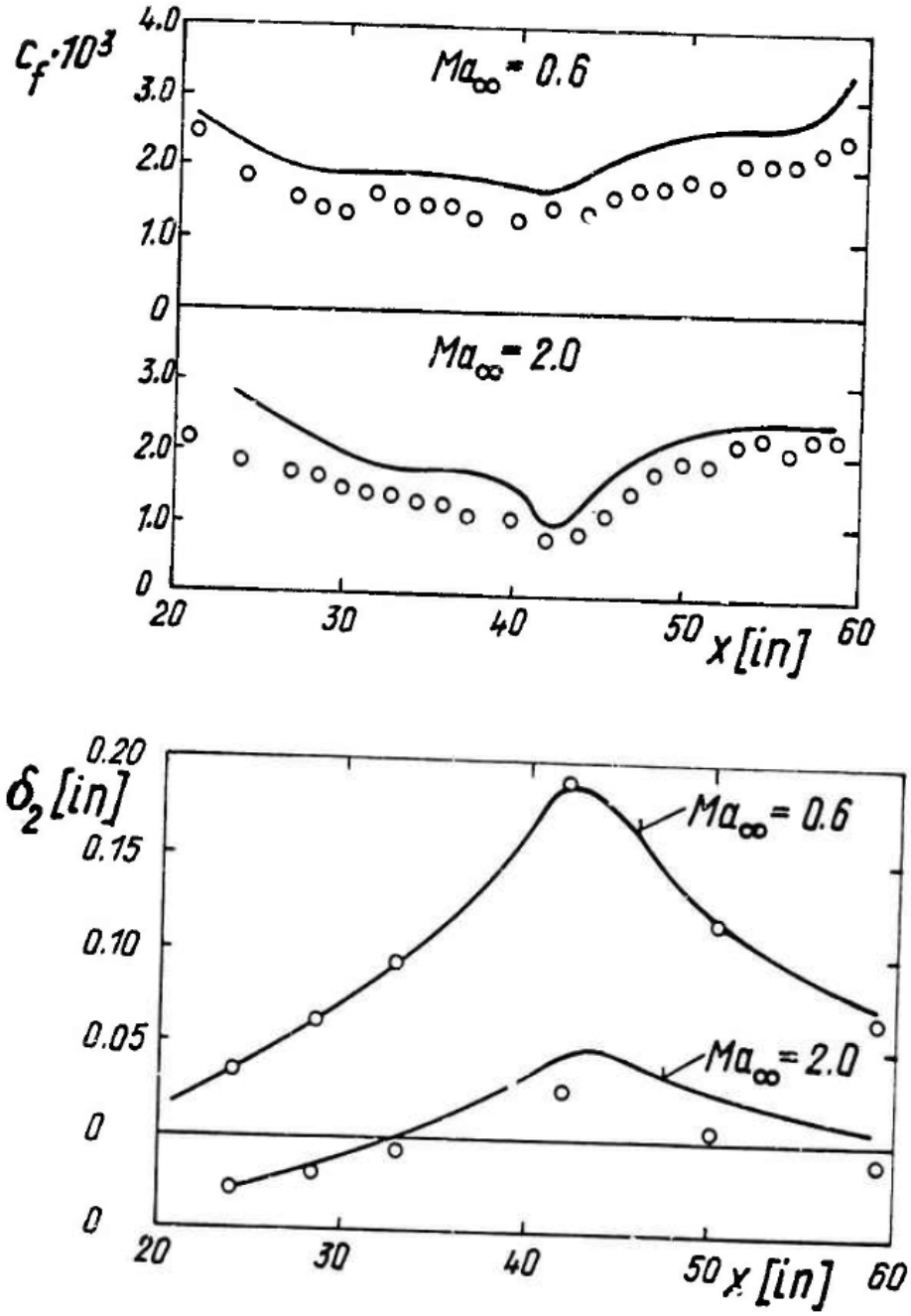

Figure A.22.
Comparison between the distributions of skin friction and momentum thickness as measured by Winter et a1. [140] and the predicted distributions as calculated by the complete field method of Herring and Mellor [58]

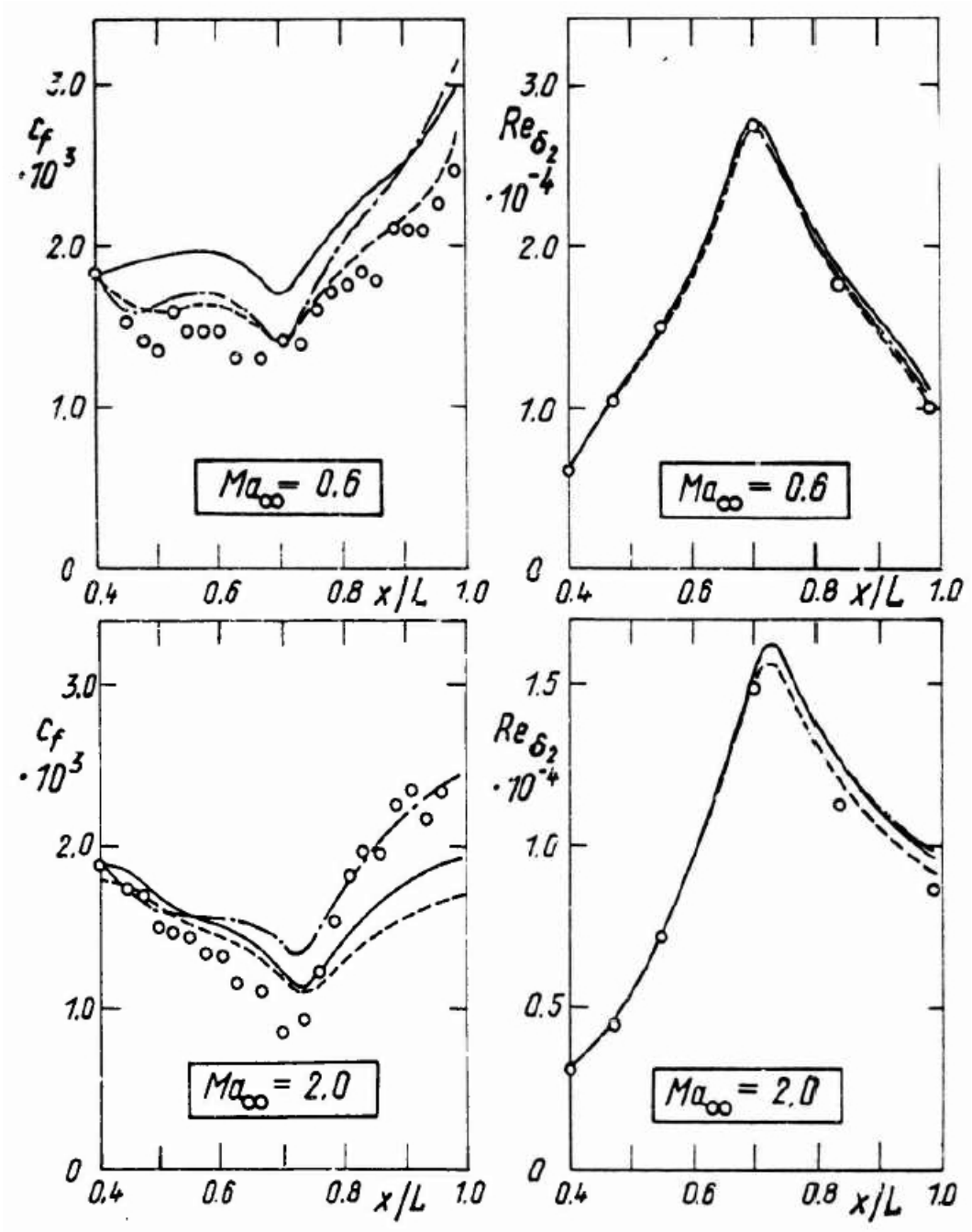

Figure A.23.
Comparison between the distributions of skin friction and momentum thickness Reynolds number as measured by Winter et al. [140] and the predicted distributions as calculated by the methods of Head [56] and Green et al. [52] including secondary effects

– – – – – *Head*
– · – · – · – *Green, corrected for longitudinal curvature, lateral strain, and dilatation*
——◯—— *Green, quasi two-dimensional*
◯ *experimental*

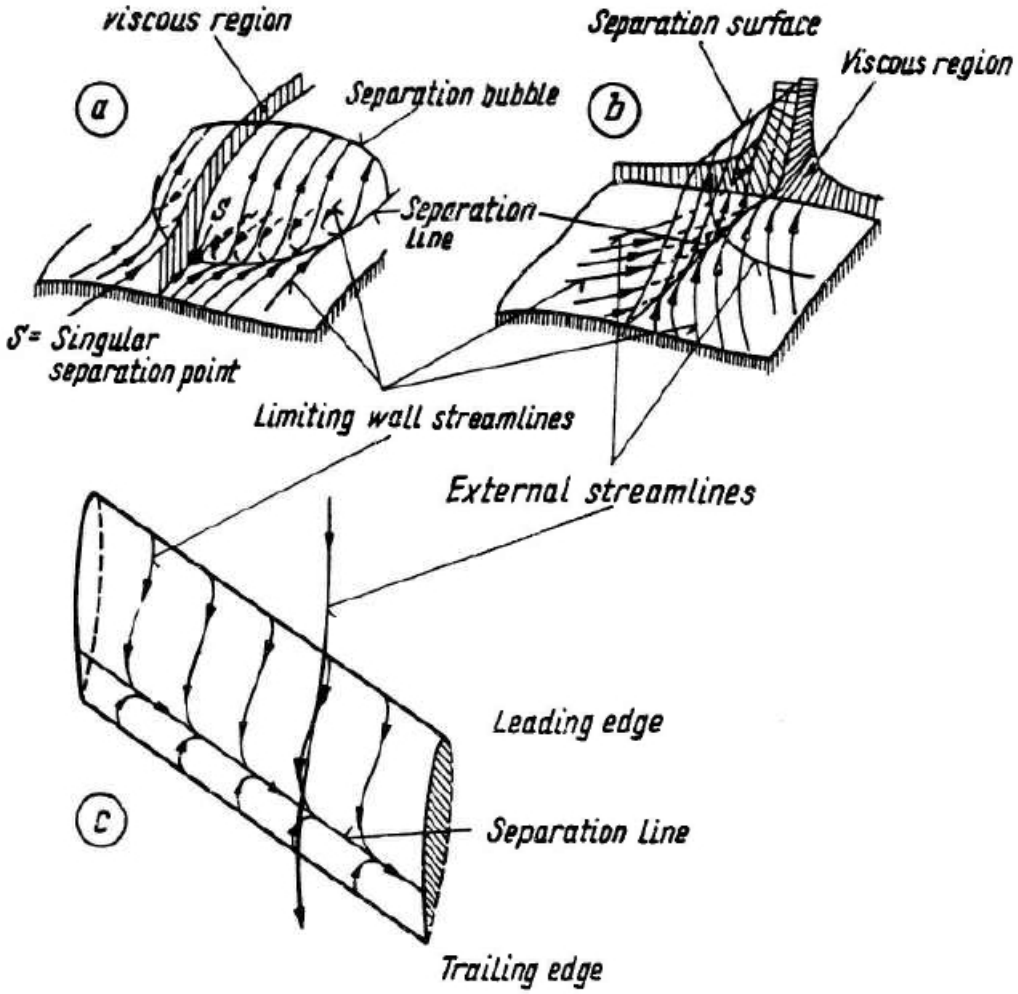

Figure A.24.

Patterns of three-dimensional boundary-layer separation: (a) separation with a singular point S, (b) separation from a line of confluent limiting wall streamline, (c) separation on a yawed infinite wing

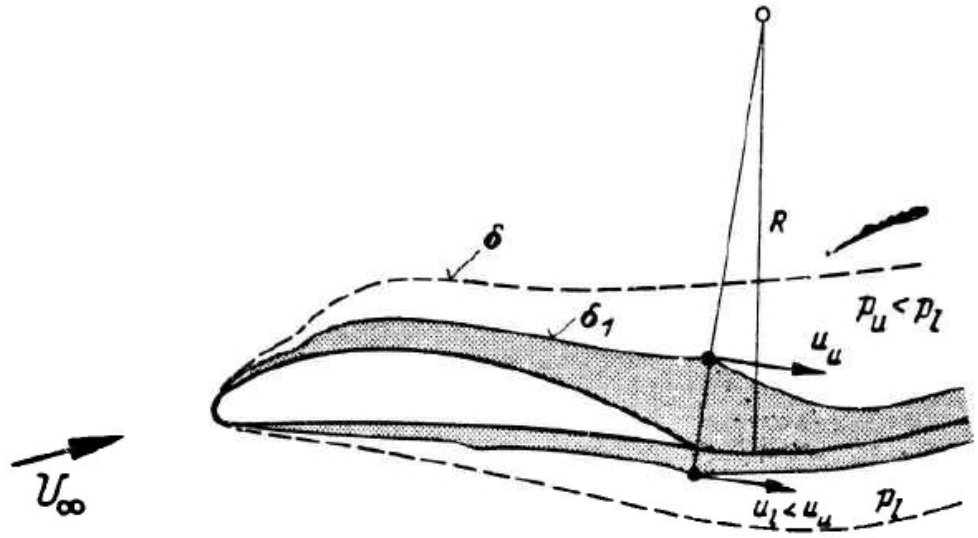

Figure A.25.
Sketch illustrating curvature effect of trailing edge wake on the external velocities and pressures

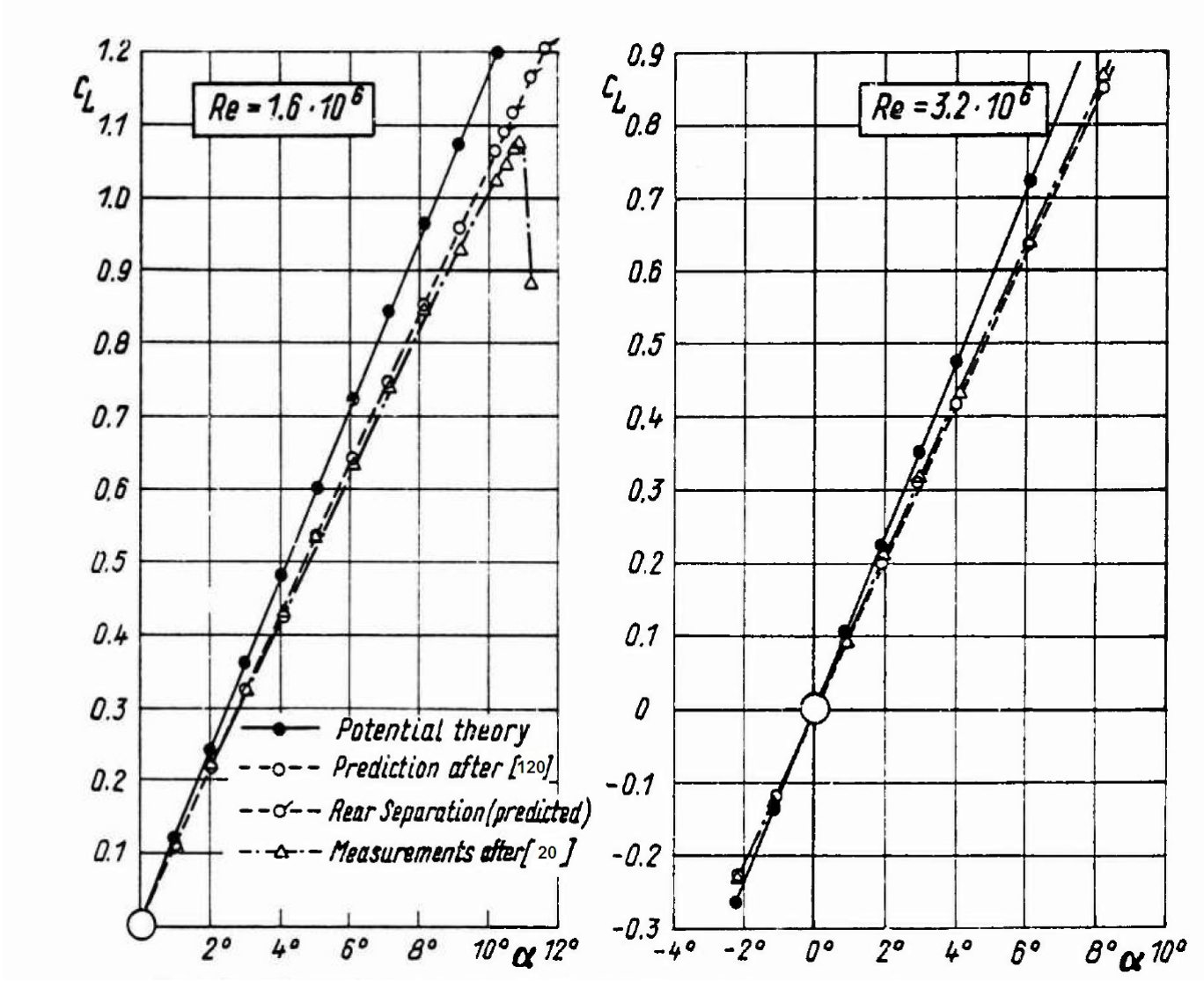

Figure A.26.
Lift coefficient of the RAE 101-airfoil vs. incidence. Comparison between calculations after [120] and experiments after [20]

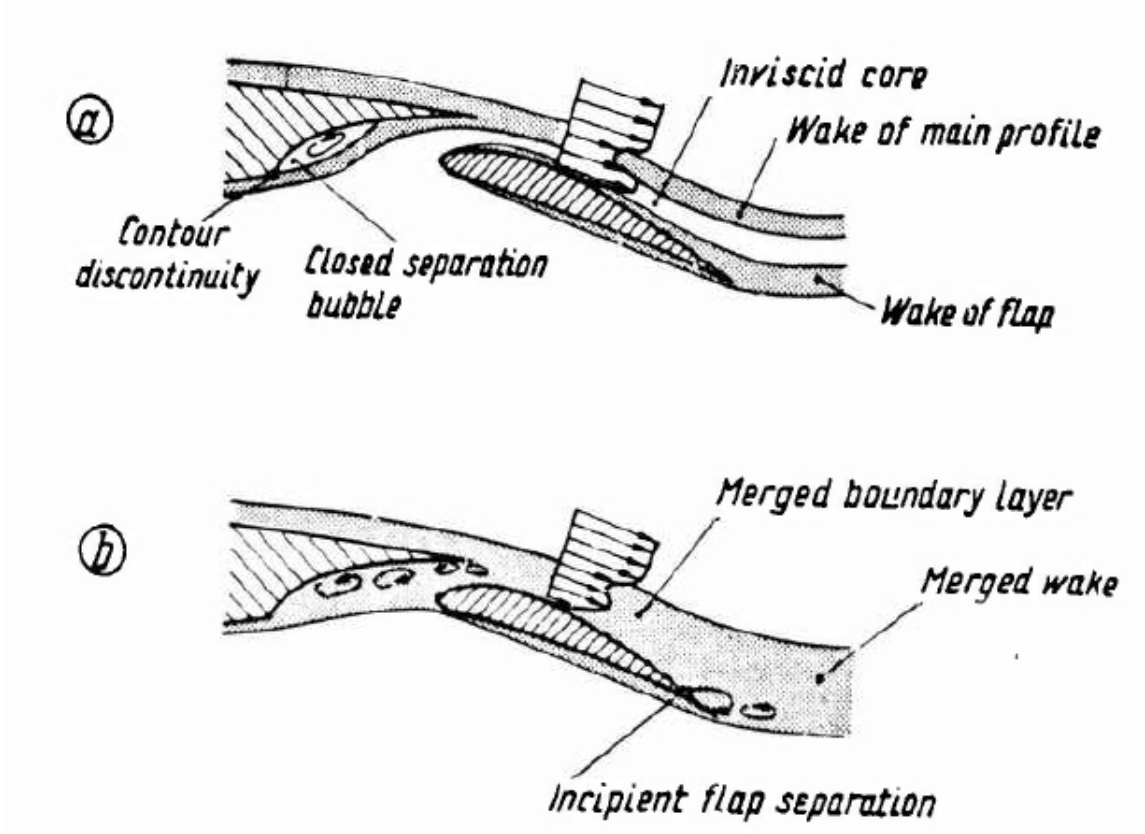

Figure A.27.
Illustration of the qualitative behavior of the viscous flow through the flap slot of a flapped airfoil: ⓐ favorable, ⓑ unfavorable flow situation

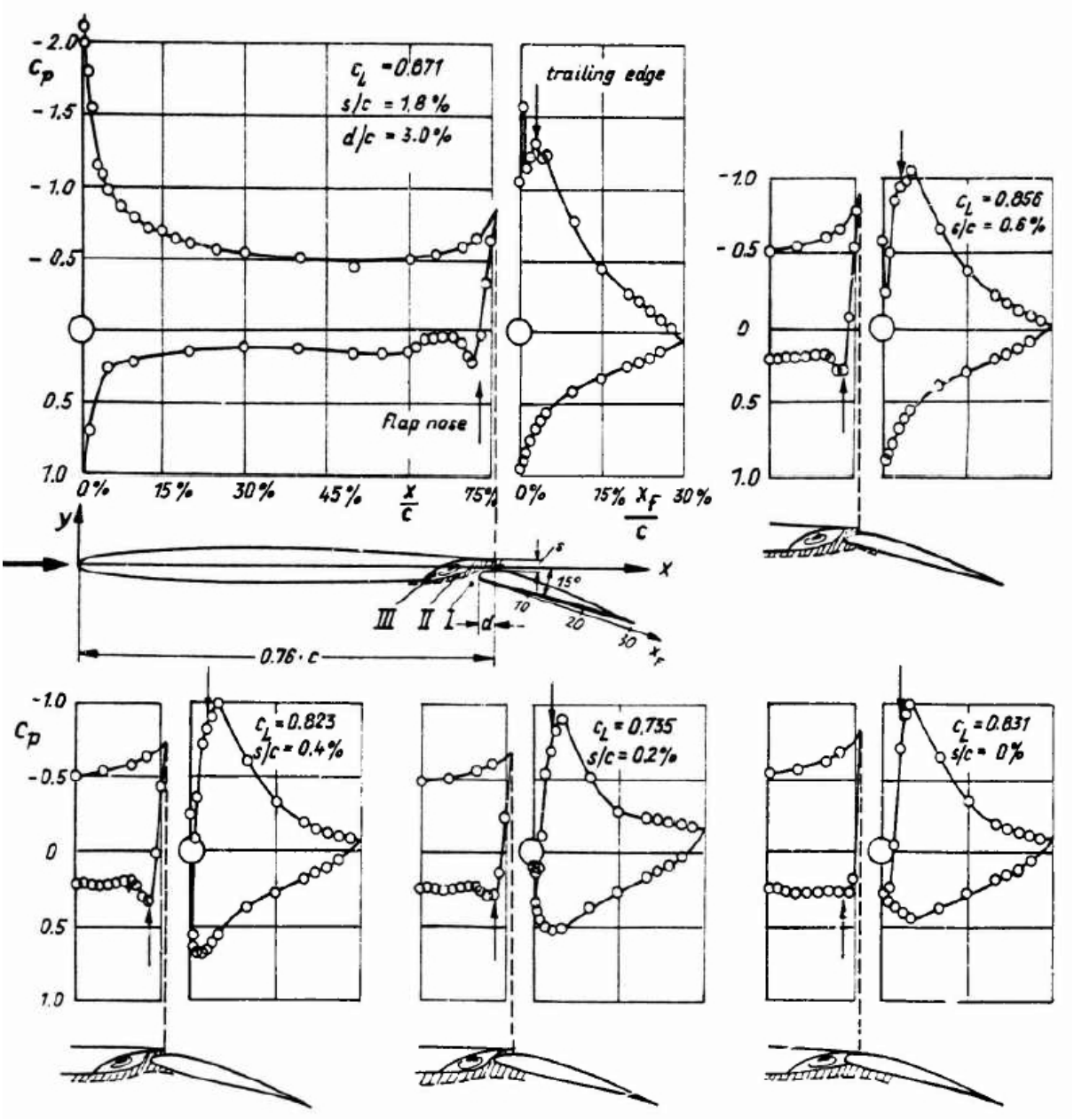

Figure A.28.
Effect of gap width on the pressure distribution over a flapped NACA 0006-airfoil at zero incidence and 15° *flap deflection as measured by Schröder [108].*
(I: region or irrotational inviscid flow, II: region of detached rotational flow, III: region of closed recirculating flow)

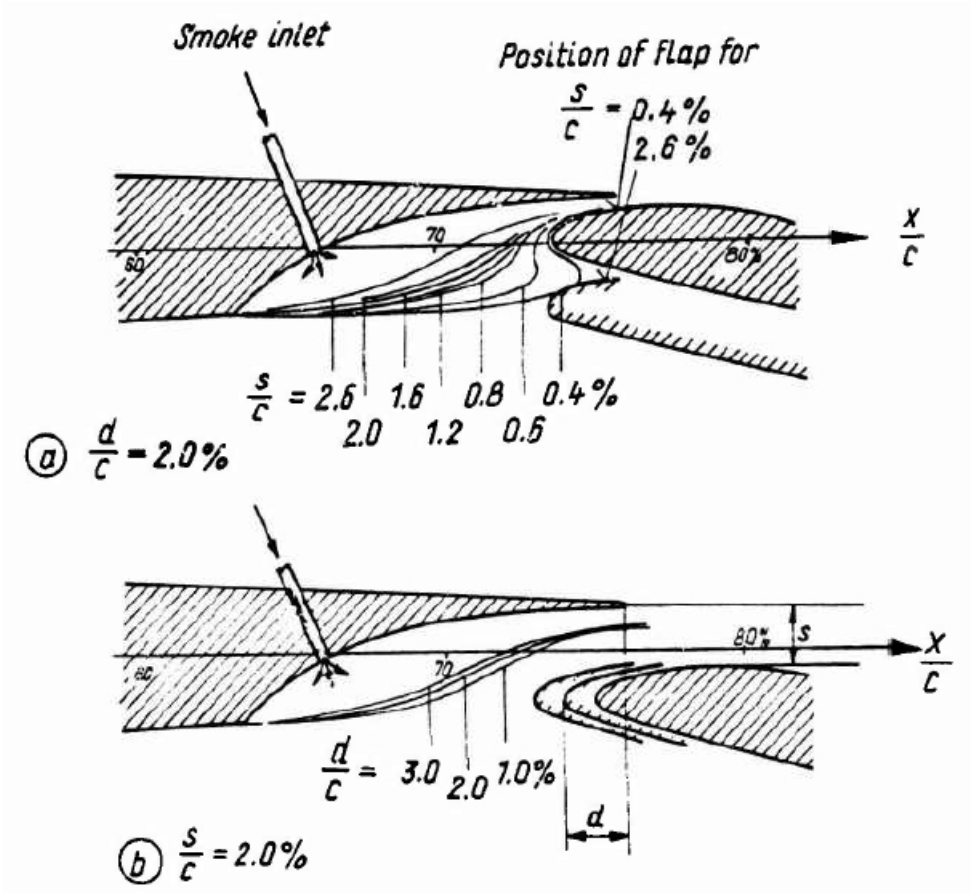

Figure A.29.
Smoke contour lines derived from flow visualization pictures in the slot region of a flapped NACA 0006-airfoil, from [108]: ⓐ for varying gap width s at constant overlap d, ⓑ for varying overlap d at constant gap width s

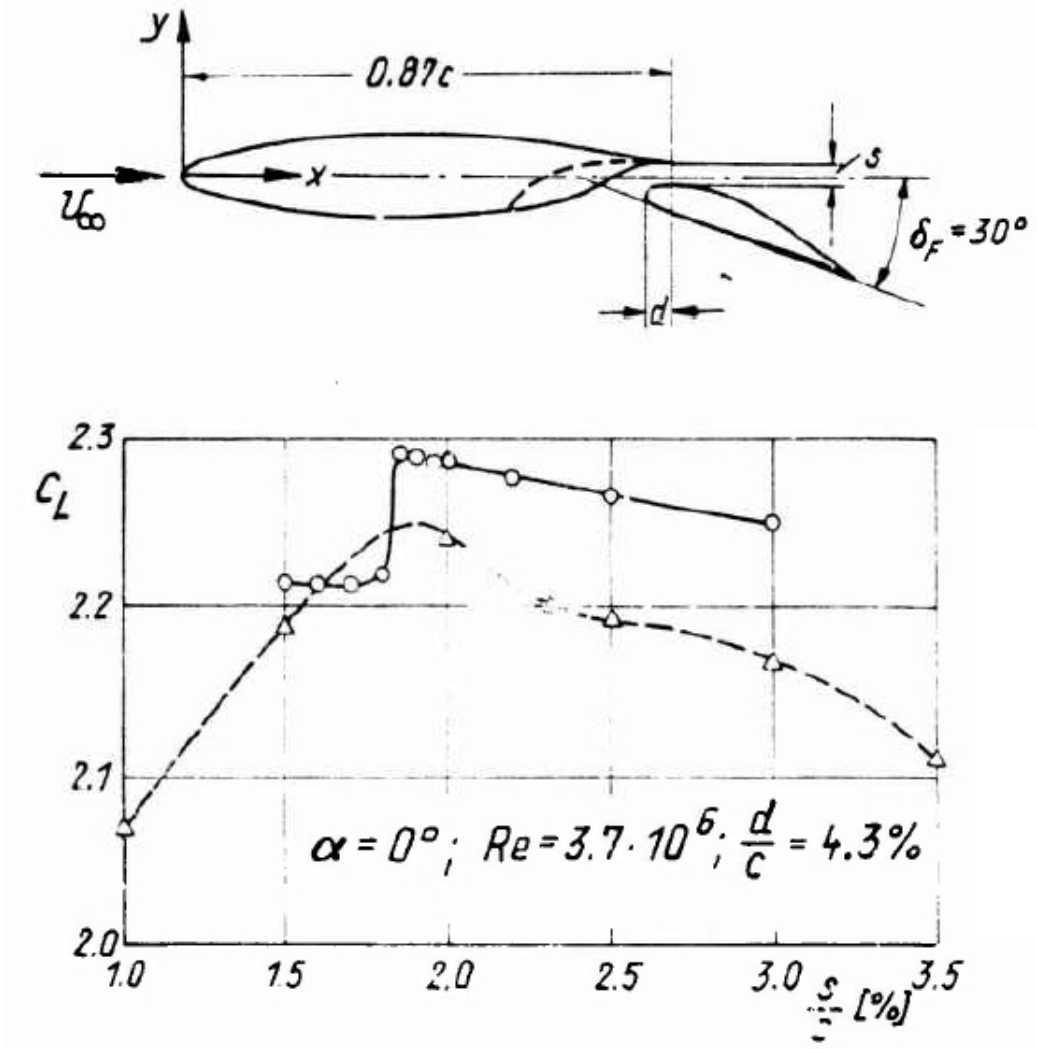

Figure A.30.
Comparison of measured [41] and calculated [120] lift coefficients showing the effect of varying gap width s at constant overlap d for a flapped NPL 3111-airfoil.
– – – △ – – – *experimental*
——◯—— *calculation*
(Note that the experiments were carried out with the broken line contour while in the calculations the solid line contour was used)

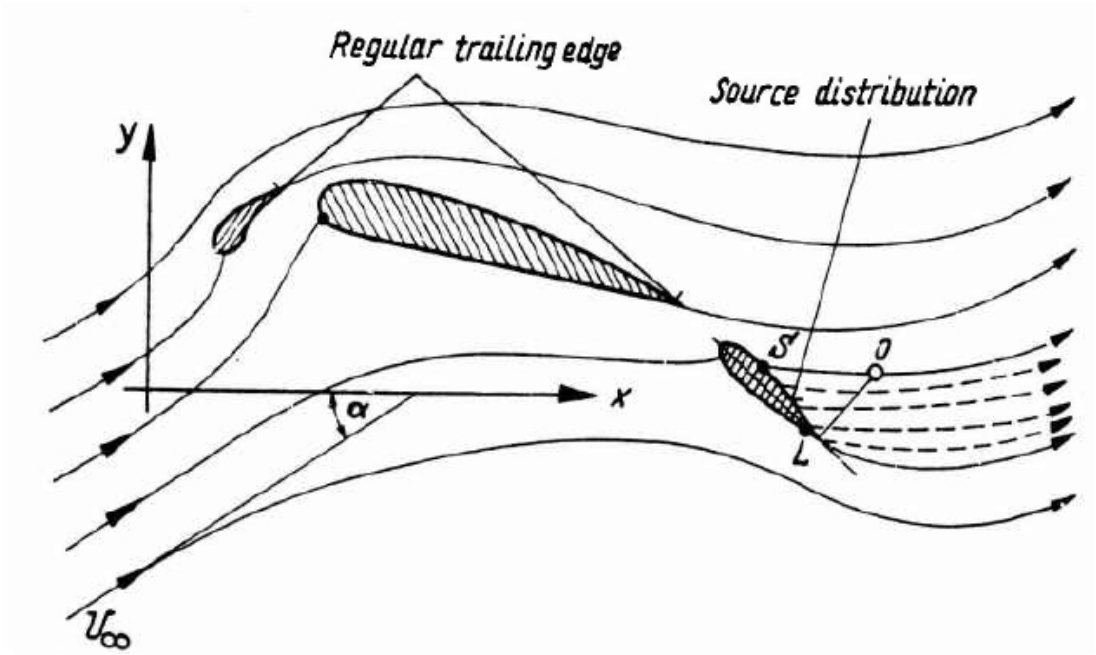

Figure A.31.
Theoretical model of the two-dimensional flow over an airfoil with slat and flap simulated by an additional source flow over the separated region according to Jacob [63]

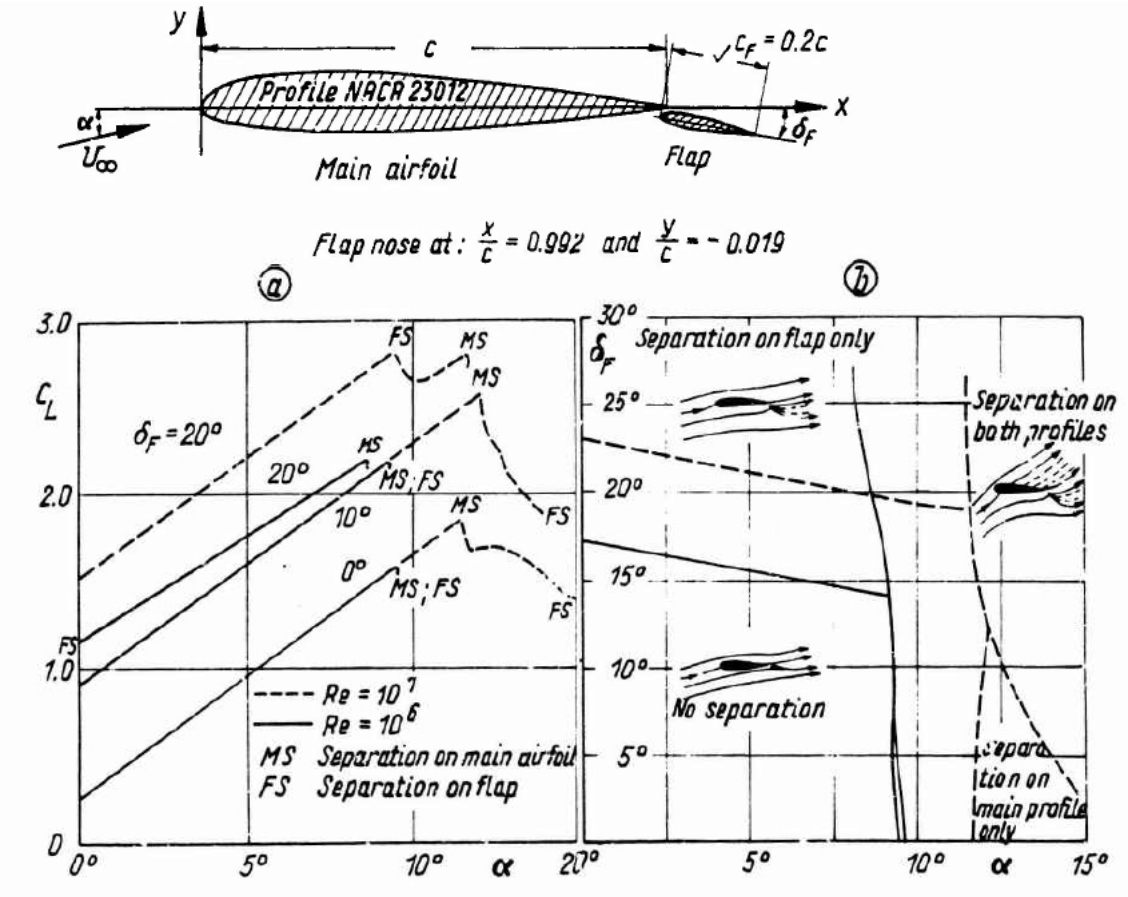

Figure A.32.
Calculated separation characteristics of a NACA 23012-airfoil with flap at two different Reynolds numbers: ⓐ lift coefficient vs. incidence for constant flap deflection, ⓑ limits of flow types dependent on incidence and flap deflection, from [63]

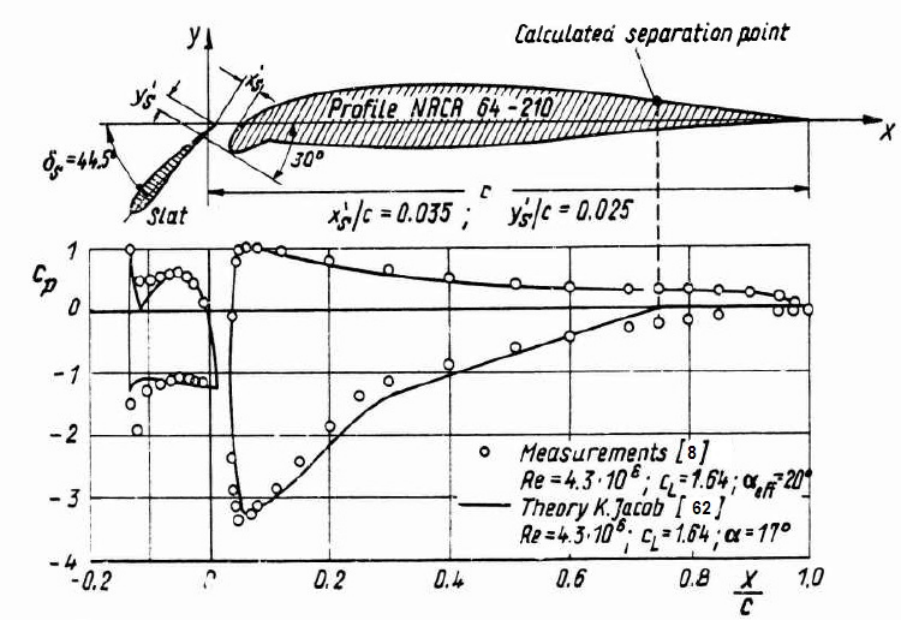

Figure A.33.
Calculated and measured pressure distribution on a slatted NACA 64-210-airfoil with drooped nose, from [63]

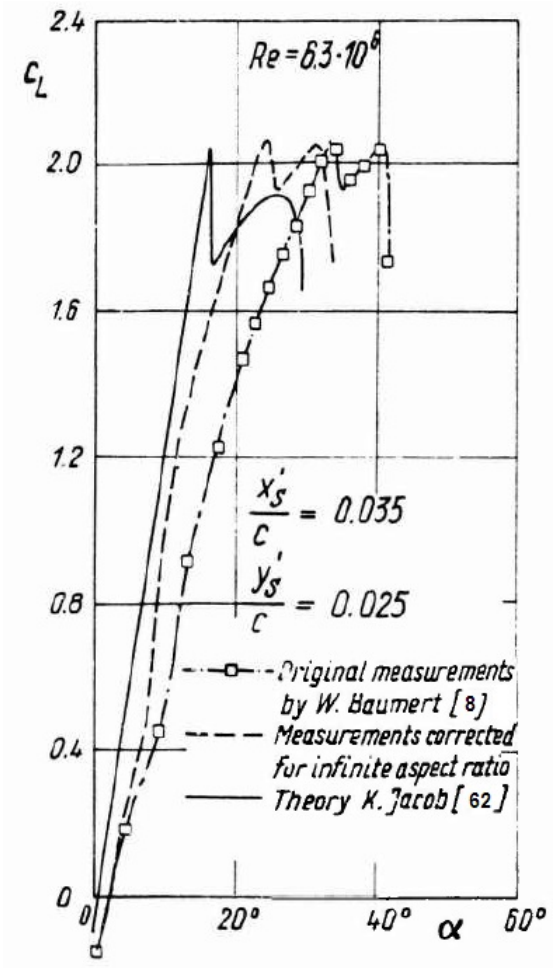

Figure A.34.
Comparison between measured and calculated lift- vs. incidence-curves of a slatted NACA 64-210-airfoil with drooped nose, from [63]

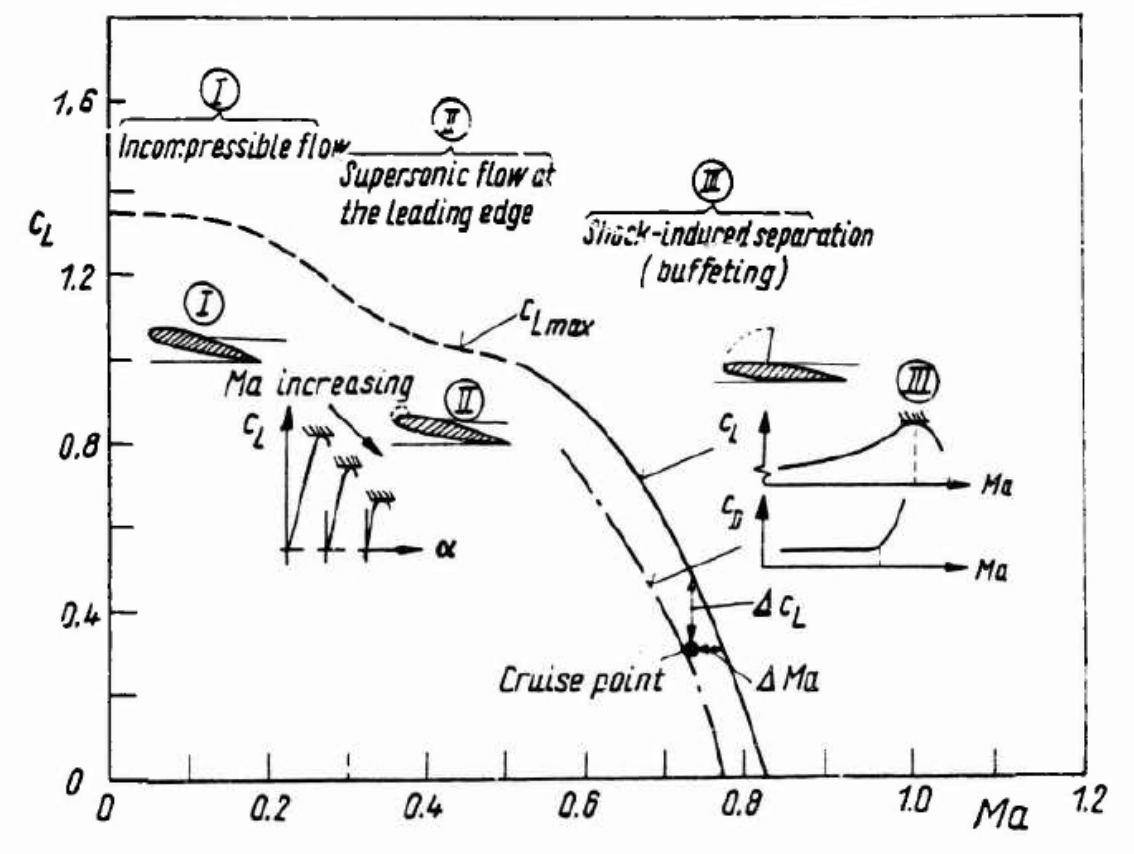

Figure A.35.
Dependence of maximum lift on Mach number and associated separation phenomena

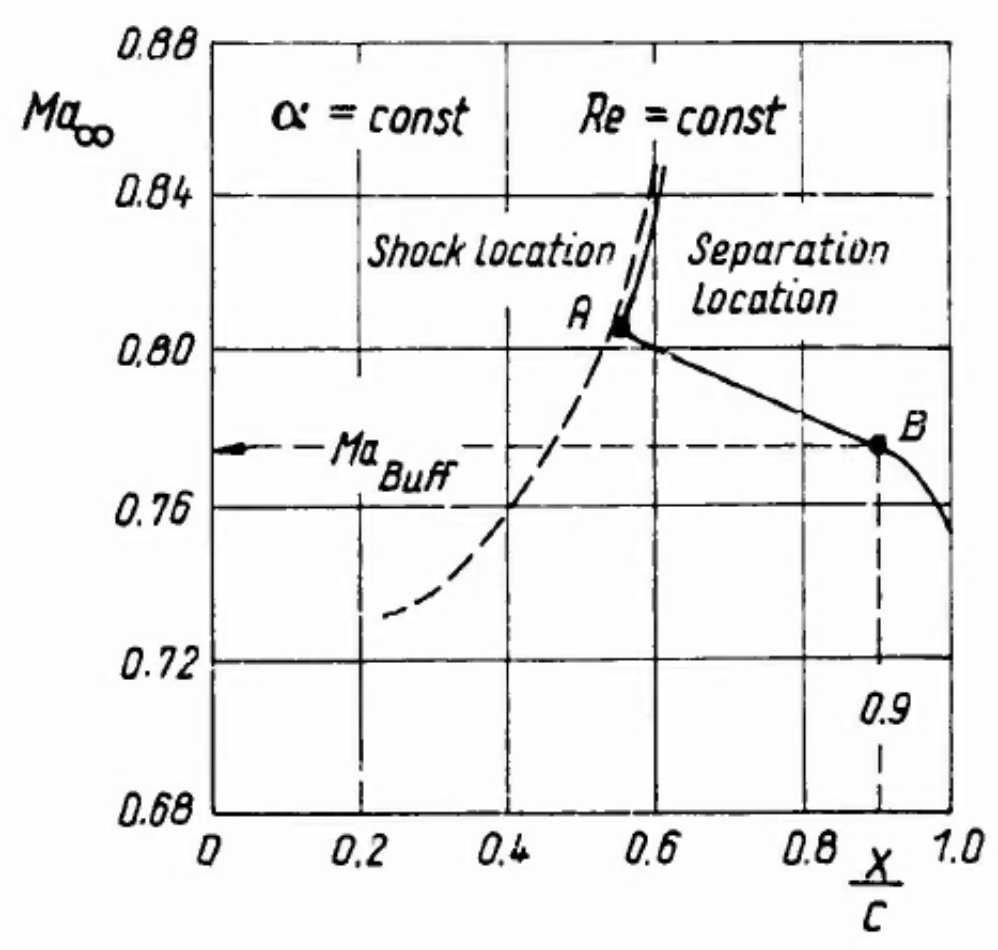

Figure A.36.
Chordwise location of normal shock and separation point depending on Nach number on a transonic wing section (schematically), point ***A*** *indicates separation immediately behind shock, point* ***B*** *explains 90 %-chord criterion of Thomas [124] for buffet-onset*

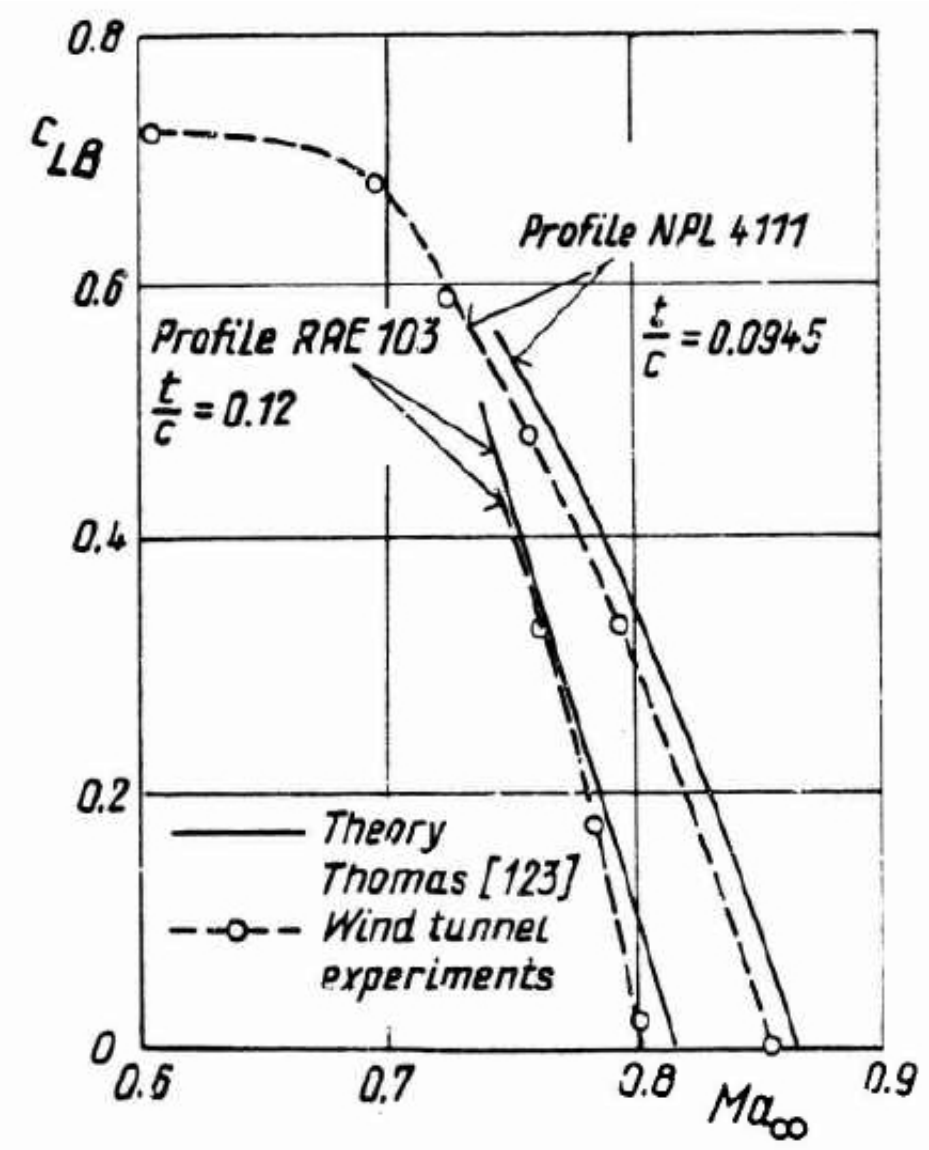

Figure A.37.
Comparison of experimentally determined buffet boundaries with the theoretical predictions after the method of Thomas [123] for two different wing sections

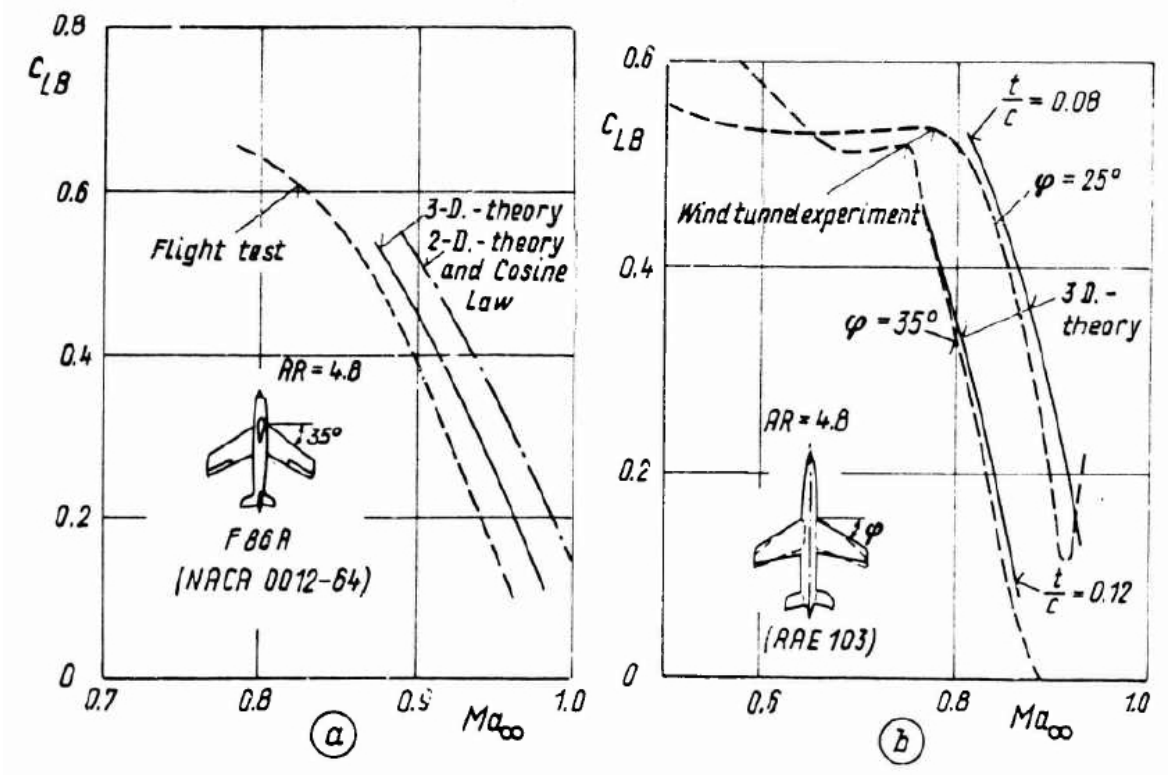

Figure A.38.
Comparison of experimentally determined buffet boundaries with theoretical predictions
ⓐ *for the fighter aircraft T-86A in flight test [42] at* $Re = 10^7$,
ⓑ *for a variable sweep wind tunnel model [131] at* $Re = 1,3 \cdot 10^6$, *from [98]*

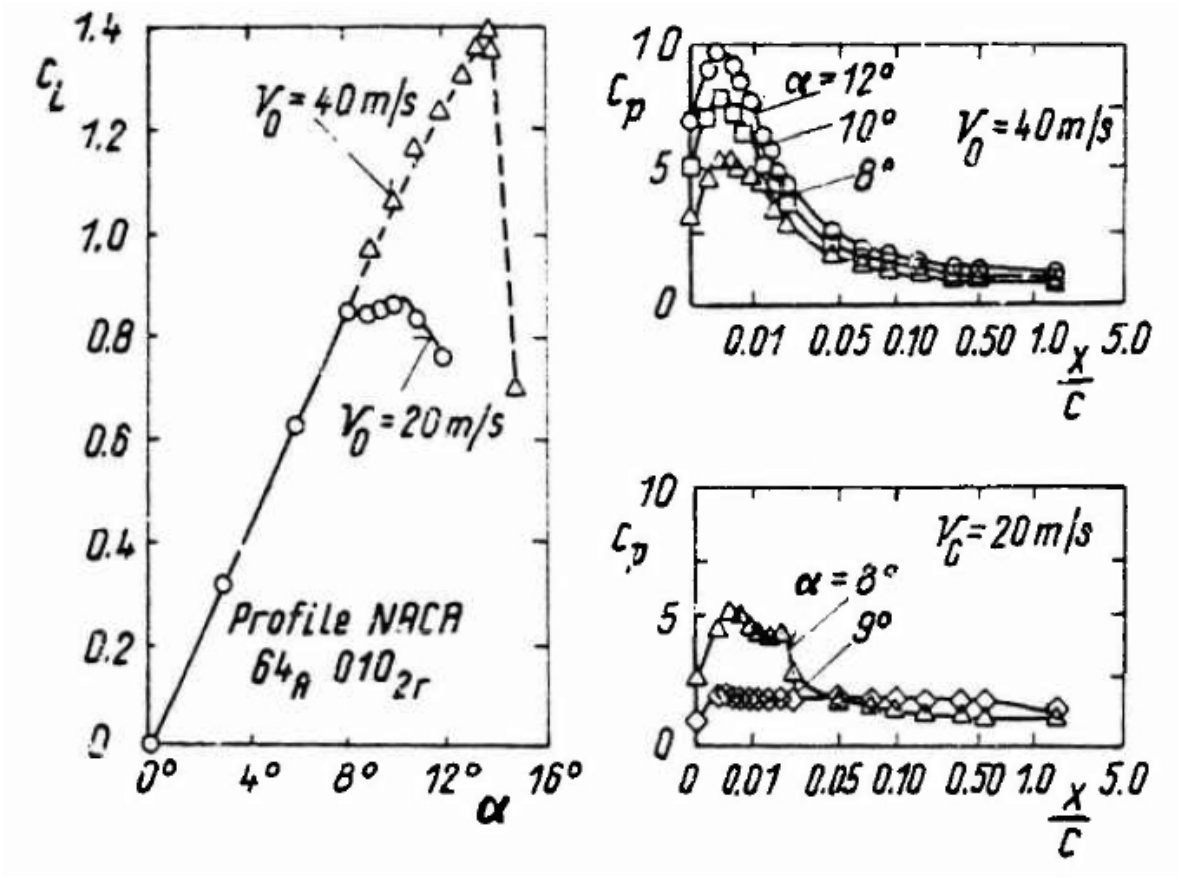

Figure A.39.
Experimental lift- vs. incidence-curve and pressure distributions in the presence of short and long bubbles, from [54]

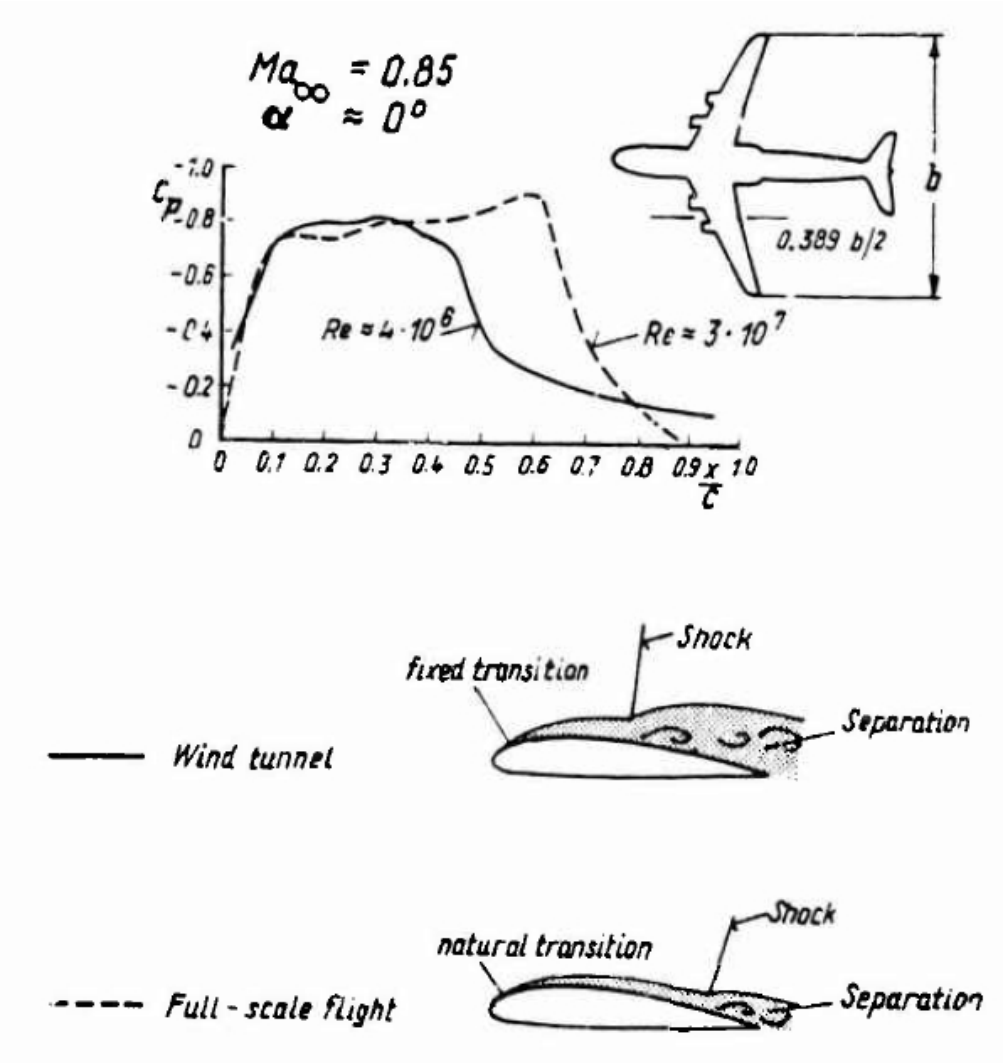

Figure A.40.
Scale effect on a transport aircraft, from [72]

List of Symbols

Re	Reynolds Number	-
Ma	Mach Number	-
α	angle of the body to the flow	$^\circ$
c_L	lift coefficient	-
c_M	pitching moment	N s
c_D	profile drag	-
c_f	local skin friction parameter	-
c_F	overall skin friction coefficient	-
δ	boundary-layer thickness	m
δ_2	momentum thickness	m
ϵ	turbulent exchange coefficient	m^2/s^3
v_e	entrainment rate	-
h_S	slat gap	m
$H_{1,2}\, H_{3,2}$	boundary-layer thickness ratio	-
$\mathscr{K}$	von Kármán constant	-
$\mathbf{k}$	turbulent kinetic energy	m^2/s^2
$\mathscr{L}$	characteristic length, e.g. length of an eddy or aircraft fuselage	m
ℓ	mixing length	m
p	pressure of the fluid	Pa
ρ	density of the surrounding fluid	kg/m^3
τ_w	wall shear stress	Pa
$u\, v\, w$	velocities in x, y and z direction along the boundary	m/s
$x\, y\, z$	coordinates in euclidian space	m
$u'\, v'\, w'$	fluctuating component of velocity	m/s
$\overline{u'}\, \overline{v'}\, \overline{w'}$	mean fluctuating component of velocity	m/s
η	dynamic viscosity of the fluid	Pa s
ν	kinematic viscosity	m^2/s
$U(x)$	undisturbed mean flow velocity (outside the boundary layer)	m/s

Bibliography

[1] Detailed exploration of the compressible, viscous flow over two-dimensional aerofoils at high reynolds numbers. volume 68 of *ICAS Paper*, page 11, New York, 1968. International Council of the Aeronautical Sciences.

[2] A morphology of the prediction methods. In S.J. Kline, M.V. Morkovin, G. Sovran, and D.J. Cockrell, editors, *Stanford conference on computation of turbulent boundary layers*, volume 1, Stanford University, 1968. Air Force Office of Scientific Research-Internal Flow Program. Two Volume Set.

[3] A morphology of the prediction methods. In S.J. Kline, M.V. Morkovin, G. Sovran, and D.J. Cockrell, editors, *Stanford conference on computation of turbulent boundary layers*, volume 2, Stanford University, 1968. Air Force Office of Scientific Research-Internal Flow Program. Two Volume Set.

[4] D.E. Abbot and H.E. Bethel. Application of the galerkin-kantorovich-dorodnitsyn method of integral relations to the solutions of steady laminar boundary layers. *Ingenieur-Archiv*, 37(2):110–124, 1968.

[5] I.H. Abbot and A.E. v. Doenhoff. *Theory of Wing Sections: Including a Summary of Airfoil Data*. Dover, 1st edition, 1960.

[6] I.E. Alber. Application of an exact expression for the equilibrium dissipation integral to the calculation of turbulent nonequilibrium flows. In S.J. Kline, M.V. Morkovin, G. Sovran, and D.J. Cockrell, editors, *Stanford conference on computation of turbulent boundary layers*, volume 1, pages 126–135, Stanford University, 1968. Air Force Office of Scientific Research-Internal Flow Program. Two Volume Set.

[7] E. Bartelt. Klärung realisierbarer möglichkeiten des hochauftriebs. Technical report, Messerschmitt-Bölkow-Blohm.

[8] W. Baumert. Messungen an druckverteilungen und geschwindigkeitsprofilen an einem rechteckflügel mit vorflügel und abgesenkter nase. Technical Report 71C31 und 71C29, Göttingen Aerodynamische Versuchsanstalt, 1971.

[9] I.E. Beckwith. *Recent advances in research on compressible turbulent boundary layers*, chapter Analytic methods in aircraft aerodynamics, pages 355–416. Number SP-228. National Aeronautics and Space Administration (NASA), 1970.

[10] I.E. Beckwith and D.M. Bushnell. Calculation of mean and fluctuating properties of the incompressible turbulent boundary layer. In S.J. Kline, M.V. Morkovin, G. Sovran, and D.J. Cockrell, editors, *Stanford conference on computation of turbulent boundary layers*, volume 1, pages 275–299, Stanford University, 1968. Air Force Office of Scientific Research-Internal Flow Program. Two Volume Set.

[11] R. Betchov and W.O. Criminale. *Stability of parallel flows*, volume 10 of *Applied Mathe- matics and Mechanics*. Academic Press, New York / London, 1st edition, 1967.

[12] I.C. Bhateley and R.G. Bradley. A simplified mathematical model for the analysis of multi-element airfoils near stall. In *Fluid Dynamics of Aircraft Stalling*, Neuilly sur Seine, France. AGARD - Advisory Group for Aerospace Research & Development. AGRARD-CP-102.

[13] F.G. Blottner. Finite difference methods of solution of the boundary-layer equations. *AIAA Journal*, 8(2):193–205, 1970.

[14] P. Bradshaw. Part 2: Calculation of boundary layer development using the turbulent energy equation. Technical Report Lecture Series 5, The Von Karman Institute for Fluid Dynamics, Sint-Genesius-Rode, Belgium, 1968.

[15] P. Bradshaw. Calculation of three-dimensional turbulent boundary layers. *Journal of Fluid Mechanics*, 46(3):417–445, 1971.

[16] P. Bradshaw. The understanding and prediction of turbulent flow. *Aeronautical Journal*, 76:403–418, 1972.

[17] P. Bradshaw. Advances in turbulent shear flows. Technical report, The Von Karman Institute for Fluid Dynamics, Sint-Genesius-Rode, Belgium, 1973.

[18] P. Bradshaw. Effects of streamline curvature on turbulent flow. AGARDOgraph, page 131, Neuilly sur Seine, France, 1973. AGARD - Advisory Group for Aerospace Research & Development. AGARD-AG-169.

[19] P. Bradshaw, D.H. Ferris, and N.P. Atwell. Calculation of turbulent boundary layer development using the turbulent energy equation. *Journal of Fluid Mechanics*, 28(3):593–616, 1967.

[20] G.G. Brebner and J.A. Bagley. Pressure and boundary-layer measurements on a two-dimensional wing at low speed. Technical Report 2886, Aeronautical Research Council, London (England), 1952.

[21] T. Cebeci, G.J. Mosinskis, and A.M.O. Smith. Calculation of separation points in incompressible turbulent flows. *Journal of Aircraft*, 9(9):618–624, 1972.

[22] K.K. Chen and N.A. Thyson. Extension of emmons' spot theory to flows on blunt bodies. *AIAA Journal*, 9(5):821–825, 1971.

[23] D. Coles. Measurements in the boundary layer on a smooth flat plate in supersonic flow. Technical Report 20-69, Jet Propulsion Laboratory, 1953.

[24] D. Coles. The law of the wake in the turbulent boundary layer. *Journal of Fluid Mechanics*, 1(2):191–226, 1956.

[25] L.F. Crabtree. The formation of regions of separated flows on wing surfaces. Technical Report 3122, Aeronautical Research Council, London (England), 1959.

[26] N.A. Cumpsty and M.R. Head. The calculation of three-dimensional turbulent boundary layers. part 1: Flow over the rear of an infinite swept wing. *The Aeronautical quarterly*, 18:55–84, 1969.

[27] N.A. Cumsty and M.R. Head. The calculation of three-dimensional turbulent boundary layers. part 4: Comparison with measurements on the rear of a swept wing. *The Aeronautical quarterly*, 21:121–132, 1970.

[28] O. De Vries. Comments on the methods developed at nlr for conducting two-dimensional research on high-lift devices. In *Fluid Dynamics of Aircraft Stalling*, Neuilly sur Seine, France, 1972. AGARD - Advisory Group for Aerospace Research & Development. AGARD-CP-102.

[29] R.O. Dietz and et al. Report of the high reynolds number wind tunnel study group of the fluid dynamics panel. Technical report. AGARD-AR-35-71.

[30] J.L. East and F.J. Pierce. Explicit numerical solution of the three-dimensional incompressible turbulent boundary-layer equations. *AIAA Journal*, 10(9):1216–1223, 1972.

[31] E.A. Eichelbrenner. Three-dimensional turbulent boundary layers with heat transfer at the wall. *Physics of Fluids*, pages S157–S160, 1967. (Supplement).

[32] E.A. Eichelbrenner. Three-dimensional boundary layers. *Annual Review of Fluid Mechanics*, 5:339–360, 1973.

[33] R. Eppler. *Airfoil Design and Data*. Springer Berlin Heidelberg, 1st edition, 1990.

[34] V.M. Falkner and S.W. Skan. Some approximate solutions of the boundary layer equations. *Philosophical Magazine*, 12:865–896, 1931.

[35] T.K. Fannelop. A simple finite difference procedure for solving the three-dimensional laminar and turbulent boundary layer equations. In *33rd EUROMECH Colloquium on three-dimensional turbulent boundary layers*, Berlin, 25-27 September 1972. European Mechanics Society.

[36] K.O. Felsch, D. Geropp, and A. Walz. Method for turbulent boundary layer prediction. In S.J. Kline, M.V. Morkovin, G. Sovran, and D.J. Cockrell, editors, *Stanford conference on computation of turbulent boundary layers*, volume 1, pages

170–176, Stanford University, 1968. Air Force Office of Scientific Research-Internal Flow Program. Two Volume Set.

[37] H. Fernholz. Three-dimensional turbulent boundary layers: a report on euromech 33. *Journal of Fluid Mechanics*, 58(1):177–186, 1973.

[38] D. Foster. The flow around wing sections with high-lift devices. In *AIAA 9th Aerospace Sciences Meeting*, number 71, page 96, New York, January 25-27, 1971. American Institute of Aeronautics and Astronautics.

[39] D.N. Foster. The flow around wing sections with high-lift devices. In *AIAA 9th Aerospace Sciences Meeting*, number 71-96, New York, 1971. American Institute of Aeronautics and Astronautics.

[40] D.N. Foster. The low-speed stalling of wings with high-lift devices. In *Fluid Dynamics of Aircraft Stalling*, page 12, Neuilly sur Seine, France, 1972. AGARD - Advisory Group for Aerospace Research & Development. AGARD-CP-102.

[41] D.N. Foster, H.P.A.H. Irwin, and B.R. Williams. The two-dimensional flow around a slotted flap. Technical Report 3681, Aeronautical Research Council, London (England), 1970.

[42] B.L. Gadeberg and H.L. Ziff. Flight-determined buffet boundaries of ten airplanes and comparisons with five buffeting criteria. Technical Report NACA-RM-A50I27, National Advisory Committee for Aeronautics. Lewis Flight Propulsion Lab.; Cleveland, OH, United States, 1951.

[43] M. Gaster. The structure and behaviour of laminar separation bubbles. In *Flow Separation, Part 2*, pages 813–854, Neuilly sur Seine, France, 1966. AGARD - Advisory Group for Aerospace Research & Development. AGARD-CP-4.

[44] A.E. Gentry. Investigation of aerodynamic analysis problems in transonic maneuvering: Volume 2. airfoil analysis computer program. Technical Report MDC-J5264-02, McDonnell Douglas Corp Long Beach California Douglas Aircraft Div., 1971.

[45] A.E. Gentry and W.R. Oliver. Investigation of aerodynamic analysis problems in transonic maneuvering: Volume 1. Technical Report MDC-J5264-01, McDonnell Douglas Corp Long Beach California Douglas Aircraft Div., 1971.

[46] J.P. Giesing. Potential flow about two-dimensional airfoils. part i.a summary of two-dimensional airfoil methods. part 2. solution of the flow field about one or more airfoils of arbitrary shape in uniform or non-uniform flows by the douglas neumann method. Technical Report LB-31946, McDonnell Douglas Corp Long Beach California Douglas Aircraft Div., 1965.

[47] F.R. Goldschmied. An approach to turbulent incompressible separation under adverse pressure gradients. *Journal of Aircraft*, 2(2):108–115, 1965.

[48] F.K. Goodwin, J.N. Nielsen, and L.L. Lynes. Inhibition of flow separation at high speed. Technical report, Air Force Flight Dynamics Laboratory (U.S.), Nielsen Engineering & Research, PALO ALTO CALIF., Wright-Patterson Air Force Base (Ohio), 1969. Two Volume Set.

[49] P.S. Granville. The calculation of the viscous drag of bodies of resolution. Technical Report 849, David Taylor Model Basin, Washington, D.C, 1953.

[50] J.E. Green. Interactions between shockwaves and turbulent boundary layers. volume 11 of *Progress in Aeronautical Science*, pages 235–340. Oxford Pergamon Press, 1970.

[51] J.E. Green. Some aspects of viscous-inviscid interactions at transonic speeds, and their dependence on reynolds number. Neuilly sur Seine, France, 1971. AGARD - Advisory Group for Aerospace Research & Development. AGARD-CP-83-71.

[52] J.E. Green, D.J. Weeks, and J.W.F. Brooman. Prediction of turbulent boundary layers and wakes in compressible flow by a lag-entrainment method. Technical Report 3791, Aeronautical Research Council, London (England), 1977.

[53] M.G. Hall and D. Küchemann. Scale effects in flows over swept wings. Technical report, Great Britain. Ministry of Technology, Royal Aircraft Establishment (Great Britain), 1971.

[54] G.J. Hancock. Problems of aircraft behaviour at high angles of attack. Neuilly sur Seine, France. AGARD - Advisory Group for Aerospace Research & Development. AGARD-AG-136.

[55] J.E. Harris. Numerical solution of the equations for compressible laminar, transitional and turbulent boundary layers and comparisons with experimental data. Technical report, National Aeronautics and Space Administration (NASA), 1971.

[56] M.R. Head. Entrainment in the turbulent boundary layer. Technical Report 3152, Aeronautical Research Council, London (England), 1958.

[57] M.R. Head and V.C. Patel. Improved entrainment method for calculating turbulent boundary layer development. Technical Report 3643, Aeronautical Research Council, London (England), 1968.

[58] H.J. Herring and L.G. Mellor. *Compressible turbulent boundary layers*, chapter A method of calculating compressible turbulent boundary layers, pages 27–132. Number SP-216. National Aeronautics and Space Administration (NASA), 1969.

[59] E.H. Hirschel. Theoretische untersuchung von transitionsphänomenen in der grenzschicht eines unendlich gestreckten gepfeilten flügels. Technical report, Deutsche Forschungs- und Versuchsanstalt für Luft- und Raumfahrt (DFVLR), 1972.

[60] E.A. Hirst and W.C. Reynolds. An integral prediction method for turbulent boundary layers using the turbulent kinetic energy equation. In S.J. Kline, M.V. Morkovin, G. Sovran, and D.J. Cockrell, editors, *Stanford conference on computation of turbulent boundary layers*, volume 1, pages 213–234, Stanford University, 1968. Air Force Office of Scientific Research-Internal Flow Program. Two Volume Set.

[61] J.H. Horlock, J.F. Norbury, and J.C. Cooke. Three-dimensional boundary layers: a report on euromech 2. *Journal of Fluid Mechanics*, 27(2):369–380, 1967.

[62] K. Jacob. Berechnung der abgelösten inkompressiblen strömung um tragflügelprofile und bestimmung des maximalen auftriebs. *Zeitschrift für Flugwissenschaften und Weltraumforschung*, 17:221–230, 1965.

[63] K. Jacob. Berechnung der inkompressiblen strömung mit ablösung für profilsysteme. Technical report, Deutsche Forschungs- und Versuchsanstalt für Luft- und Raumfahrt (DFVLR), 1972.

[64] J.P. Johnston. On the three-dimensional turbulent boundary layer generated by secondary flow. *Journal of Basic Engineering*, 82(1):233–246, 1960.

[65] E. Krause. Numerical treatment of boundary layer problems. In *Advances in Numerical Fluid Dynamics*, Neuilly sur Seine, France, 1973. AGARD - Advisory Group for Aerospace Research & Development. AGARD-LS-64.

[66] J.L. Krause, E.H. Hirschel, and E.H. Kordulla. Finite difference solutions for three-dimensional turbulent boundary layers. In *33rd EUROMECH Colloquium on three-dimensional turbulent boundary layers*, Berlin, 25-27 September 1972. European Mechanics Society.

[67] D. Küchemann. Types of flow on swept wings with special reference to free boundaries and vortex sheets. *Journal of the Royal Aeronautical Society*, 57:683–699, 1953.

[68] T.E. Labrujere, G.J. Schipholt, and O. De Vries, editors. *Potential flow calculations to support two-dimensional wind tunnel tests on high-lift devices*, volume 72 of *ICAS Paper*. International Council of the Aeronautical Sciences, 1972.

[69] B.E. Launder and D.B. Spalding. *Mathematical models of turbulence*. Academic Press, London, New York, 1st edition, 1972.

[70] B.H. Little. Scaling effects on shock induced separation. In *High Reynolds Number Subsonic Aerodynamics*, Neuilly sur Seine, France, 1970. AGARD - Advisory Group for Aerospace Research & Development. AGARD-LS-37-70.

[71] B.L.G. Ljungstrøm. Boundary layer studies on a two-dimensional high-lift wing. Technical Report AU-862, Flygtekniska førsøksanstalten, Aeronautical Research Institute of Sweden, Bromma, 1972.

[72] D.L. Loving. Wind-tunnel-flight correlations of shock-induced separated flow. Technical Report TN D-3580, National Aeronautics and Space Administration (NASA), 1966.

[73] H. Ludwieg and W. Tillmann. Untersuchungen über die wandschubspannung in turbulenten reibungsschichten. *Ingenieur-Archiv*, 17(4):288–299, 1949.

[74] A. Mager. Generalization of boundary-layer momentum-integral equations to three-dimensional flows including those of rotating system. Technical Report NACA-TR-1067, National Advisory Committee for Aeronautics. Lewis Flight Propulsion Lab.; Cleveland, OH, United States, 1952.

[75] G. Maise and H. McDonald. Mixing length and eddy viscosity in a compressible boundary-layer. *AIAA Journal*, 6:73–80, 1968.

[76] H. McDonald and F.J. Camarata. An extended mixing length approach for computing the turbulent boundary layer development. In S.J. Kline, M.V. Morkovin, G. Sovran, and D.J. Cockrell, editors, *Stanford conference on computation of turbulent boundary layers*, volume 1, pages 83–98, Stanford University, 1968. Air Force Office of Scientific Research-Internal Flow Program. Two Volume Set.

[77] H. McDonald and R.W. Fish. Practical calculations of transitional boundary layers. AGARDograph, Neuilly sur Seine, France, 1972. AGARD - Advisory Group for Aerospace Research & Development. AGARD-AG-164.

[78] G.L. Mellor and H.J. Herring. Two methods of calculating turbulent boundary layer behavior based on numerical solutions of the equations of motion. In S.J. Kline, M.V. Morkovin, G. Sovran, and D.J. Cockrell, editors, *Stanford conference on computation of turbulent boundary layers*, volume 1, pages 331–345, Stanford University, 1968. Air Force Office of Scientific Research-Internal Flow Program. Two Volume Set.

[79] R. Michel, C. Quémard, and J. Cousteix. Méthode pratique de prévision des couches limites turbulentes bi- et tri-dimensionnelles. *La Recherche Aérospatiale*, 1:1–14, 1972.

[80] R. Michel, C. Quémard, and R. Durant. Hypotheses on the mixing length and application to the calculation of the turbulent boundary layers. In S.J. Kline, M.V. Morkovin, G. Sovran, and D.J. Cockrell, editors, *Stanford conference on computation of turbulent boundary layers*, volume 1, pages 195–212, Stanford University, 1968. Air Force Office of Scientific Research-Internal Flow Program. Two Volume Set.

[81] M.V. Morkovin. Effects of compressibility on turbulent flows. In A. Favre, editor, *Mécanique de la Turbulence*, pages 367–380, Paris, 1961. Centre national de la recherche scientifique.

[82] E.M. Murman and J.D. Cole. Calculation of plane steady transonic flows. In *AIAA 8th Aerospace Sciences Meeting*, volume 70, page 40, New York, 1970. American Institute of Aeronautics and Astronautics.

[83] D.F. Myring. An integral prediction method for three-dimensional turbulent boundary-layers in incompressible flow. Technical report, Great Britain. Ministry of Technology, Royal Aircraft Establishment (Great Britain), 1970.

[84] J.F. Nash. Turbulent-boundary-layer behaviour and the auxiliary equation. Technical Report 835, Aeronautical Research Council, London (England), 1966.

[85] J.F. Nash. The calculation of three-dimensional turbulent boundary layers in incompressible flow. *Journal of Fluid Mechanics*, 37(4):625–642, 1969.

[86] J.F. Nash and J.G. Hicks. An integral method including the effect of upstream history on the turbulent shear stress. In S.J. Kline, M.V. Morkovin, G. Sovran, and D.J. Cockrell, editors, *Stanford conference on computation of turbulent boundary layers*, volume 1, pages 37–45, Stanford University, 1968. Air Force Office of Scientific Research-Internal Flow Program. Two Volume Set.

[87] J.F. Nash and A.G.J. Macdonald. The calculation of momentum thickness in a turbulent boundary layer at mach numbers up to unity. Technical Report 963, Aeronautical Research Council, London (England), 1966.

[88] J.F. Nash and V.C. Patel. *Three-dimensional turbulent boundary layers*. Scientific and Business Consultants Technical Books, Atlanta, 1st edition, 1972.

[89] V.W. Nee and L.S.G. Kovasznay. The calculation of the incompressible turbulent boundary layers by a simple theory. In S.J. Kline, M.V. Morkovin, G. Sovran, and D.J. Cockrell, editors, *Stanford conference on computation of turbulent boundary layers*, volume 1, pages 300–319, Stanford University, 1968. Air Force Office of Scientific Research-Internal Flow Program. Two Volume Set.

[90] H.J. Obremski, M.V. Morkovin, and M Landahl. A portfolio of stability characteristics of incompressible boundary layers. AGARDograph, page 146, Neuilly sur Seine, France, 1969. AGARD - Advisory Group for Aerospace Research & Development. AGARD-AG-134.

[91] P.R. Owen and L. Klanfer. On the laminar boundary layer separation from the leading edge of a thin airofoil. Technical report, Aeronautical Research Council, London (England), 1953.

[92] S.V. Patankar and D.B. Spalding. *Heat and mass transfer in boundary layers*. Intertext Books, 2nd edition, 1970.

[93] J.H. Paterson. Scaling effects on drag prediction. In *High Reynolds Number Subsonic Aerodynamics*, Neuilly sur Seine, France, 1970. AGARD - Advisory Group for Aerospace Research & Development. AGARD-LS-37-70.

[94] D.J. Peake, G. Brakmann, and J.M. Romeskie. Comparisons between some high reynolds number turbulent boundary layer experiments at mach 4 and various recent calculation procedures. In *Turbulent shear flows*, page 11, Neuilly sur Seine, France, 1971. AGARD - Advisory Group for Aerospace Research & Development. AGARD-CP-93.

[95] H.H. Pearcey, J. Osborns, and A.B. Haines. The interaction between local effects at the shock and rear separation - a source of significant scale effects in wind tunnel tests on airofoils and wings. In *Transonic Aerodynamics*, pages 11–1–11–23, Neuilly sur Seine, France, 1968. AGARD - Advisory Group for Aerospace Research & Development. AGARD-CP-35.

[96] B.J. Powell. The calculation of the pressure distribution of a thick cambered aerofoil at subsonic speeds including the effect of the boundary layer. Technical Report 1005, Aeronautical Research Council, London (England), 1967.

[97] L. Prandtl. über flüssigkeitsbewegung bei sehr kleiner reibung. In *Verhandlungen III, Internationaler Mathematiker-Kongresses*, pages 484–491, Heidelberg, 1904.

[98] G. Redeker. Die berechnung der schüttelgrenzen von pfeilflügeln. *Zeitschrift für Flugwissenschaften und Weltraumforschung*, 21:345–359, 1973.

[99] W.C. Reynolds. A morphology of the prediction methods. In S.J. Kline, M.V. Morkovin, G. Sovran, and D.J. Cockrell, editors, *Stanford conference on computation of turbulent boundary layers*, volume 1, pages 1–15, Stanford University, 1968. Air Force Office of Scientific Research-Internal Flow Program. Two Volume Set.

[100] F.W. Riegels. *Aerodynamische Profile*. Oldenbourg Verlag München, 1st edition, 1958.

[101] F.W. Riegels and K. Jacob. Berechnung der druckverteilung endlich dicker profile: ohne und mit klappen und vorflügeln. Technical Report 63, Göttingen Aerodynamische Versuchsanstalt, 1963.

[102] L. Rosenhead. *Laminar Boundary Layers*. Fluid Motion Memoirs. Clarendon Press, Oxford, England, 1st edition, 1963.

[103] J. Rotta. Fortran iv - rechenprogramm für grenzschichten bei kompressiblen, ebenen und achsensymmetrischen strömungen. Technical Report 68-R-03, Aerodynamische Versuchsanstalt Göttingen, 1968.

[104] J. Rotta. Turbulent boundary layer calculations with the integral dissipation method. In S.J. Kline, M.V. Morkovin, G. Sovran, and D.J. Cockrell, editors, *Stanford conference on computation of turbulent boundary layers*, volume 1, pages 177–181, Stanford University, 1968. Air Force Office of Scientific Research-Internal Flow Program. Two Volume Set.

[105] J. Rotta, editor. *Turbulente Strömungen*. Leitfäden der angewandten Mathematik und Mechanik, Band 15. B. G. Teubner, Stuttgart, 1st edition, 1972.

[106] H. Schlichting. *Boundary-Layer Theory*. McGraw Hill series in mechanical engineering. McGraw Hill, New York, 6th edition, 1968.

[107] H. Schlichting. *Boundary-Layer Theory*, chapter Origin of turbulence. McGraw Hill series in mechanical engineering. McGraw Hill, New York, 6th edition, 1968.

[108] W. Schröder. Investigation of the flow field in the slot region of a two-dimensional slotted trailing edge flap on a naca-0006 aerofoil. Technical Report 73-12, The Von Karman Institute for Fluid Dynamics, Sint-Genesius-Rode, Belgium, 1973.

[109] G.B. Schubauer and P.S. Klebanoff. Investigation of separation of the turbulent boundary layer. Technical Report 1030, National Advisory Committee for Aeronautics, 1951.

[110] G.B. Schubauer and W.G. Spangenberg. Forced mixing in boundary layers. *Journal of Fluid Mechanics*, 8(1):10–32, 1966.

[111] C.S. Sinnot. On the prediction of mixed subsonic/supersonic pressure distributions. *Journal of Aerospace Sciences*, 27(10):767–778, 1960.

[112] A.M.O. Smith. Aerodynamics of high-lift airfoil systems. In *Fluid Dynamics of Aircraft Stalling*, page 24, Neuilly sur Seine, France, 1972. AGARD - Advisory Group for Aerospace Research & Development. AGARD-CP-102.

[113] A.M.O. Smith and T. Cebeci. Numerical solution of the turbulent boundary-layer equations. Technical Report DAC 33735, Douglas Aircraft Co., 1967.

[114] A.M.O. Smith and N. Gamberoni. Transition, pressure gradient and stability theory. Technical Report ED 26388, Douglas Aircraft Co., 1956.

[115] P.D. Smith. Calculation methods for three-dimensional turbulent boundary layers. Technical Report 3523, Aeronautical Research Council, London (England), 1966.

[116] D.B. Spalding and S.W. Chi. The drag of a compressible turbulent boundary layer on a smooth flat plate with and without heat transfer. *Journal of Fluid Mechanics*, 18(1):117–143, 1964.

[117] D.A. Spence. Prediction of the characteristics of two-dimensional airfoils. *Journal of Aeronautical Sciences*, 21(9):577–588, 1954.

[118] D.A. Spence and J.A. Beasley. The calculation of lift slopes, allowing for boundary layer, with applications to the rae 101 and l04 aerofoils. Technical Report 3137, Aeronautical Research Council, London (England), 1958.

[119] H. B. Squire and A. D. Young. The calculation of the profile drag of aerofoils. Technical Report 1838, Aeronautical Research Committee, London (England), 1937.

[120] J. Steinheuer. Berechnung des reibungseinflusses auf den auftrieb eines spaltklappenprofils. Technical Report 73-04, Deutsches Zentrum für Luft- und Raumfahrt, 1973.

[121] B.S. Stratford. The prediction of separation of the turbulent boundary layer. *Journal of Fluid Mechanics*, 5(1):1–16, 1959.

[122] I. Tani. *Progress in Aeronautical Science*, volume 5, chapter Low-speed flows involving bubble separations, pages 70–103. The Macmillan Company, New York, 1964.

[123] F. Thomas. Die ermittlung der schüttelgrenzen von tragflügeln im transsonischen geschwindigkeitsbereich. In *Jahrbuch d. Wissenschaftlichen Gesellschaft f. Luft- u. Raumfahrt*, pages 126–144. Braunschweig, 1966.

[124] F. Thomas and G. Redeker. A method for calculating the transonic buffet boundary including the influence of reynolds number. In *Facilities and Techniques for Aerodynamic Testing at Transonic Speeds and High Reynolds Number*, Neuilly sur Seine, France, 1971. AGARD - Advisory Group for Aerospace Research & Development.

[125] B.G.J. Thompson. A critical review of existing methods of calculating the turbulent boundary layer. Technical Report 3447, Aeronautical Research Council, London (England), 1964.

[126] B. Thwaites. *Incompressible Aerodynamics*. Fluid Motion Memoirs. Clarendon Press, Oxford, England, 1st edition, 1960.

[127] W. Tollmien. Berechnung turbulenter ausbreitungsvorgänge. *Zeitschrift für angewandte Mathematik und Mechanik*, 6(6):468–478, 1926.

[128] E. Truckenbrodt. Ein quadraturverfahren zur berechnung der laminaren und turbulenten reibungsschicht bei ebener und rotationssymmetrischer strömung. *Ingenieur-Archiv*, 20(4):211–228, 1952.

[129] E.R. van Driest. Turbulent boundary layer in compressible fluids. *Journal of Aeronautical Sciences*, 18(3):146–160, 1951.

[130] E.R. Van Driest. On turbulent flow near a wall. *Journal of the Aeronautical Sciences*, 23(11):1007–1011, 1956.

[131] R. Vanino and E. Wedemeyer. Wind tunnel investigations of buffet loads on four airplane models. In *Facilities And Techniques For Aerodynamic Testing At Transonic Speeds And High Reynolds Number*, Neuilly sur Seine, France, 1971. AGARD - Advisory Group for Aerospace Research & Development. AGARD-CP-83-71.

[132] A.J. Vermeulen. *Measurements of three-dimensional turbulent boundary layers*. PhD thesis, University of Cambridge, 1971.

[133] A. Walz. *Strömungs- und Temperaturgrenzschichten*. G. Braun, Karlsruhe, 1st edition, 1966.

[134] H. Werlé. Sur l'écoulement au bord d'attaque d'un profil portant. *La Recherche Aérospatiale*, (4):197–218, 1973.

[135] P. Wesseling and J.P.E. Lindhout. Three-dimensional incompressible turbulent boundary layers: comparison between calculations and experiments. In *33rd EUROMECH Colloquium on three-dimensional turbulent boundary layers*, Berlin, 25-27 September 1972. European Mechanics Society.

[136] A.J. Wheeler and J.P. Johnston. Three-dimensional turbulent boundary layers: an assessment of prediction methods. Technical report, Thermosciences Division, Dept. of Mechanical Engineering, Stanford University, 1971.

[137] A.J. Wheeler and J.P. Johnston. Three-dimensional turbulent boundary layers: Data sets for two-space coordinate flows. Technical report, Thermosciences Division, Dept. of Mechanical Engineering, Stanford University, 1972.

[138] J. Williams and A.J. Ross. Some airframe aerodynamic problems at low speeds. In *International Congress on Subsonic Aeronautics*, volume 154 of *Annals of the New York Academy of Sciences*, pages 264–305, 1968.

[139] R.E. Wilson. Turbulent boundary layer characteristics at supersonic speeds - theory and experiment. *Journal of Aeronautical Sciences*, 17(9):585–594, 1950.

[140] K.G. Winter, J.C. Rotta, and K.G. Smith. Studies of the turbulent boundary layer on a waisted body of revolution in subsonic and supersonic flow. Technical Report 3633, Aeronautical Research Council, London (England), 1968.

[141] F.J. Zwarts. Turbulent boundary layer predictions using a dissipation integral method. In S.J. Kline, M.V. Morkovin, G. Sovran, and D.J. Cockrell, editors, *Stanford conference on computation of turbulent boundary layers*, volume 1, pages 154–169, Stanford University, 1968. Air Force Office of Scientific Research-Internal Flow Program. Two Volume Set.